NTNU
Norwegian University of
Science and Technology

Dynamic Analysis of Connected Jackets

Tarjei Nærø Sandal

Marine Technology
Submission date: June 2018
Supervisor: Jørgen Amdahl, IMT
Co-supervisor: Ole Gabrielsen, DNV GL

Norwegian University of Science and Technology
Department of Marine Technology

NTNU – Trondheim
Norwegian University of
Science and Technology

Dynamic Analysis of Connected Jackets

Tarjei Nærø Sandal

11.06.2018

Master Thesis
Department of Marine Technology
Norwegian University of Science and Technology (NTNU)

Supervisors: Jørgen Amdahl (NTNU), Ole Gabrielsen (DNV GL)

NTNU
Norges teknisk-naturvitenskapelige universitet
Institutt for marin teknikk

MASTER THESIS 2018

for

Stud. Techn. Tarjei Nærø Sandal

Dynamic Analysis of Connected Jackets
Dynamisk analyse avkoblede fagverksplattformer

Introduction

An increasing number of jacket platforms, both in the North Sea and other parts of the world, are approaching or has passed their original design life. The oil and gas industry is constantly developing techniques to ensure safe use of these assets. Online monitoring of environmental data, improved analysis tools, development of inspection technologies, re-analysis tools and inspection planning are important in this respect. In addition, on-going developments within sensor technology open for new opportunities with regards to structural monitoring of offshore structures. Increasing sensor robustness, accuracy, efficiency and lower cost make it possible to collect valuable data of structural response. These data may be used primarily for two purposes:

1. Online structural monitoring to ensure safe use, prevent failures and control further degradation.

2. Assessment of the accuracy of the structural models used in design and verification.

It is the first item that is the focus of this thesis proposal as it is important to understand how interaction between connected jackets may influence acceleration measurements. This understanding needs to be established before the measurements of such systems are assessed.

Description of how to perform instrumented condition monitoring can be found in NORSOK N-005 /2/, and summaries from some monitoring projects are given in NORSOK N-006 /3/. The Kvitebjørn jacket was instrumented to assess its dynamic behaviour /4/. In other cases, topside accelerations are measured as part of a monitoring scheme in order to detect possible defects. However, if two or more jackets are connected by bridges, the dynamic behaviour of a jacket might be affected by neighbouring jacket(s).

Aim of the Project and Master thesis work

The aim of the project (fall 2017) and master thesis work (spring 2018) is to assess how/if the behaviour jackets connected with bridges is affected by the neighbouring jacket(s).

Scope of work:

The work is proposed carried out in the following steps

1. Conduct a dynamic analysis of the response of one, two and three simplified "jacket" models by means of USFOS. It is suggested that the jacket be modelled as cantilever beams with topside masses where the stiffness is scaled such that a realistic eigenperiod and topside displacement are obtained. The water depth shall be realistic. The cantilever beams can be connected with 2-node springs at the top representing the bridge/piping system. Initially, the environmental force may be represented by concentrated harmonic forces at the top nodes with given phase lags. Compare the results those obtained with the MATLAB program developed in the project work. In addition to deck displacements other response quantities relevant for condition monitoring should also be considered. To ease parametric studies it is recommended to use scripting techniques for USFOS analyses.

2. Analyse the structure subjected to Morrison type environmental loads from waves. The hydrodynamic coefficient and /or the hydrodynamic diameter may be varied to obtain the desired load level. Wave phase lags may be adjusted by varying the distance between the "jackets" Analysis should be carried out for wave loads integrated up to (approximately) mean surface level (small amplitude) and true surface level. Initial calculations shall be done with an inertia dominated structure and small amplitude (linear system). Next, for a dragdominated structure. Identify and discuss any super - or sub-harmonic response component due top nonlinearity in wave load formulation and integration to true surface level.

3. A brief review of structural configurations, weight and stiffnesses for representative bridges that support process piping between two jackets. Estimate by analyses and simplified models representative springs for interconnecting bridges.

4. Establish finite models of real jacket(s) to be used in numerical studies. To reduce the computational effort, it shall be considered to reduce the extent and the fineness of the models without compromising accuracy. Verify that the wave loads obtained are reasonable. Estimate the phase lag of the resultant forces for given separation distances and wave frequencies. Platforms may be connected with realistic bridges and piping models or equivalent springs. Perform eigenvalue analysis of the platforms alone and interconnected. Estimate the period needed to obtain stationary response for harmonic loading. Perform parametric, dynamic simulation of the response to harmonic loading. Discuss the results with special reference to those obtained for the simple models. Can 2 or 3 DOF models be applied? Can pseudo transfer functions be developed?

5. Conduct simulations of interconnected jacket response subjected to irregular waves. Dynamic – and static response histories should be compared. Estimate the statistical

properties and power spectra of key response data. Can an equivalent DAF be defined? Discuss how thew resulst can be used in condition monitoring.

6. Conclusions and recommendations for further work.

References

/1/ NORSOK standard N-001, "Integrity of offshore structures", edition 8, September 2012.

/2/ NORSOK standard N-005:2017, "In-service Integrity of Managments of Structures and Maritime Systems

/3/ NORSOK standard N-006, "Assessment of structural integrity for existing offshore load-bearing structures", revision 3, February 2013.

/4/ D. Karunakaran and S. Haver, "Dynamic behaviour of Kvitebjørn jacket structure – Numerical predictions versus full-scale measurements", Eurodyn 2005.

/5/ B. Skallerud and J. Amdahl, "Nonlinear Analysis of Offshore Structures", January 2002, ISBN 0-86380-258-3.

Literature studies of specific topics relevant to the thesis work may be included.

The work scope may prove to be larger than initially anticipated. Subject to approval from the supervisor, topics may be deleted from the list above or reduced in extent.

In the thesis the candidate shall present his personal contribution to the resolution of problems within the scope of the thesis work.

Theories and conclusions should be based on mathematical derivations and/or logic reasoning identifying the various steps in the deduction.

The candidate should utilise the existing possibilities for obtaining relevant literature.

The thesis should be organised in a rational manner to give a clear exposition of results, assessments, and conclusions. The text should be brief and to the point, with a clear language. Telegraphic language should be avoided.

The thesis shall contain the following elements: A text defining the scope, preface, list of contents, summary, main body of thesis, conclusions with recommendations for further work, list of symbols and acronyms, references and (optional) appendices. All figures, tables and equations shall be numerated.

The supervisor may require that the candidate, in an early stage of the work, presents a written plan for the completion of the work. The plan should include a budget for the use of computer and laboratory resources, which will be charged to the department. Overruns shall be reported to the supervisor.

The original contribution of the candidate and material taken from other sources shall be clearly defined. Work from other sources shall be properly referenced using an acknowledged referencing system.

The report shall be submitted in two copies:

- Signed by the candidate
- The text defining the scope included
- In bound volume(s)
- Drawings and/or computer prints which cannot be bound should be organised in a separate folder.

Supervisor:
Prof. Jørgen Amdahl

Contact person at DNV GL : Ole Gabrielsen

Deadline:, June 11, 2018

Trondheim, January 18 2018

Jørgen Amdahl

Preface

This master thesis is the closing submission of the 5-years master's degree program in Marine Technology, at the Department of Marine Technology, Norwegian University of Science and Technology (NTNU). It was carried out in the period from January 2018 to June 2018. The thesis builds upon a preparatory work performed during the autumn/winter of 2017. The work has been done in cooperation with the offshore structure section of DNV GL in Stavanger, under supervision of Ole Gabrielsen, who initially suggested the topic of the thesis. The scope of the thesis was suggested by Jørgen Amdahl, who is my supervisor at NTNU.

I would like to express my gratitude to Ole Gabrielsen in DNV GL for giving me the opportunity to write my master thesis for DNV GL and for proposing a very interesting topic. Further, I would like to thank him for his guidance and for providing an excellent working facility in a good atmosphere among professionals. Additionally, I would like to thank my supervisor at NTNU, Jørgen Amdahl. It has been a pleasure to work under the supervision of such a highly experienced professor. Despite of his tight schedule, he has payed high attention to my work and has always found time to assist me. The cooperation between NTNU and DNV GL has worked out well, and it has been truly inspiring to write my master thesis with such a good team behind me. Finally, I would like to thank my other colleagues in DNV GL, and especially Kjetil Dahl and Robert Ganski for being helpful and always answering questions.

Tarjei Nærø Sandal
Stavanger, June 8, 2018

Abstract

The dynamic behavior of jacket platforms connected by a bridge has been studied by time-domain simulations in USFOS, which is a nonlinear finite element program. The main motivation behind studying this, is to be able to do condition monitoring of connected jackets by assessing acceleration measurement. In order to do this, it is essential to gain an understanding of how the interaction between connected jackets may influence the acceleration measurements. The simulations have been done for a system consisting of two identical jackets, connected by a linear spring representing the bridge. The system has been subjected to waves from one direction only.

Initially, the simulations were done on a simplified model with jackets modelled as cylindrical cantilevered beams. The response was plotted in the frequency domain by running many simulations at different force frequencies. The phase lag of the force on the second jacket was kept constant by varying the distance between the jackets. Results from the simplified model were compared with results obtained in the specialization project. The hydrodynamic loads have been calculated by Morison's equations, and the nonlinear effects due to the wave load formulation have been studied.

A finite element model of two connected "real" jackets has been developed, and this model has been subjected to irregular waves. The response data from both static and dynamic analyses have been compared, to investigate to what extent the system is affected by dynamics. Additionally, it has been conducted a sensibility study on how the bridge stiffness influences the response values. The responses from the irregular waves were compared with respect to fatigue, extreme long term response and mean square response.

Sammendrag

Den dynamiske oppførselen til fagverksplattformer sammenkoblet av ei bru har blitt analysert ved å kjøre simuleringer i tidsplanet i programvaren USFOS. Hovedmotivasjonen for å studere dette, er å kunne gjøre tilstandsovervåkning av sammenkoblede jacket-plattformer ved å følge med på endringer i akselerasjonsmålinger. For å kunne gjøre dette, er det essensielt å forstå hvordan interaksjonen mellom de sammenkoblede jacket-plattformene påvirker akselerasjonsmålingene. Simuleringene har blitt gjort for et system bestående av to identiske jacket-plattformer, sammenkoblet med en lineær fjær. Systemet har blitt påtrykt bølger fra bare én retning.

Innledningsvis ble analysene gjort for en forenklet modell, hvor jacket-plattformene var modellert som sylindriske utkragerbjelker. Responsen ble plottet i frekvensplanet ved å kjøre mange simuleringer med ulike frekvenser for kraften. Faseforsinkelsen (phase lag) for kraften på den andre plattformen ble holdt konstant ved å variere avstanden mellom plattformene. Resultater fra analyser for den forenklede modellen ble sammenlignet med resultater fra prosjektoppgaven. De hydrodynamiske kreftene har blitt gitt ved Morisons ligning, og ikke-lineære effekter fra formuleringen av bølgelasten har blitt studert.

En elementmetodemodell for to reelle jacket-plattformer har blitt påtrykt irregulære bølger. Responsdata fra statiske og dynamiske analyser har blitt sammenlignet for å undersøke i hvilken grad systemet er påvirket av dynamikk. Det var også gjort en sensitivitetsstudie av hvordan brustivheten påvirker responsene. Responsene fra irregulære bølger ble sammenlignet med hensyn på utmatting, ekstrem langtidsrespons og som gjennomsnittsverdi av kvadratet til responsen for de ulike tidsstegene.

Nomenclature

$\ddot{r_i}$	Acceleration of oscillatory translation motion for degree of freedom i
$\dot{r_i}$	Velocity of oscillatory translation motion for degree of freedom i
ω_{ni}	Eigenfrequency [rad/s] corresponding to mode shape ϕ_i
ϕ_i	Mode shape corresponding to eigenfrequency ω_{ni}
α	Parameter in Gumbel distribution
α_1, α_2	Coefficients used for Rayleigh damping
β	Parameter in Gumbel distribution
β_j	Phase lag of the excitation acting on jacket j due to the force acting on jacket 1
δ	Constant in JONSWAP spectrum
$\Delta\sigma_i$	Stress range at the center of stress range interval i
γ	Constant in JONSWAP spectrum
λ	Wave length
u	Flow velocity of fluid
μ	Stiffness ratio $= \frac{k_b}{K_j}$
ω	Wave frequency
ω_l, ω_u	Lower and upper frequency limits in wave spectrum
ω_p	Peak frequency in JONSWAP spectrum
Φ	Velocity potential
ρ	Water density
σ	Constant in JONSWAP spectrum
σ^2	Variance
$\mathbf{C}$	Damping matrix for multi degree of freedom system
$\mathbf{K}$	Stiffness matrix for multi degree of freedom system
$\mathbf{M}$	Mass matrix for multi degree of freedom system
θ_j	Random phase angle for describing irregular waves
υ	Constant in JONSWAP spectrum
ξ	Damping ratio

ζ Wave elevation

ζ_{aj} Amplitude for wave component j

a Constant used to define straight line from linear regression

$a_0, a_1, ..., a_k, ...$ Coefficients of Fourier series

a_n Acceleration component normal to the pipe longitudinal axis, used in Morison's equation

b Constant used to define straight line from linear regression

$b_0, b_1, ..., b_k, ...$ Coefficients of Fourier series

C Fatigue damage

c Damping coefficient for single degree of freedom system

C_D Drag coefficient in Morison's equation

C_M Inertia/mass coefficient in Morison's equation

D Diameter of cylinder

E_j Energy per unit area for wave component j

F(t) External load

F_D Force from drag term in Morison's equation

F_I Force from inertia term in Morison's equation

$F_{0,q}$ q- annual probability force response

g Gravitational acceleration constant = 9.81 m/s^2

h Water depth

H(ω) Complex frequency response function

h, Δt Time step used in time domain method

H_j Jacket height

H_s Significant wave height in JONSWAP spectrum

H_{cyl} Height of cylinders used in simplified model

k Stiffness coefficient for single degree of freedom system

k_b Stiffness coefficient for bridge modelled as a spring

k_j Stiffness coefficient for jacket displacement in deck

L_π Length between jackets corresponding to phase lag $\beta_2 = \pi$

$L_\pi/2$	Length between jackets corresponding to a phase lag $\beta = \pi/2$
m	Mass for single degree of freedom system
N	Number of wave frequencies used to describe irregular waves
N_i	Number of cycles to failure for stress range $\Delta\sigma_i$
$R_\zeta(\tau)$	Autocorrelation function for the wave elevation
r_i	Oscillatory translation motion for degree of freedom i
$r_{0,q}$	q- annual probability displacement response
r_{0i}	Amplitude of oscillatory translation motion for degree of freedom i
$S_\zeta(\omega)$	Wave spectrum
$S_F(\omega)$	Force spectrum
$S_r(\omega)$	Response spectrum
T	Wave period
t	Time
t_k	Discrete points of time where solution is found in time domain method
T_p	Peak period in JONSWAP spectrum
T_{nj}	Eigenperiod corresponding to mode shape ϕ_j
u_n	Velocity component normal to the pipe longitudinal axis, used in Morison's equation
x,y,z	Coordinates used to describe the model, with x pointing to the right, y into the paper and z upwards
z'	Scaled vertical coordinate used in stretched Airy theory (Wheeler stretching)

Contents

List of Figures

List of Tables

1 Introduction

1.1 Background and Motivation

Many jacket offshore platforms around the world are approaching their design life. During their service time, the jackets have been exposed to environmental loads which have gradually weakened the structure and made them more vulnerable to defects.

To ensure adequate safety of a jacket platform, the operator is responsible for doing structural integrity management. NORSOK N-005 [2] is a standard of how this can be performed, and is applicable for all types of offshore structures. In this standard, integrity management is defined as: "a continuous process to manage all changes that will occur during service life (from fabrication until decommissioning) that may affect the integrity of structures and marine systems". This can be performed by inspection and/or monitoring. Monitoring is when instruments are used to collect data for integrity assessment. New technology and increasingly accurate sensors, has opened for new methods of doing structural monitoring of jackets. According to the latest revision of NORSOK N-005, accelerometers may be used for monitoring changes in response. This can be done by assessing the power spectrum obtained from the measured accelerations. A change in the power spectrum, e.g. a shifted eigenfrequency, may indicate a defect in the structure. To do this kind of monitoring, it is essential to understand how the interaction between connected jackets may influence the acceleration measurements. This understanding needs to be established before measurements of such systems can be assessed.

1.2 Objective and Scope

This master thesis aims to provide a basic understanding on how the behavior of jackets connected with bridges are affected by the neighboring jacket. This has been done both by examining how the bridge stiffness affects the response plotted in the frequency domain, as well as comparing key response values for different bridge stiffnesses. The simulations have been done in the computer program USFOS, where the responses are solved in the time domain. The main work of this master thesis has been carried out in the following steps:

1. The work presented in this thesis, builds upon a preparatory work that was carried out in the specialization project (TMR 4500) during the autumn/winter of 2017. In the specialization project, Matlab was used to analyze a very simplified model by means of the frequency response method. Hence, a natural first step for this master thesis was to verify the results from the specialization project by use of USFOS. This was also done in order to get an initial simplified USFOS model, verified by the Matlab simulation.

2. The simplified model was subjected to wave loads given by Morison's equation. The super-harmonic force components from the drag term in Morison's equation and integration up to true surface level were studied. This was carried out by doing simulations for both inertia dominated systems and drag dominated systems, separately.
3. A brief review was done for the structural configurations of a representative bridge.
4. A finite element model of "real" connected jackets was established, by copying an already established model, and connecting them with a linear sprig.
5. Similar simulations as was done for the simplified model, were carried out for the complete jacket model.
6. The "real" jacket model was subjected to irregular waves, and key response data from static and dynamic analyses were compared. Additionally, it was conducted a sensitivity study on how the bridge stiffness influences the responses. The responses were compared with respect to fatigue, extreme long term response and mean square response.

The study is limited to a very simplified system. However, when studying the behavior of a complex system, it is essential to first establish a good understanding of the behavior of a simplified system. Thus, this thesis will hopefully provide an understanding of some basic concepts, which can be used in further studies.

The initial task given by Jørgen Amdahl, included studies of three connected jackets. In this work, a system of three connected jackets has only been used to verify the Matlab simulations from the specialization project. Other than this, no other simulations have been conducted on three connected jackets, due to the already existing complexity in a system with two connected jackets.

1.3 Software Tools

The response simulations were carried out with USFOS, a computer program which can be used for static or dynamic analysis in the time domain. USFOS is especially designed for nonlinear progressive collapse and accident analysis for frame structures [3]. Even though this is not the field of study in this thesis, USFOS was chosen due to several reasons:

- USFOS is well suited for analysis of jacket platforms.
- USFOS has a built-in hydrodynamic load module using Morison's equation.
- A jacket FE-model for use in USFOS was available.
- The response is solved by nonlinear analysis in the time domain. In this way, the super-harmonic force components from hydrodynamic loads can be captured.

To streamline the parametric studies, scripting techniques were used by calling the USFOS simulations with various parameters. The software Cygwin was used as a shell to get UNIX-like commands on the Windows operating system. Appendix X contains the command line scripts used to automate the simulations.

Matlab was used for the post-processing of the data from USFOS. The USFOS module Dynres was used to extract the time series data from USFOS into txt.files, which were used as input in the Matlab programs.

The bridge stiffness from the pipes was estimated with GeniE, which is a module in the Sesam suite provided by DNV GL. GeniE is a FEM software which among other things may be used for analyses of beam, plate and shell structures [4].

1.4 A Brief Review of Structural Configurations for Connected Jackets

A jacket platform is a bottom-fixed platform made up of tubular steel members to a truss of the shape of a truncated pyramid, see Figure 1. They are widely used in the North Sea (i.e. Ekofisk and Valhall field), and are mostly installed on water depths of less than 100 meters [5]. There are also examples of jackets installed on deeper water, such as the Kvitebjørn platform which is installed on 190 m [6]. The main task for the tubular members is to take axial forces (tension and compression), and the members are normally dimensioned against buckling[7]. On the other hand, the joints which connect the tubular members are dimensioned against fatigue. Jacket platforms have typically between three and eight vertical tubular legs with large diameter. These are connected by smaller tubular members called braces. The bracing can be arranged in different ways, as shown in Figure 2 [8].

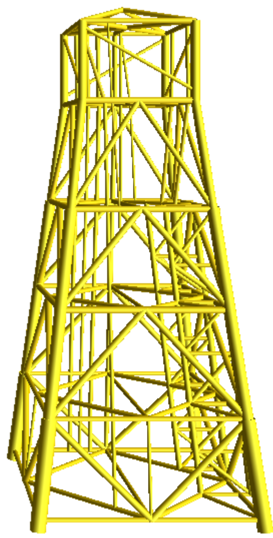

Figure 1: A four-legged jacket, as used in this thesis

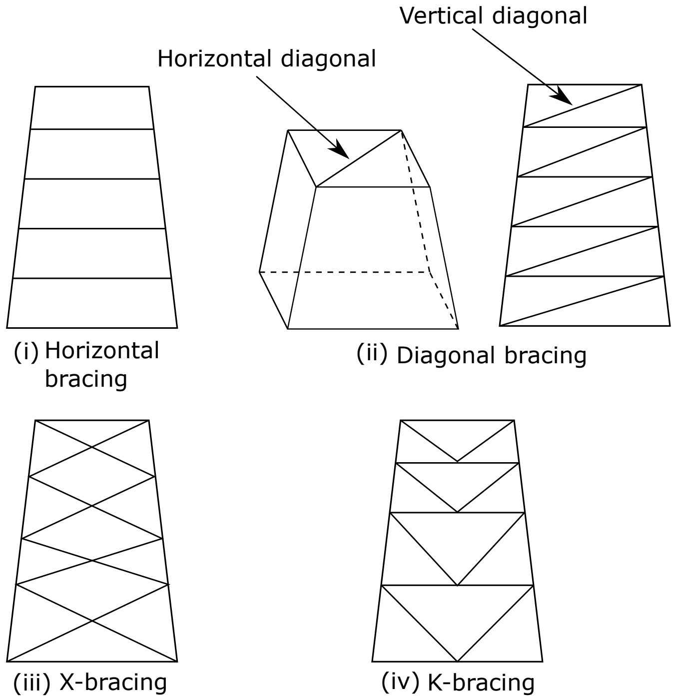

Figure 2: Different types of bracing

A typical weight of a four-legged jacket as shown in Figure 1 is between 5000 t and 8000 t. The topside, where equipment are installed, is connected to the top of the jacket above the splash zone. The weight of the topside can typically be between 10000 t and 25000 t. In this report, a system with jackets connected with bridges that support process piping is studied. Normally the bridge carrying the piping is also a truss made of steel. Most of the axial bride stiffness comes from the piping, since the bridge is connected to one of the platform with a roller support. In reality, there is some friction in the roller support, but still most of the axial stiffness comes from the piping. To ensure that the bridge is not too stiff and to allow thermal expansion, the piping has expansion loops as shown in Figure 3. In this way, most of the stiffness is related to bending of the piping, rather than stretching/compressing the piping.

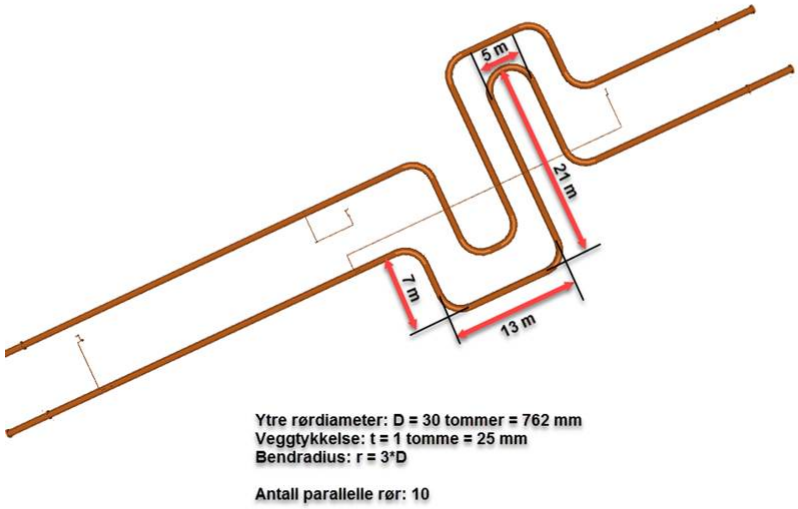

Figure 3: An example of expansion loops given by DNV GL. In reality there are many pipes of different dimensions

2 Theory

This chapter aims to cover the most important theory needed in order to read this thesis. Initially, techniques for solving the dynamic equation of motion (2.1) are presented, with focus on the time domain method which is used in this thesis. Subsequently, theory behind the hydrodynamic loading is given, and then the concept of spectral density is described, together with how it can be applied as a measurement of the response. Finally, the chapter gives a brief discussion on when a structure can be considered quasi-static versus dynamic.

2.1 Equation of Motion

The motion r of a single degree of freedom (SDOF) system subjected to external loading can be described by the dynamic equation of motion given by

$$m\ddot{r}(t) + c\dot{r}(t) + kr(t) = F(t) \tag{2.1}$$

where

- m: mass of the system, including the added mass for structures moving in water
- c: damping coefficient, which in this case is assumed to be viscous
- k: stiffness coefficient
- $F(t)$: external load
- t: time

The equation of motion (2.1) can be generalized to a multi-degree-of-freedom (MDOF) system by introducing matrices including the properties listed above for all the degrees of freedom, together with the couplings between them. The solution to the equation of motion (2.1) can be found in two different ways: in the frequency domain and in the time domain. In the specialization project, the frequency domain method was used, while in this master thesis, the time domain method is used. The following subsection describes the applicability of the frequency domain method, and subsequently the time domain method will be described.

2.2 Applicability of the Frequency Domain Method

Due to the simple relation between the wave spectrum and response spectrum, (2.65), the frequency domain method is well suited for analyses of response from stochastic loads. Additionally, the method is useful for systems with frequency-dependent mass, damping or stiffness [9]. Since the statistically properties of the response can be calculated directly from the response spectrum, the frequency domain method is suited for fatigue analysis. However, the method assumes linearity. This means that nonlinear effects, like the drag term from Morison's equation[1], must be neglected or linearized, such that the response becomes proportional to the wave amplitude. In addition, all transient effects are neglected. In this way the response is oscillating harmonically with the same frequency as the load. A system can also have several other nonlinear effects[2]. Some of them can be linearized, while other are highly nonlinear, and then a time domain analysis is necessary.

2.3 Time Domain Method

In this method, the dynamic analysis is done in the time domain. This means that the solution is obtained during a given time interval. The time interval is divided into many small subintervals (time steps) Δt, normally with equal length $\Delta t = h$. When the initial conditions are known (displacement, velocity and/or acceleration), the solution at the end of the first time step can be determined by assuming a certain variation of the motion during the interval. Further, this solution can be used as starting values for the next time step, and so on [9]. In this way, an approximated solution is obtained for given points along the time axis. Obviously, the smaller time step, the more accurate the solution will be. The time domain method demands much more computer resources than the frequency domain method. On the other hand, it can be used to capture nonlinear effects, and should therefore be used when these are important. Examples of such effects are [11]

- Nonlinear drag term in Morison's equation
- Integration up to the exact surface, see Section 2.4.2
- Transient slamming response
- Simulation of low-frequency motions (slow drift)
- Highly non-linear high-frequency response (e.g. ringing)
- Coupled floater, riser and mooring response

The solution is given directly as a function of time, and it is therefore convenient to use this method with deterministic loading given as a function of time. In the following, two different methods for obtaining the solution in the time domain will be presented.

2.3.1 Methods Based on a Difference Formulation

For these methods, the derivatives in (2.1) are replaced by a difference expression of the order that is required.

[1]See Section 2.4.3
[2]See 2.3 or, for instance, Faltinsen, [10] ch.5 for details

2.3.1.1 Second Central Difference

The velocities and accelerations at the current time step are approximated by

$$\begin{aligned}\dot{\mathbf{r}}_k &= \frac{1}{2\Delta t}(\mathbf{r}_{k+1} - \mathbf{r}_{k-1}) \\ \ddot{\mathbf{r}}_k &= \frac{1}{\Delta t^2}(\mathbf{r}_{k+1} - 2\mathbf{r}_k + \mathbf{r}_{k-1})\end{aligned} \tag{2.2}$$

Substituting this into (2.1) gives

$$\left[\frac{1}{\Delta t^2}\mathbf{M} + \frac{1}{2\Delta t}\mathbf{C}\right]\mathbf{r}_{k+1} = \mathbf{F}_i - \mathbf{K}\mathbf{r}_k(t) + \frac{1}{\Delta^2}\mathbf{M}(2\mathbf{r}_k - \mathbf{r}_{k-1}) + \frac{1}{2\Delta t}\mathbf{C}\mathbf{r}_{k-1} \tag{2.3}$$

This shows that the displacements at step $k+1$ can be calculated from the two foregoing steps. This method is conditionally stable and requires that [12]

$$\Delta t < \frac{2}{\omega_{max}} \tag{2.4}$$

where ω_{max} is the highest eigenfrequency.

2.3.2 Methods Based on Numerical Integration

Considering first a SDOF system, and the dynamic equilibrium for a discrete point of time t_k is then given by

$$m\ddot{r}_k + c\ddot{r}_k + kr_k = F_k \tag{2.5}$$

Between t_k and t_{k+1} we have no exact representation of the displacement $r(t)$ and the dynamic equilibrium. The displacement at time t_{k+1} is found by introducing assumptions regarding the acceleration between t_k and t_{k+1}. These assumptions give the basis for the different methods based on numerical integration.

2.3.2.1 Constant Average Acceleration

In this method, the acceleration is assumed to be the average value for the acceleration within the interval.

$$\ddot{r}(t) = \frac{1}{2}(\ddot{r}_k + \ddot{r}_{k+1}) \tag{2.6}$$

This is a very simple model, which is given here to illustrate how numerical time integration can be done. In modern computer programs, more sophisticated and accurate methods are used. In USFOS, the numerical time integration is based on the HHT-α method.[3] From the assumed acceleration (2.6), the velocity is found by

$$\dot{r}(t) = \dot{r}_k + \frac{t}{2}(\ddot{r}_k + \ddot{r}_{k+1}) \tag{2.7}$$

[3]See the USFOS Theory Manual [13] Section 14.4 for details

The velocity and displacement at time t_{k+1} are found by integrating the assumed acceleration $\ddot{r}(t)$ and the corresponding velocity $\dot{r}(t)$ over $\Delta t = h$

$$\dot{r}_{k+1} = \dot{r}_k + \int_0^h \ddot{r}(t)dt = \dot{r}_k + \frac{h}{2}(\ddot{r}_k + \ddot{r}_{k+1}) \tag{2.8}$$

$$r_{k+1} = r_k + \int_0^h \dot{r}(t)dt = r_k + h\dot{r}_k + \frac{h^2}{4}(\ddot{r}_k + \ddot{r}_{k+1}) \tag{2.9}$$

where $\ddot{r}_{k+1}$ is given by requiring dynamic equilibrium at step k+1

$$\ddot{r}_{k+1} = \frac{1}{m}\left(F_{k+1} - c\dot{r}_{k+1} - kr_{k+1}\right) \tag{2.10}$$

The three equations (2.8) - (2.10) are sufficient to find the three unknowns $\ddot{r}_{k+1}$, $\dot{r}_{k+1}$ and r_{k+1}. From (2.8) and (2.9) we get

$$\begin{aligned} \ddot{r}_{k+1} &= \frac{4}{h^2}(r_{k+1} - r_k) - \frac{4}{h}\dot{r}_k - \ddot{r}_k, \\ \dot{r}_{k+1} &= \frac{2}{h}(r_{k+1} - r_k) - \dot{r}_k \end{aligned} \tag{2.11}$$

Substituting this into (2.10), and get

$$\left(\frac{4}{h^2}m + \frac{2}{h}c + k\right) r_{k+1} = F_{k+1} + \left(\frac{4}{h^2}m + \frac{2}{h}c\right) r_k + \left(\frac{4}{h}m + c\right)\dot{r}_k + m\ddot{r}_k \tag{2.12}$$

where r_{k+1} is the only unknown value.

2.3.2.2 MDOF-Systems

The methods based on numerical integration can also be used directly on coupled MDOF-systems

$$\mathbf{M}\ddot{\mathbf{r}} + \mathbf{C}\dot{\mathbf{r}} + \mathbf{K}\mathbf{r} = \mathbf{F}(t) \tag{2.13}$$

To solve (2.13) directly by a stepwise method is equivalent to solve N uncoupled equations, using the same method and same the time step for all mode-shapes. The stability requirements for the different methods for solving (2.5), can also be applied for solving (2.13). This means that a method is stable with respect to the highest eigenfrequency, even though the mode-shape corresponding to this frequency has no influence on the solution. Hence, to solve a MDOF-system in the time domain requires very small time steps and is therefore computationally heavy. [9]

2.3.3 Eigenfrequencies with Corresponding Mode-Shapes for a 2-DOF System

A system consisting of two equal jackets connected with a bridge modelled as a linear spring, will behave like the system in Figure 4. A N-DOF system will generally have

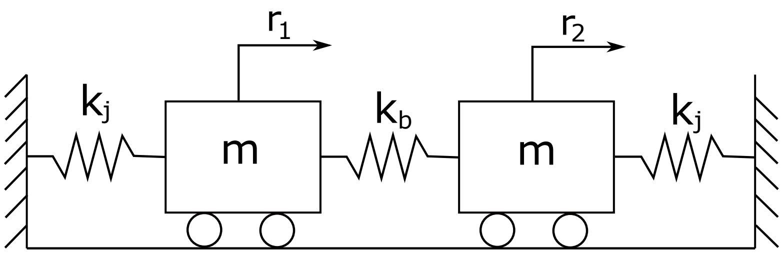

Figure 4: Oscillating system with 2 DOF, used to illustrate the behaviour of two connected jacket. k_j represents the jacket stiffness in sway, while k_b represents the bridge stiffness

N eigenfrequencies $(\omega_{n1}, \omega_{n2}, ..., \omega_{nN})$ with corresponding mode shapes $(\phi_1, \phi_2, ..., \phi_N)$. The eigenfrequencies are found by setting the damping and the external load in (2.1) to zero, i.e. $c = F(t) = 0$. The equations of motion are then found by equilibrium of forces acting on the two masses

$$m\ddot{r_1} + (k_j + k_b)r_1 - k_b r_2 = 0 \tag{2.14}$$

$$m\ddot{r_2} - k_b r_1 + (k_b + k_j)r_2 = 0 \tag{2.15}$$

which in matrix form becomes

$$\begin{bmatrix} m & 0 \\ 0 & m \end{bmatrix} \begin{bmatrix} \ddot{r_1} \\ \ddot{r_2} \end{bmatrix} + \begin{bmatrix} (k_j + k_b) & -k_b \\ -k_b & (k_j + k_b) \end{bmatrix} \begin{bmatrix} r_1 \\ r_2 \end{bmatrix} = \begin{bmatrix} 0 \\ 0 \end{bmatrix} \tag{2.16}$$

The motion is assumed to be harmonic, and can be expressed in complex form as

$$\begin{aligned} r_1 &= r_{01} e^{i\omega t} \\ r_2 &= r_{02} e^{i\omega t} \end{aligned} \tag{2.17}$$

with second derivatives

$$\begin{aligned} \ddot{r_1} &= \omega^2 r_{01} e^{i\omega t} \\ \ddot{r_2} &= \omega^2 r_{02} e^{i\omega t} \end{aligned} \tag{2.18}$$

Substituting (2.17) and (2.18) into (2.16)

$$\begin{bmatrix} k_j + k_b - \omega^2 m & -k_b \\ -k_b & k_j + k_b - \omega^2 m \end{bmatrix} \begin{bmatrix} r_{01} \\ r_{02} \end{bmatrix} = \begin{bmatrix} 0 \\ 0 \end{bmatrix} \tag{2.19}$$

Equation (2.19) has its non-trivial solution when the determinant of the matrix is equal to zero

$$\begin{vmatrix} k_j + k_b - \omega^2 m & -k_b \\ -k_b & k_j + k_b - \omega^2 m \end{vmatrix} = 0 \tag{2.20}$$

This gives the characteristic equation for the system

$$(k_j + k_b - \omega^2 m)^2 - k_b^2 = 0 \tag{2.21}$$

In the result part of this thesis, the bridge stiffness k_b is given by the jacket stiffness k_j through the stiffness ratio defined as

$$\mu = \frac{k_b}{k_j} \tag{2.22}$$

Introducing (2.22) into (2.21)

$$(k_j(1+\mu) - \omega^2 m)^2 - (\mu k_j)^2 = 0 \tag{2.23}$$

which on expanded form becomes

$$\omega^4 - 2(1+\mu)\frac{k_j}{m}\omega^2 + (1+2\mu)(\frac{k_j}{m})^2 = 0 \tag{2.24}$$

Solving this equation for ω^2

$$\omega^2 = (1+\mu \pm \mu)\frac{k}{m} \quad \Rightarrow \quad \omega_{n1}^2 = \frac{k}{m}, \qquad \omega_{n2}^2 = (1+2\mu)\frac{k}{m} \tag{2.25}$$

The first line of (2.19) gives

$$\frac{r_{01}}{r_{02}} = \frac{k_b}{k_j + k_b - \omega^2 m} = \frac{\mu k_j}{k_j(1+\mu) - \omega^2 m} \tag{2.26}$$

The two mode-shapes are now found by introducing the two eigenfrequencies, ω_{n1} and ω_{n2}, into (2.26)

$$\left.\frac{r_{01}}{r_{02}}\right|_{\omega_{n1}} = \frac{\mu k_j}{k_j(1+\mu) - \frac{k_j}{m}m} = \frac{\mu k_j}{\mu k_j} = 1 \tag{2.27}$$

$$\left.\frac{r_{01}}{r_{02}}\right|_{\omega_{n2}} = \frac{k_j \mu}{k_j(1+\mu) - (1+2\mu)\frac{k_j}{m}m} = \frac{\mu k_j}{-\mu k_j} = -1 \tag{2.28}$$

This means that for ω_{n1} the displacements will be in phase with each other, while for ω_{n2}, the displacements will be in counter-phase with each other. Thus, the two mode shapes, ϕ_1 and ϕ_2, can be expressed as

$$\phi_1 = \begin{bmatrix} 1 \\ 1 \end{bmatrix} \tag{2.29}$$

$$\phi_2 = \begin{bmatrix} 1 \\ -1 \end{bmatrix} \tag{2.30}$$

when the amplitudes are normalized such that r_{01}=1. [14]

2.4 Hydrodynamic Loading

2.4.1 Governing Equations for Potential Flow

In potential flow theory, the flow velocity $\mathbf{u}$ is described by the velocity potential Φ

$$\mathbf{u} = \nabla \boldsymbol{\Phi} \tag{2.31}$$

The fluid motion is irrotational, which mathematically can be written

$$\nabla \times \mathbf{u} = 0 \tag{2.32}$$

Additionally, the fluid is assumed to be incompressible, which mathematically can be written

$$\nabla \cdot \mathbf{u} = 0 \tag{2.33}$$

Consequently, the velocity potential Φ satisfies the Laplace equation

$$\nabla^2 \Phi = 0 \tag{2.34}$$

This equation can be solved by introducing the kinematic free-surface condition

$$\frac{\partial \zeta}{\partial t} + \frac{\partial \Phi}{\partial x}\frac{\partial \zeta}{\partial x} + \frac{\partial \Phi}{\partial y}\frac{\partial \zeta}{\partial y} - \frac{\partial \Phi}{\partial z} = 0 \qquad \text{on} \quad z = \zeta(x, y, t) \tag{2.35}$$

and the dynamic free-surface condition

$$g\zeta + \frac{\partial \Phi}{\partial t} + \frac{1}{2}\left(\left(\frac{\partial \Phi}{\partial x}\right)^2 + \left(\frac{\partial \Phi}{\partial y}\right)^2 + \left(\frac{\partial \Phi}{\partial z}\right)^2\right) = 0 \qquad \text{on} \quad z = \zeta(x, y, t) \tag{2.36}$$

These free-surface conditions (2.35) and (2.36) are non-linear, and can therefore not be implemented directly in USFOS.

2.4.2 Airy Wave Theory

In Airy wave theory, the free-surface conditions (2.35) and (2.36) are linearized, which means that the velocity potential is proportional to the wave amplitude. By a Taylor expansion the free-surface condition from the free-surface position $z = \zeta(x, y, t)$ is transferred to the mean free-surface $z = 0$. By keeping the linear terms, the new free-surface conditions becomes

$$\frac{\partial \zeta}{\partial t} = \frac{\partial \Phi}{\partial z} \qquad \text{on} \quad z = 0 \tag{2.37}$$

$$g\zeta + \frac{\partial \Phi}{\partial t} = 0 \qquad \text{on} \quad z = 0 \tag{2.38}$$

which can be combined to give

$$\frac{\partial^2 \Phi}{\partial t^2} + g\frac{\partial \Phi}{\partial z} = 0 \qquad \text{on} \quad z = 0 \tag{2.39}$$

In Airy wave theory, the velocity potential is oscillating harmonically with time, such that (2.39) can be written

$$\omega^2 \Phi + g\frac{\partial \Phi}{\partial z} = 0 \qquad \text{on} \quad z = 0 \tag{2.40}$$

The last condition that is needed to find a complete mathematically solution to the velocity potential corresponding to Airy theory, is the sea bottom condition

$$\frac{\partial \Phi}{\partial z} = 0 \qquad \text{on} \quad z = -h \tag{2.41}$$

where h is the water depth. Now, it can be shown (e.g. Newman, 1977, chapter 6) that the velocity potential for Airy theory is given by

$$\Phi = \frac{g\zeta_a}{\omega}\frac{\cosh k(z+h)}{\cosh kh}\cos(\omega t - kx) \qquad \text{(for finite water depth)} \tag{2.42}$$

$$\Phi = \frac{g\zeta_a}{\omega}e^{kz}\cos(\omega t - kx) \qquad \text{(for infinite water depth)} \tag{2.43}$$

From the velocity potential, the dynamic pressure in the fluid can be determined by [10]

$$p_{dyn} = -\rho\frac{\partial \Phi}{\partial t} = \rho g\zeta_a e^{kz}\sin(\omega t - kx) \qquad \text{(for infinite water depth)} \tag{2.44}$$

The x- and z-component of the fluid velocity can also be found directly from the velocity potential by

$$u = \frac{\partial \Phi}{\partial x} = \omega\zeta_a e^{kz}\sin(\omega t - kx) \qquad \text{(for infinite water depth)} \tag{2.45}$$

$$w = \frac{\partial \Phi}{\partial z} = \omega\zeta_a e^{kz}\cos(\omega t - kx) \qquad \text{(for infinite water depth)} \tag{2.46}$$

Finally, the x- and z-component of the acceleration are found from the corresponding velocity components

$$a_x = \frac{\partial u}{\partial t} = \omega^2\zeta_a e^{kz}\cos(\omega t - kx) \qquad \text{(for infinite water depth)} \tag{2.47}$$

$$a_z = \frac{\partial w}{\partial t} = -\omega^2\zeta_a e^{kz}\sin(\omega t - kx) \qquad \text{(for infinite water depth)} \tag{2.48}$$

Since Airy theory is based on a Taylor expansion at the mean free-surface $z = 0$, the theory is only valid for infinitesimal waves. Hence, assumptions regarding the wave kinematics have to be made when the waves have finite amplitudes. One option, which is used in this thesis, is called *extrapolated* Airy theory. This theory assumes the velocity potential to be constant from the mean free-surface and up to the free-surface level, while the "true" velocity potential is used below the mean free-surface, see Figure 5. Figure 5 shows that the hydrostatic pressure cancel the hydrodynamic pressure at the wave crest, while there is a higher order error at the wave trough.

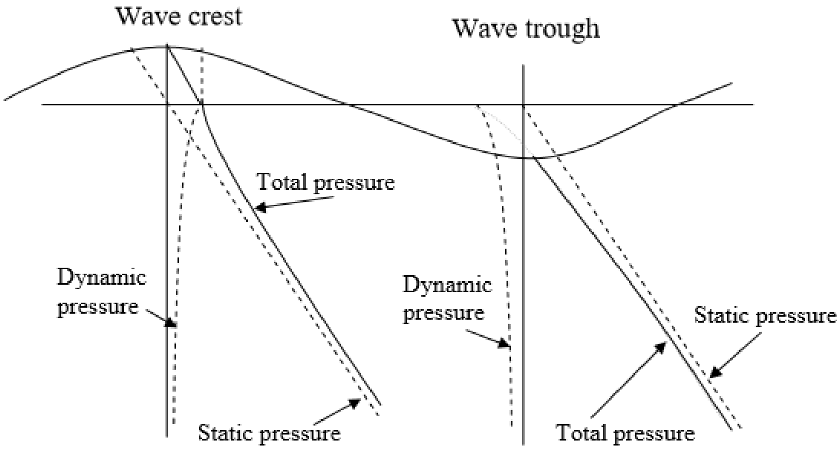

Figure 5: Hydrodynamic and hydrostatic pressure under waves with extrapolated Airy theory. The figure is taken from [1]

2.4.2.1 Stretched Airy Theory (Wheeler Stretching)

The representation of the free-surface conditions can be improved by introducing Wheeler stretching. In this thesis, Wheeler stretching was applied in the irregular wave analysis. In this method, the vertical coordinate z is replaced by the scaled coordinate z':

$$z' = (z - \eta)\frac{d}{d + \eta} \tag{2.49}$$

The Wheeler stretching method has the advantage that it has fast computation time since it is based on linear theory. However, since it is based on linear theory, it will lead to inaccurate wave kinematics due to the nonlinear free-surface condition. To get a more accurate description of the wave kinematics, higher order terms can be introduced. An example of this is Stoke's 5^{th} order theory, where the velocity potential is given as a series expansion with five terms. See the USFOS hydrodynamics manual [1] section 1.2.2.3 for further details.

2.4.3 Morison's Equation

The hydrodynamic forces in USFOS are calculated by Morison theory, which states that the wave force on a slender cylindrical element can be expressed as a linear combination of two components:

– An inertia force proportional to the acceleration of the wave particles

– A drag force proportional to the square of the velocity of the wave particles.

Mathematically, the wave force per unit length dF is given by [10]

$$dF = \left\{ \rho \frac{\pi D^2}{4} C_M a_n + \frac{1}{2} \rho C_D D u_n |u_n| \right\} ds \tag{2.50}$$

where

- ρ is the water density
- D is the diameter of the cylinder
- C_M is the inertia/mass coefficient
- C_D is the drag coefficient
- a_n is the instantaneous acceleration component normal to the pipe longitudinal axis
- u_n is the instantaneous velocity component normal to the pipe longitudinal axis

When applying Morison's equation, it is assumed that the fluid field characteristics are not affected by the presence of the structure. This implies that the equation only is valid for structures which are much smaller than the wave length, where the limit is normally given by

$$\frac{D}{\lambda} \leq 0.2 \tag{2.51}$$

For structures with larger diameter than this, Mac-Camy and Fuchs theory based on linear potential theory may be applied[4]. An inherent uncertainty when using Morison's equation is the choice of the hydrodynamic coefficients C_M and C_D. They must be determined empirically, and the main factors influencing them are: [10]

- Reynolds number $Rn = UD/\nu$
- Roughness number = K/D
- Keulegan-Carpenter number $KC = U_M T/D$
- Relative current number = U_c/U_M
- Body form
- Free-surface effects
- Sea-floor effects
- Nature of ambient flow relative to the structure's orientation
- Reduced velocity $U_R = U/(f_n D)$

[4]See USFOS Hydrodynamics [1] section 1.3.5 for further details

Since the inertia force is given by the acceleration (2.47), it has its maximum when the wave elevation is at mean water level. On the other hand, the drag force is given by the velocity (2.45), meaning that the drag force has maximum absolute values at the wave crest and wave trough. It can be shown [10] that the inertia force decays with $e^{2\pi z/\lambda}$ and the drag force decays with $e^{4\pi z/\lambda}$. This means the drag force is more concentrated near the free-surface than the inertia force.

2.4.3.1 Non-linearities from Hydrodynamic Loading

When applying Morison's equation, there are two sources to non-linearity: the quadratic drag term and integration of forces up to the true water level. The drag and inertia forces on a cylinder piercing the wave surface, subjected to extrapolated Airy waves can be shown to be [15]

$$F_D \propto u_n|u_n| \cdot H[\zeta(t)] \propto \sin(\omega t)|\sin(\omega t)| \cdot H[\sin(\omega t)] \tag{2.52}$$

and

$$F_I \propto a_n H[\zeta(t)] \propto \cos(\omega t) H[\sin(\omega t)] \tag{2.53}$$

Where H[x] is the Heaviside function, defined as

$$H[x] = \begin{cases} 0 & \text{when } x < 0 \\ \frac{1}{2} & \text{when } x = 0 \\ 1 & \text{when } x > 0 \end{cases} \tag{2.54}$$

By use of Fourier series, the periodic force components(2.52) and (2.53) can be represented as infinite series of cosines and sines. Generally, the Fourier series of a periodic function f(t) with period $2\pi/\omega$ can be written

$$f(t) = \frac{a_0}{2} + \sum_{n=1}^{\infty} a_n \cos(n\omega t) + \sum_{n=1}^{\infty} b_n \sin(n\omega t) \tag{2.55}$$

where

$$a_n = \frac{\omega}{\pi} \int_{-\pi/\omega}^{\pi/\omega} f(t) \cos(n\omega t) dt \tag{2.56}$$

$$b_n = \frac{\omega}{\pi} \int_{-\pi/\omega}^{\pi/\omega} f(t) \sin(n\omega t) dt \tag{2.57}$$

Fourier series expansion applied on the two force components (2.52) and (2.53), gives the following results

$$\begin{aligned} F_D &\propto \frac{1}{4}(1 - \cos(2\omega t)) + \frac{2}{\pi} \sum_{n=1}^{\infty} \frac{1 - (-1)^n}{(4 - n^2)n} \sin(n\omega t) \\ &= 0.25 + 0.424 \sin(\omega t) - 0.25 \cos(2\omega t) - 0.085 \sin(3\omega t) - 0.012 \sin(5\omega t) - ... \end{aligned} \tag{2.58}$$

and

$$\begin{aligned} F_I &\propto \frac{1}{2}\cos(\omega t) + \frac{1}{\pi}\sum_{n=1}^{\infty}\frac{(-1)^n - 1}{1-n^2} n\sin(n\omega t) \\ &= \frac{1}{2}\cos(\omega t) + 0.424\sin(2\omega t) + 0.170\sin(4\omega t) + 0.109\sin(6\omega t) + ... \end{aligned} \tag{2.59}$$

This shows that non-linearity creates *super-harmonic force components* with frequency at multiples of the wave frequency ω. Thus, waves of lower frequencies than the eigenfrequency may have force components with frequency equal to the eigenfrequency.

2.5 Spectral density

Since the sea surface $\zeta(t)$ is composed of random waves with random amplitude and frequency, they need to be described statistically. This is done by introducing the wave spectrum, which gives all necessary statistical information for the waves.

It is well known that the arbitrary sea surface can be broken down to a sum of harmonic wave components with different frequency, amplitude and phase angle. The energy per unit area of wave component j is given by

$$E_j = \frac{1}{2}\rho g \zeta_{aj}^2 \tag{2.60}$$

Since ρ and g are constants, $\frac{\zeta_{aj}^2}{2}$ will be a measure of the energy for wave component j. Now the wave spectrum is introduced as

$$S_\zeta(\omega_j)\Delta\omega = \frac{1}{2}\zeta_{aj}^2 \tag{2.61}$$

Which means that the area of the spectrum inside a small frequency interval $\Delta\omega$ is equal to the total energy of all the wave components inside this frequency interval. The total energy is then given by

$$\frac{E}{\rho g} = \sum_{j=1}^{N}\frac{1}{2}\zeta_{aj}^2 = \sum_{n=1}^{N} S_\zeta(\omega_j)\Delta\omega \tag{2.62}$$

We recognize the left hand side of (2.62) as the Riemann sum, and get

$$\lim_{x\to\infty}\sum_{n=1}^{N} S_\zeta(\omega_n)\Delta\omega = \int_0^\infty S_\zeta(\omega)d\omega \tag{2.63}$$

From (2.63) and (2.62), the total amount of energy is given by

$$\frac{E}{\rho g} = \sum \frac{1}{2}\zeta_{aj}^2 = \int_0^\infty S_\zeta(\omega)d\omega \tag{2.64}$$

This shows that the wave spectrum gives the distribution of energy as a function of the frequency ω. [16] A structure excited by random waves will also have a random response which can be described statistically by the response spectrum. For a SDOF system, it can be shown that the relation between the wave spectrum and the response spectrum is given by [5]

$$S_r(\omega) = |H(\omega)|^2 S_\zeta(\omega). \tag{2.65}$$

where $H(\omega)$ is the complex frequency response function.

2.5.1 Relation Between the Variance of the Wave Elevation and the Wave Spectrum

By assuming that the wave elevation is Gaussian with zero mean, the variance is given by

$$\sigma^2 = E[\zeta(t)^2] \tag{2.66}$$

The relation between the variance of the wave elevation and the wave spectrum is found by introducing the autocorrelation function $R_\zeta(\tau)$ which is defined as

$$R_\zeta(\tau) = E[\zeta(t)\zeta(t+\tau)] \tag{2.67}$$

Such that

$$R_\zeta(0) = E[\zeta(t)^2] \tag{2.68}$$

Combining (2.66) and (2.68) which gives

$$\sigma^2 = R_\zeta(0) \tag{2.69}$$

It can be shown [17] that the autocorrelation function is related to the spectrum by the inverse Fourier transform

$$R_\zeta(\tau) = \int_{-\infty}^{\infty} S_\zeta(\omega) e^{i\omega\tau} d\omega \tag{2.70}$$

Such that

$$R_\zeta(0) = \int_{-\infty}^{\infty} S_\zeta(\omega) d\omega \tag{2.71}$$

Now, substituting (2.71) into (2.69) gives

$$\sigma^2 = \int_{-\infty}^{\infty} S_\zeta(\omega) d\omega \tag{2.72}$$

This shows that the variance is equal to the area under the graph of the wave spectrum $S_\zeta(\omega)$ against ω. [17]

[5] See, for instance, Newland [17] p. 71-72

2.5.2 Mean Square Response

The relation between the variance and the spectrum derived in Section 2.5.1 does only apply to Gaussian processes with zero mean. It was shown in Section 2.4.3.1 that the mean drag force due to waves with zero mean is not equal to zero, and the relation in (2.72) can therefore not be used for the response spectrum $S_r(\omega)$. However, (2.68) and (2.71) can be combined and applied for the response spectrum, which gives

$$E[r(t)^2] = \int_{-\infty}^{\infty} S_r(\omega)d\omega \tag{2.73}$$

where $E[r(t)^2]$ is denoted as the *mean square response* and will be used as to a measurement of the responses in the result part.

2.6 Quasi-static vs. Dynamically Behaving Jackets

When a structure is subjected to oscillating loads with periods well above the highest eigenperiod of the structure, it may be considered as a quasi-static structure. For quasi-static structures the mass term and the damping term in (2.1) can be neglected, and the equation of motion becomes

$$r(t) = \frac{F(t)}{k} \tag{2.74}$$

which is way less demanding to solve than the full dynamic equation of motion (2.1). As a rule of thumb, structures exposed to wave forces can be considered quasi-static if the largest natural period is lower than 2-3 s [18]. For jacket structures, the stiffness will generally decrease with the water depth. Consequently, the natural period will increase with the water depth, and jackets can typically be considered as quasi-static for water depths up to around 150 m, depending on the design.

3 Method

This chapter describes the different models analyzed in this thesis, including their physical properties and assumptions made. The assumptions made for the input to the USFOS simulations are presented, together with related theory. In the result part, the key response data will be compared with respect to:

- Mean square response
- Fatigue damage
- Extreme long term response

What is meant by these three terms, and how they are found, is presented in the end of this method chapter.

3.1 Simplified Model

The same simplified model that was used in the Matlab program in the specialization project, has been studied by use of USFOS. This was done to verify the results in the specialization project. Figure 6 shows a sketch of the simplified model for two connected jackets, while Figure 7 shows how the model appears in USFOS. It is emphasized that the stiffnesses k_j act in the horizontal direction, as shown in Figure 4.

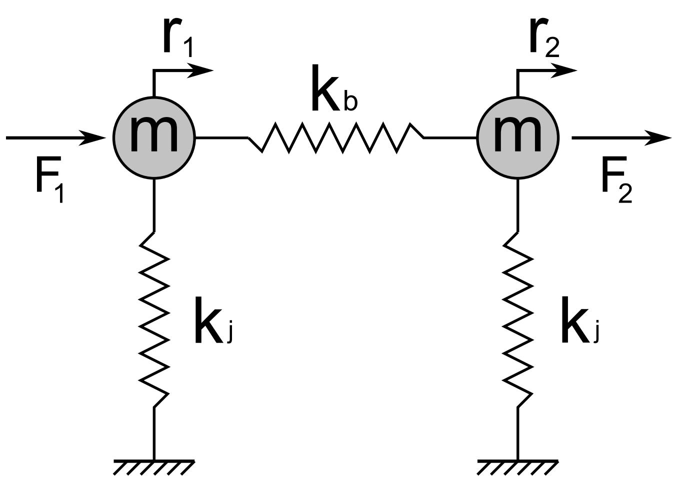

Figure 6: A sketch of the simplified model for two connected jackets

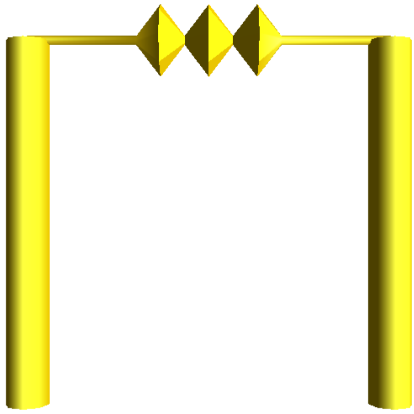

Figure 7: Simplified model in USFOS representing two connected jackets

The assumptions/simplifications made are:

- The jackets and the bridges are identical to each other.
- The bridges are massless springs with stiffness k_b.
- The mass of the jackets are concentrated in the decks and equal to $m_j = 15\,000$ t.
- Rayleigh-damping is assumed, which means that the damping matrix $\mathbf{C}$ is expressed as a linear combination of the mass matrix $\mathbf{M}$ and the stiffness matrix $\mathbf{K}$: [9]

$$\mathbf{C} = \alpha_1 \mathbf{M} + \alpha_2 \mathbf{K} \tag{3.1}$$

  with $\alpha_1 = \alpha_2 = 0.01$.

- The jackets are modelled as cylindrical cantilever beams, such that the deflection in the deck can be expressed as a linear spring with stiffness k_j, see Figure 8. To ensure linearity, the displacements are kept small by scaling the applied force.
- The height of the cylinders were set to be $H_{cyl} = 100$ m. The diameter and the wall-thickness were tuned in order to give the same eigenperiod as was used in the specialization project, $T_{nj} = 2.0$ s. The tuned dimensions used for the cylinders are given in Table 1.

Height, H_{cyl}	100 m
Diameter, D	12 m
Thickness, t	0.39 m

Table 1: Dimensions of the cylinders, giving eigenperiod in sway equal to $T_{n1} = 2.0$ s

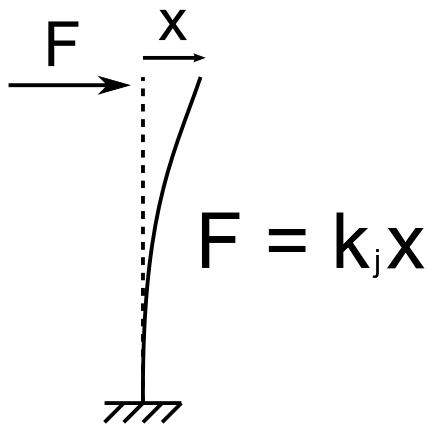

Figure 8: Jackets modelled as a cantilever beam

- The bridge stiffness was set to be half of the jacket stiffness: $\mu = \frac{k_b}{k_j} = \frac{1}{2}$.
- The jacket stiffness was calculated from the eigenperiod by

$$k_j = m_j \omega_{nj}^2 = m_j \left(\frac{2\pi}{T_{nj}} \right)^2 = 15 \times 10^6 kg \left(\frac{2\pi}{2s} \right)^2 = 148.04 \times 10^6 N/m \tag{3.2}$$

This stiffness was verified by applying a point load $F = 148.04 \times 10^6 N$ to the top node of one single cylinder, see Figure 9.

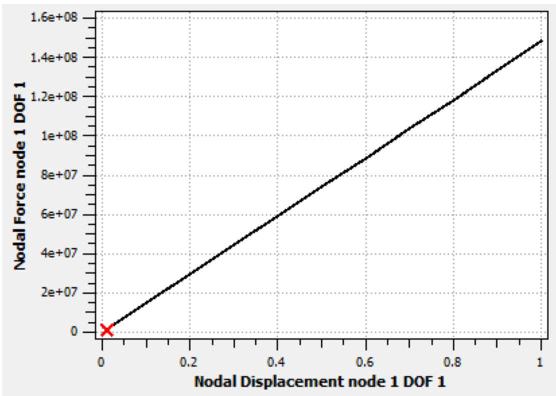

Figure 9: Verification of the calculated bridge stiffness

3.1.1 Simplified Model Subjected to Wave Loads

The simplified model has also been subjected to wave loads. In this case, the model was placed at a water depth of $h = 80$ m, and needs to move away water when accelerating. This leads to an added mass which depends on the mass coefficient C_M in Morison's equation. The added mass increases the eigenperiods, but not sufficient to be in the range of the lowest wave periods applied to the model. To be able to include the eigenfrequencies in the frequency plots (see Section 3.4) the eigenperiods were increased by increasing the topside mass, and reducing the jacket stiffness by decreasing the diameter of the cylinder. The updated data for the simplified model subjected to wave loads are found in table 2.

Height, H_{cyl}	100 m
Diameter, D	10 m
Thickness, t	0.5 m
Stiffness, k_j	106.06×10^6 N/m
Topside mass, m_j	20 000 t

Table 2: Updated data for the simplified model subjected to wave loads

3.2 Jacket Model

The jacket model consists of two equal jacket platforms connected by a linear spring, see Figure 10. The FE-model of the jackets is the DS jacket taken from the appendix of the PhD thesis of Katrine van Raaij [19]. The water depth is $h = 80$ m. The topside is modelled as a pyramid, with topside weight 11 000 t given as node mass in the uppermost node. When the jacket model is subjected to irregular waves, the distance between them is set to be $L_{jacket} = 80$ m. The beams in the top pyramid were set to have E-module and yield stress 1000 times the other beams of the jacket. In this way, they can transfer the force from the self-weight of the topside and the force transmitted from the spring down to the jacket.

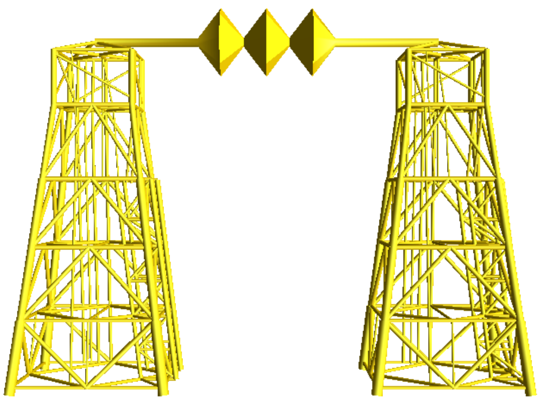

Figure 10: Jacket model used in USFOS

3.2.1 Jacket Stiffness in Sway

The jacket stiffness in sway is found by applying a point load to the uppermost node. Figure 11 shows that the stiffness is linear until a displacement of 0.22 m, where one the braces starts to yield. To ensure linearity, the maximum displacement in all the simulations done in this report has been kept lower than 0.22 m. From Figure 11, the stiffness is found to be $k_j = 182.65 \times 10^6$ N/m.

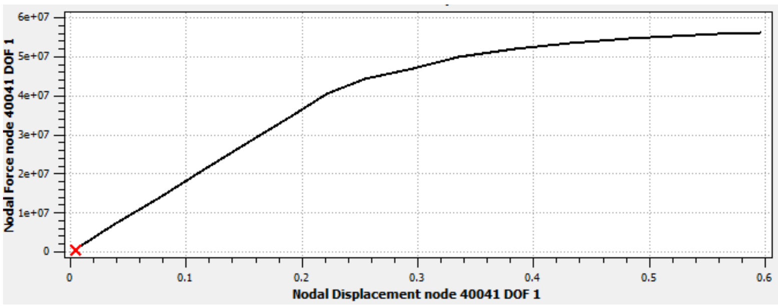

Figure 11: Applied force as function of displacement. The jacket stiffness k_j was found from the slope of the linear part

3.2.2 Damping

In the jacket model, the damping is given by the damping ratio ξ at two frequencies, rather than the two damping coefficients α_1 and α_2 connected to Rayleigh damping. This was chosen to get a more intuitive input value of the magnitude of the damping. The damping ratio is given by

$$\xi = \frac{c}{c_{cr}} = \frac{c}{2m\omega_0} \tag{3.3}$$

where c_{cr} is the critical damping, which is a characteristic measure of the structure. The equivalent modal damping ratio for a MDOF system is given by

$$\xi_i = \frac{\bar{c_i}}{2\bar{m_i}\omega_{0i}} \tag{3.4}$$

Now, the relation between Rayleigh damping and the damping ratio can be found. The modal damping coefficients from Rayleigh damping are given by

$$\bar{c_i} = \alpha_1\bar{m_i} + \alpha_2\bar{k_i} = \bar{m_i}(\alpha_1 + \omega_{0i}^2\alpha_2) \tag{3.5}$$

Substituting (3.5) into (3.4)

$$\xi_i = \frac{1}{2}(\frac{\alpha_1}{\omega_{0i}} + \alpha_2\omega_{0i}) \tag{3.6}$$

When knowing the damping ratio for two frequencies in the domain of interest, α_1 and α_2 are found by

$$\alpha_1 = \frac{2\omega_1\omega_2}{\omega_2^2 - \omega_1^2}(\xi_1\omega_2 - \xi_2\omega_1) \tag{3.7}$$

$$\alpha_2 = \frac{2(\omega_2\xi_2 - \omega_1\xi_1)}{\omega_2^2 - \omega_1^2} \tag{3.8}$$

By substituting α_1 and α_2 into (3.6), the damping ratio can be given as function of eigenfrequency. Figure 12 shows an example of this with the values given in Table 3. These values are used to describe the damping of the jacket model used in this thesis. It is observed that the damping ratio becomes asymptotically proportional to $\frac{1}{2}\alpha_2\omega_i$ for large frequencies and increases quickly towards infinity for frequencies lower than ω_1.

Specified frequency	Damping ratio ξ
$2\pi/15s$	0.02
$2\pi/1.5s$	0.02

Table 3: Damping ratio specified at two frequencies, used to describe the damping of the jacket model

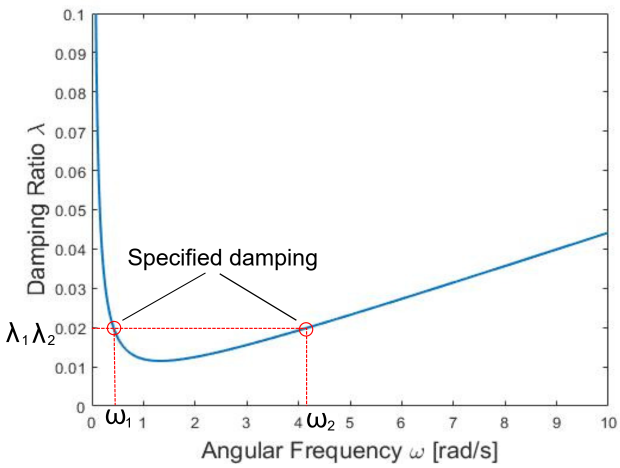

Figure 12: Damping ratio as function of eigenfrequency with $\omega_1 = \pi$, $\omega_2 = \pi/5$, $\xi_1 = 0.1$ and $\xi_2 = 0.1$

3.3 Structural Configurations of the Bridge

Figure 13 shows the bridge connecting the two Draupner platforms. In this report the FE-model of the Drapner S platform (the one in the front) is used on both sides of the bridge. The exact structural configurations of the bridge have not been provided. Hence, several assumptions to the structural configurations have been made. The weight of the bridge was set to be m_{bridge}=430 tons, and the length L_{bridge}=80 m. The bridge is pinned to one of the jackets, and is allowed to move with a friction pad at the other jacket, see Figure 14. The processing piping are connected directly to the top sides, and are therefore assumed to be fixed at both ends.

Figure 13: The bridge connecting the Draupner platforms. The picture is taken from the photo library on www.equinor.com

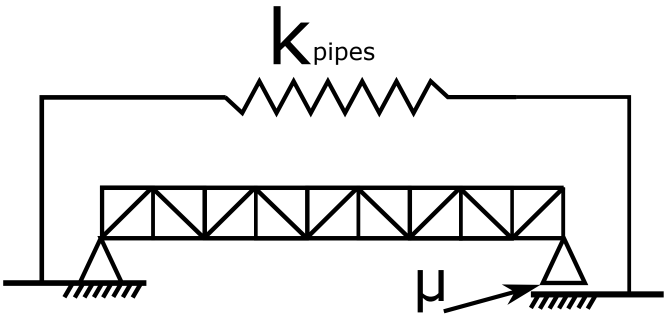

Figure 14: Schematic drawing of the bridge

Hence, the two main mechanisms from the bridge that restrict the two jackets from moving relative to each other are: stiffness from the piping and the friction force from the sliding support. To get a vague idea of the magnitudes of these two contributions, rough estimates are presented in the result part, while the parameters/dimensions used are presented in the following.

3.3.1 Friction Force

The static friction coefficient μ_{stat} at the sliding support is assumed to be $\mu_{stat} = 0.1$. This assumption is based upon the catalogue of bearings provided by the company Oiles [20], which has delivered bearings to bridges in the North Sea.[6]

[6]Due to Ole Gabrielsen, DNV GL

3.3.2 Stiffness from Piping with Expansion Loops

The stiffness contribution from the pipes is estimated by several analyses in GeniE, with representative dimensions of the pipes. The stiffness of each pipe is given by the reaction force due to a prescribed displacement. All of the pipes are assumed to follow the shape shown in Figure 15. The loop shown is an expansion loop which lower the stiffness.

Figure 15: Shape of the piping used in GeniE analyses

Table 4 shows different pipe dimensions that were considered, together with the number of each pipe. When the dimensions were chosen, it was ensured that the pipes can

Diameter [m]	Thickness [m]	# Pipes
1.0	0.012	2
0.5	0.006	4
0.2	0.003	10

Table 4: Pipe dimensions and the number of each dimension used in the estimation of total stiffness from piping

withstand an internal pressure of 5 MPa. In the FE-model used in this thesis, the bridge was modelled as a linear massless spring. Hence, the static friction from the sliding support was neglected.

3.4 Plot in the Frequency Domain

In USFOS, finite element analysis is used to simulate response in the time domain, see Figure 16.

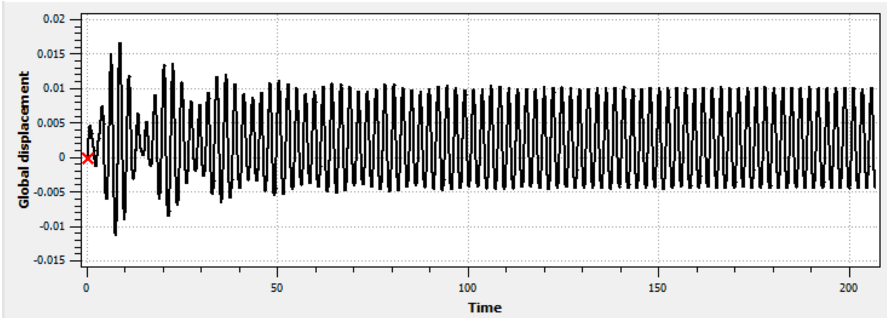

Figure 16: Time series of displacement due to a harmonic load

The solution to a nonhomogeneous differential equation consists of two parts, a homogeneous and a particular part. The homogeneous part is transient and dies out with time, while the particular solution continues to oscillate with the excitation frequency. It is the response from the particular solution that is of interest in this thesis, and it is therefore important to do the time series until the homogeneous solution has died out. In Figure 16, it is seen that the homogeneous solution has died out after about 100 s. The maximum absolute value of the response amplitude is found by DynMax, which is a built-in utility in USFOS. Each time series is excited by an excitation with a given frequency. Hence, several time series are needed to represent the behavior in the frequency domain. To do this effectively, scripting techniques were used to automatically call the USFOS simulations with different parameters. The desired responses are written to a file together with their corresponding excitation frequency. In this way, plots of the response amplitude as function of frequency can be made in a program like Excel. Since the responses are calculated in the time domain, the frequency plots may include higher order peaks.

3.5 Application of Loads

3.5.1 Concentrated Harmonic Excitation

Concentrated harmonic excitation is applied on the top nodes of the jackets. Each harmonic excitation is connected to a time series in USFOS, and the phase lags are given by varying the start time of the time series. E.g., consider a system of two jackets subjected to harmonic excitation with period 6 s, a start time of 3 s for the second jacket will then give a phase lag equal to $\beta_2 = \pi$.

3.5.2 Wave Loads

The relative velocity between the structure and the wave particles has not been accounted for in the calculations of drag forces. When the system is subjected to regular wave loads, the phase lag is adjusted by varying the distance between the jackets. E.g., a distance of half a wave length corresponds to a phase lag of $\beta_2 = \pi$. For high frequencies, the wave length λ might be lower than the width of the jacket. To overcome this, a number k of wavelengths can be added to the distance between the jackets. In Figure 17b, one additional wave length is added to the distance, such that the distance is 1.5λ. The distance L_π between the jackets to obtain a phase lag of $\beta_2 = \pi$ is generally given by

$$L_\pi = \left(\frac{1}{2} + k\right)\lambda, \qquad k = 0, 1, 2... \tag{3.9}$$

where a suitable value of k is selected based on the wave frequency. Similarly, for a phase lag of $\beta_2 = \pi/2$, the distance between the jackets is given by

$$L_{\pi/2} = \left(\frac{1}{4} + k\right)\lambda, \qquad k = 0, 1, 2... \tag{3.10}$$

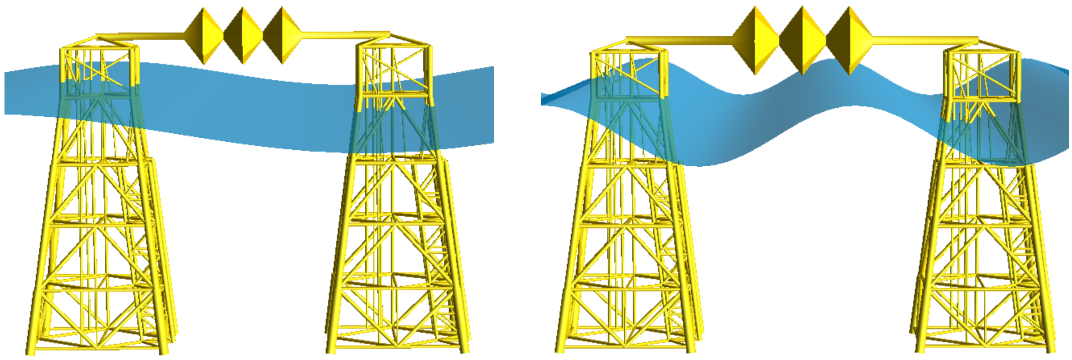

(a) Distance between jackets given by $L_\pi = \frac{1}{2}\lambda$ **(b)** Distance between jackets given by $L_\pi = \frac{3}{2}\lambda$

Figure 17: Phase lag $\beta_2 = \pi$ for two different wave frequencies

The wave length is calculated from the wave period T according to the USFOS hydrodynamics theory manual [1]

$$\lambda = \begin{cases} \frac{g}{2\pi}T^2 & \text{if } T < T_{lim} \\ 2d\left(2\frac{T}{T_{lim}} - 1\right) & \text{if } T < T_{lim} \end{cases} \tag{3.11}$$

where

$$T_{lim} = \sqrt{\frac{2d}{g/2\pi}} = 10.12 \text{ [s]} \tag{3.12}$$

3.5.2.1 Irregular Waves

For analyses where dynamic effects and/or nonlinear effects are significant, irregular wave analysis in the time domain represents the reality in the best way. As explained in Section 2.5, a sea state can be described statistically by an appropriate wave spectrum.

The wave spectrum gives all the necessary statistical information for the waves. The JONSWAP spectrum is widely used in the North Sea, and was therefore chosen as an appropriate spectrum for this work. In USFOS, the spectrum is described by the spectral peak period T_p and the significant wave height H_s [1]

$$\begin{aligned} S_\varsigma(\omega) &= \upsilon \frac{g^2}{\omega^5} \exp\left[-\frac{5}{4}\left(\frac{\omega_p}{\omega}\right)\right]\gamma^r, \\ r &= \exp\left[-\frac{1}{2}(\frac{\omega-\omega_p}{\sigma\omega_p})^2\right] \end{aligned} \tag{3.13}$$

where ω_p is the peak frequency, and given by

$$\omega_p = \frac{2\pi}{T_p} \tag{3.14}$$

γ is the peak enhancement factor. The higher γ the more energy is concentrated near the peak frequency ω_p. γ is given by

$$\begin{aligned} \gamma &= \exp\left[3.483\left(1-\frac{0.1975\delta T_p^4}{H_s^2}\right)\right], \\ \delta &= 0.036 - \frac{0.0056T_p}{\sqrt{H_s}} \end{aligned} \tag{3.15}$$

υ determines the shape of the spectrum for high frequencies, and is given by

$$\upsilon = 5.061(1-0.2871\log\gamma)\frac{H_s^2}{T_p^4} \tag{3.16}$$

and σ describes the spectrum width, and is given by

$$\sigma = \begin{cases} \sigma_a = 0.07 & \text{for } \omega \le \omega_p \\ \sigma_b = 0.09 & \text{for } \omega > \omega_p \end{cases} \tag{3.17}$$

The JONSWAP spectrum should only be used for combinations of H_s and T_p that satisfies the following requirement [16]

$$3.6\sqrt{H_s} \le T_p \le 5\sqrt{H_s} \tag{3.18}$$

Based on this, the following two sea states have been used in this thesis: The sea states have a duration of three hours, which is a standard period for sea states [11]. Within these three hours the sea sate is assumed to be a stationary random process. For the first sea state, the waves have almost no energy, however this sea state was chosen to

Sea State no.	T_p [s]	H_s [m]
1	6	2
2	10	5
3	15	10
4	16.3	14.9

Table 5: Sea states used in this thesis

see if the system behaves more dynamically for a low peak period. For the second and the third sea state, the peak period increases, and the system should therefore behave less dynamically. The fourth sea state is the 10^{-2} annual probability sea state, which is applied in the extreme response analysis, see Section 3.6.3. Figure 18 shows the JONSWAP spectrum for $H_s = 5$ m and $T_p = 10$ s.

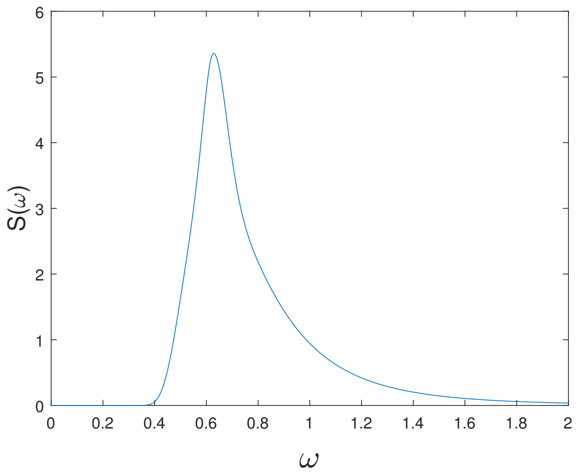

Figure 18: JONSWAP spectrum for $H_s = 5$ m and $T_p = 10$ s

The surface elevation is described as a sum of many harmonic waves with a given amplitude ζ_{Aj}, angular frequency ω_j and a random phase angle θ_j. The surface elevation at a particular location (x=0) is then given by

$$\zeta(t) = \sum_{j=1}^{m} \zeta_{Aj} \cos(\omega_j t + \theta_j) \tag{3.19}$$

where the random phase angle θ_j is uniformly distributed between 0 and 2π. From the definition of the wave spectrum in Section 2.5, the amplitude of each wave component can be determined by

$$\zeta_{Aj} = \sqrt{2 \int_{\omega_{l,j}}^{\omega_{u,j}} S_\zeta(\omega) d\omega} \tag{3.20}$$

where $\omega_{l,j}$ and $\omega_{u,j}$ are the lower and upper frequency limits for wave component j. There are several options in USFOS on how to discretize the wave components.

In this work, the range of frequencies is divided into N=120 intervals of equal length, $\Delta\omega = \frac{\omega_u - \omega_l}{N}$. The upper and lower limits for angular frequencies in the wave spectrum are chosen to be $\omega_u = \frac{2\pi}{2}$ and $\omega_l = \frac{2\pi}{20}$, respectively. The built-in dicretization option in USFOS uses the midpoint in each interval as the frequency from where corresponding amplitudes in the JONSWAP spectrum is given. In this way, the intervals between these points will also be constant and equal to $\Delta\omega$ and the time series will repeat itself after an amount of time. To avoid this, the frequencies are selected randomly within each interval. See Matlab script in Appendix C.3.

3.6 Key Response Data from Irregular Wave Analysis

To investigate the influence from the bridge on the system, a sensitivity study has been performed for various bridge stiffnesses. This has been done for both quasi-static and dynamic analysis, to investigate to what extent the system is affected by dynamics. The following responses have been studied:

- Horizontal displacement in deck
- Force in diagonal brace (part of K-stiffener) located between elevation 40 m and 21 m below mean free surface

These responses are given as time series in USFOS. Two Matlab scripts have been made for post-processing of the data from the time series into different comparable quantities/magnitudes of the responses, see Appendix C.1 and C.2. How the responses were quantified will be described in the following subsections. The program Dynres was used to extract the data from USFOS to a .txt-file, which was used as input in the Matlab program.

3.6.1 Mean Square Response $E[r(t)^2]$

Equation (2.73) shows that the mean square response is equal to the area under the response spectrum. Responses from different configurations of the analysis, have been compared in terms of their mean square response. The mean square responses were calculated both directly from the time series, and from the area under the response spectrum. Both of the methods gave the same results, which verifies the Matlab program that calculates the response spectrum from the time series, see Appendix C.1.

3.6.2 Fatigue Damage C

The fatigue damage can be studied from the force in the selected brace by the following procedure:

1. The beam stress was calculated from the beam force divided by the cross section area. A stress concentration factor has not been included since it is the relative fatigue damage that is of importance in this study.
2. The irregular beam stress was "counted" by use of rainflow counting algorithm[7].
3. A histogram was made to express the stress distribution, see Figure 19. The histogram consists of 30 bars[8], meaning that the stress ranges from the rainflow-counting are ordered into 30 intervals. The height of bar number i, is the number of cycles n_i with stress range within the limits of the bar.
4. For the stress range corresponding to the centre of each of the bars, $\Delta\sigma_i$, the number of cycles to failure N_i is calculated from the S-N curve given by[9]

$$\log N_i = 16.13 - 5\Delta\sigma_i \tag{3.21}$$

   where σ_i is the stress range

5. The fatigue damage C is determined by

$$C = \sum_{i}^{n} \frac{n_i}{N_i} \tag{3.22}$$

3.6.3 Extreme Response Analysis

Extreme response analysis was performed for all of the three key responses by the following procedure: [18]

1. The worst sea state along a 10^{-2} annual probability contour line is found. In [23], a sea-state with T_p=16.3 s and H_s=14.9 m was identified to be appropriate. To limit the work, this sea-state was used for the extreme response analysis in this report.
2. The extreme response from 20 3-hour simulations with different seeds were found. The extremes were ordered in an increasing order $\{x_1 \leq x_2 \leq ... \leq x_i \leq ... \leq x_n\}$, and the sample distribution was found by

$$F_i^\star = \frac{i}{20+1} \tag{3.23}$$

[7]See, for instance, Schijve [21] p. 273-275 for detail regarding rainflow counting

[8]The number of bars should be at least 20 to ensure reasonably numerical accuracy [22]

[9]S-N curve for tubular joints from DNV GL - RP-C203 p.25 [22]

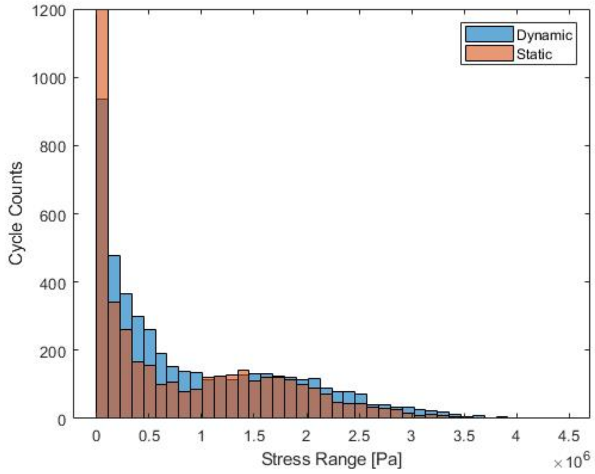

Figure 19: An example of a histogram that shows the stress distribution for the selected brace, for both quasi-static and dynamic analysis

3. The Gumbel distribution is assumed to be an appropriate model for the long term extreme value, and is given by

$$F_X(x) = \exp\left[-\exp\left(-\frac{x-\alpha}{\beta}\right)\right] \tag{3.24}$$

4. The sample distribution is plotted in a Gumbel probability paper, with coordinate system that has x_i on the horizontal axis and $y_i = -ln[-ln(F_i^{\star})]$ on the vertical axis. If the data plotted in the probability paper seem to lie more or less along a straight line, the Gumbel distribution may be a good model.

5. A straight line $y = ax + b$ is fitted by use of linear regression. The parameters α and β are found from the regression line by

$$\beta = \frac{1}{a} \tag{3.25}$$

$$\alpha = -\beta \cdot b = -\frac{b}{a} \tag{3.26}$$

6. The 90-percentile is assumed to be a good estimate for the 100 year extreme response. The 100 year extreme response is then found by

$$r_{100} = \alpha - \beta \ln(-\ln(0.9)) \tag{3.27}$$

3.6.3.1 Equivalent Dynamic Amplification Factors, EDAFs

EDAFs are defined as the q-probable dynamic response divided by the q-probable quasi-static response: [23]

$$EDAF = \frac{r_{q,d}}{r_{q,s}} \tag{3.28}$$

This means that the dynamic q-probability response can be estimated from the quasi-static q-probable response by multiplying the quasi-static q-probable response with the EDAF. In this way, EDAFs can be used to estimate ALS and ULS of the platform by performing quasi-static analysis, which requires less computer time than dynamic analysis.

4 Results and Discussion

Before presenting the results, different magnitudes/parameters that are used as inputs and outputs for the results are clarified, such that there will be no doubt about which physical properties they represent:

- Displacement response, r_0 [m]: The amplitude of the horizontal response at the topside of the first jacket.
- Phase lag, β_j [rad]: The phase lag of the excitation acting on jacket j due to the excitation acting on jacket 1. For simplicity, the values of β given in the results are written without the unit [rad].
- Stiffness ratio, μ [-]: The ratio between the bridge stiffness and the jacket stiffness, i.e. $\mu = \frac{k_b}{k_j}$.
- Excitation frequency/wave frequency, ω [rad/s]: When the harmonic excitation is given by concentrated nodal loads, ω refers to *excitation frequency*. When the load is given by wave loads, ω refers to *wave frequency*. For simplicity, the values of ω given in the results are written without the unit [rad/s].

4.1 Simplified Model Subjected to Concentrated Harmonic Excitation

The simplified model described in Section 3.1 has been subjected to concentrated harmonic excitation acting on the top nodes of the jackets. The stiffness of the jackets k_j was scaled to give the eigenperiod in sway equal to $T_{n,j} = 2.0$ s, which is same eigenperiod as used in the specialization project. Figure 20 compares results from the Matlab program made in specialization project with results from USFOS. Both of the plots are given for a system with two jackets, phase lag $\beta_2 = \pi/2$ and stiffness ratio $\mu = 0.5$. The USFOS plot is made in Excel where each of the dots in Figure 20b corresponds to a simulation in USFOS. The dots are combined with smoothed lines made by Excel. Figure 20 shows that USFOS and the Matlab program give nearly identical results. Figure 21 shows that this is also valid for a system with three jackets.

4.2 Simplified Model Subjected to Extrapolated Airy Waves

The same simplified model is now subjected to extrapolated Airy waves. The water depth is set to be $d = 80$ m and the jackets are 100 m tall. The bridge stiffness is kept constant to $\mu = 0.5$. Wave forces are calculated in USFOS by Morison's equation (2.50). The drag term and the inertia term of this equation have been studied individually by varying the hydrodynamic coefficients C_M and C_D. It was also considered to study the effect of integrating up to true wave height by doing simulations for small and large wave heights (0.1 m and 15 m), but this didn't show any difference other than scaling

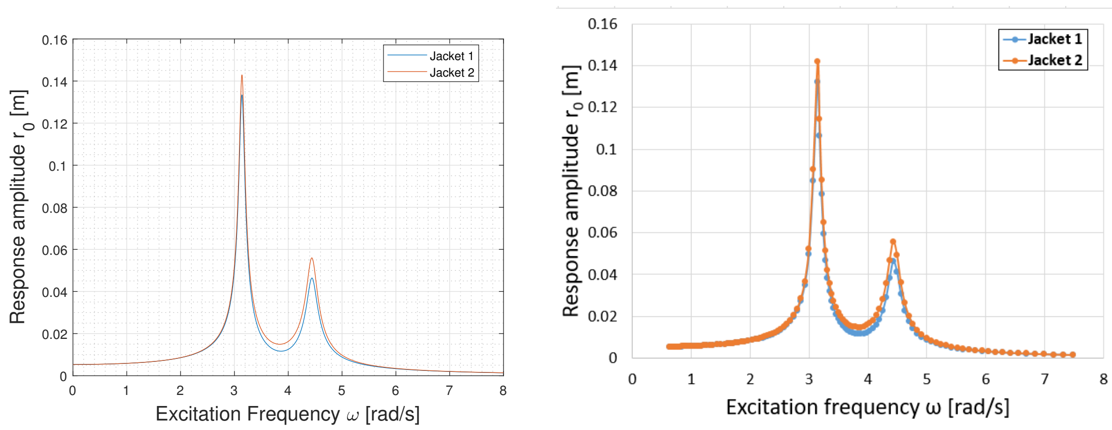

(a) From Matlab program

(b) From USFOS

Figure 20: Response amplitude as function of excitation frequency for a system with two jackets, phase lag $\beta_2 = \pi/2$ and stiffness ratio $\mu = 0.5$

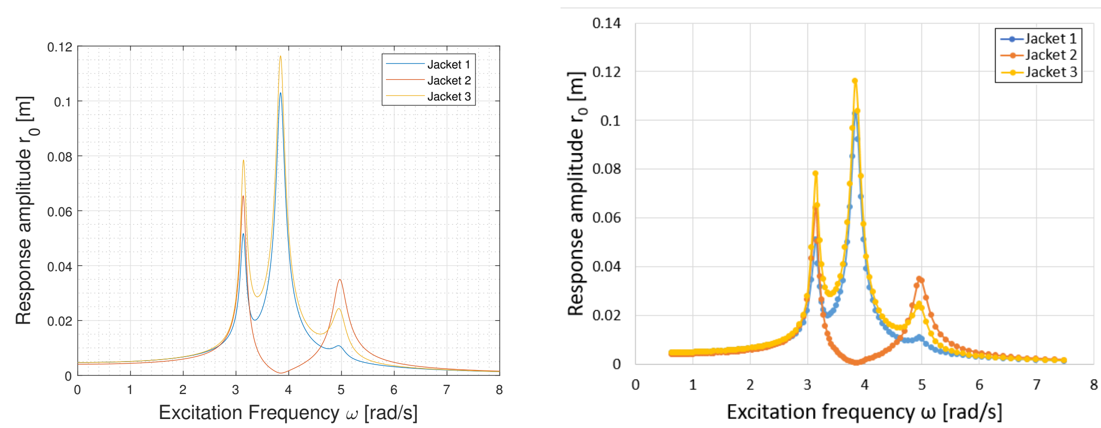

(a) From Matlab program

(b) From USFOS

Figure 21: Response amplitude as function of excitation frequency for a system with three jackets, $\mu = 0.5$ and phase lags $\beta_2 = \pi/2$ and $\beta_3 = \pi$

the values of the results. Thus, a wave height of 10 m was chosen to be used in the simulations of the simplified model. As explained in Section 2.4.3, the non-linear nature of the wave load gives harmonic excitations at multiples of the wave frequency. In the following section, these super-harmonic force components are investigated and compared with the analytic expressions (2.58) and (2.59).

4.2.1 Super-Harmonic Force Components

Figure 22 shows a time series of the total force from extrapolated Airy waves with period T = 5 s acting on a single pipe piercing the sea surface. The forces are calculated by

Morison's equation with only the inertia term present. By use of fast Fourier transform in Matlab[10], the time series was transformed into the frequency domain, as seen in Figure 23.

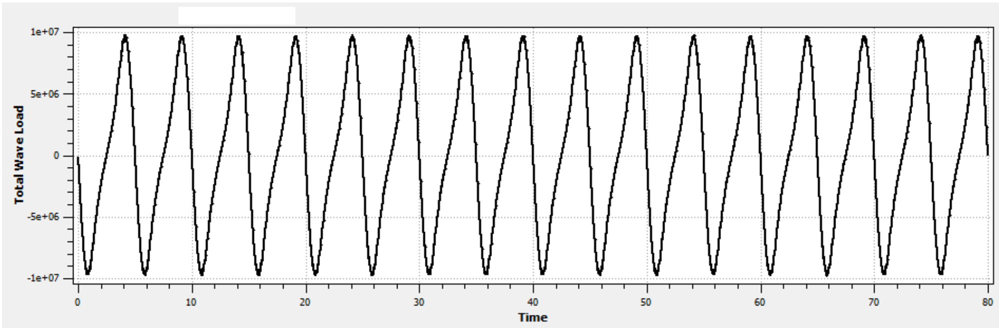

Figure 22: Time series of total wave load on a pipe piercing the sea surface. The load is calculated by Morison's equation (2.50) with only the inertia term present

The highest peak in Figure 23, at frequency $f = 0.2$ Hz, corresponds to the wave period $T = 5$ s. This means that most of the wave force acts with the wave frequency $f_{wave} = 0.2$ Hz. The two peaks at $2f_{wave}$ and $3f_{wave}$ are explained by the super-harmonic force components, see Section 2.4.3.1. However, the analytic expression for the force components due to inertia loading, (2.59), does not include a force component at $3f_{wave}$. Additionally, in the analytic expression the force component with frequency $2f_{wave}$ is almost as high as the force component with frequency f_{wave}, while in Figure 23 the force component with frequency f_{wave} is governing. This shows that (2.59) is not valid for calculating the super-harmonic force components from inertia loads given by USFOS.

Figure 24 shows the force components when only the drag term is present. It is observed that the super-harmonic forces are more important for drag-dominated systems than for inertia-dominated systems. This is due to the squared velocity term in the drag term of Morison's equation. The peak at $\omega = 0$ is related to the constant positive force term from drag forces, see (2.58). By comparing Figure 24 with the analytic expression for the force components due to drag loading (2.58), it is seen that (2.58) is not valid for calculating the super-harmonic force components from drag loads given by USFOS.

4.2.2 Inertia dominated system, $C_M = 2$ and $C_D = 0$

4.2.2.1 Phase lag equal to $\beta_2 = \pi$

When the distance between the jackets gives a phase lag of $\beta_2 = \pi$, the wave forces on the two jackets act in counter-phase with each other. This corresponds to the second eigenmode ϕ_2, see (2.30). Figure 25 shows a high peak at $\omega = 3.1$ which corresponds to

[10] See Appendix C.1

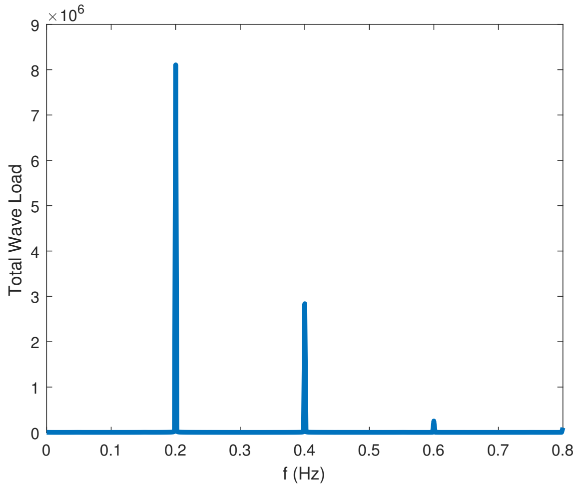

Figure 23: Force components with only the inertia term C_M present

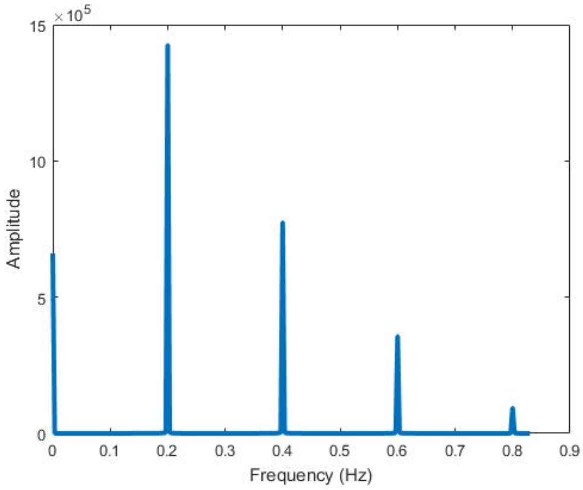

Figure 24: Force components with only the drag term C_D present

the second eigenfrequency ω_{n2}. There is no peak at the first eigenfrequency $\omega_{n1} = 2.2$ since the system is excited with the second eigenmode ϕ_2. However, there is a smaller peak at $\omega = 1.1$ which is half of the first eigenfrequency. This is explained by the first super-harmonic force component with frequency 2ω. Hence, this frequency coincides with the first eigenfrequency when the wave frequency is $\omega = \omega_{n1}/2$. On the other hand, there is no peak at half of the second eigenfrequency.

Figure 26 is given to explain that the super-harmonic force component with frequency 2ω gives a peak at $\omega_{n1}/2$ not at $\omega_{n2}/2$, although the system is excited with the second eigenmode ϕ_2. The blue line represents force acting with the wave frequency ω and the red line represents the force component acting with double the wave frequency 2ω. It

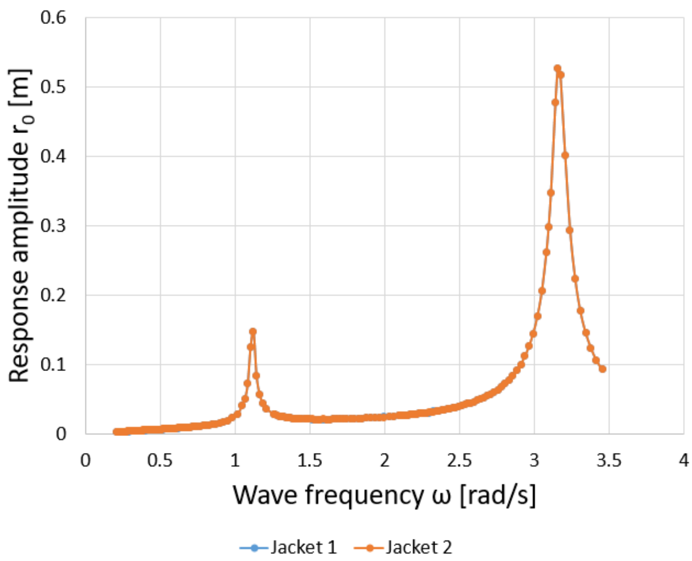

Figure 25: Response amplitude as function of wave frequency for a inertia dominated system with phase lag $\beta_2 = \pi$ and stiffness ratio $\mu = 0.5$

is seen that the excitation from the red line has maximum at both of the jackets, while the blue line has maximum and minimum at the two jackets (counter-phase). Thus, the excitation from the blue line excites the system with the second mode shape ϕ_2, while the excitation from the red line excites the system with the first mode shape ϕ_1.

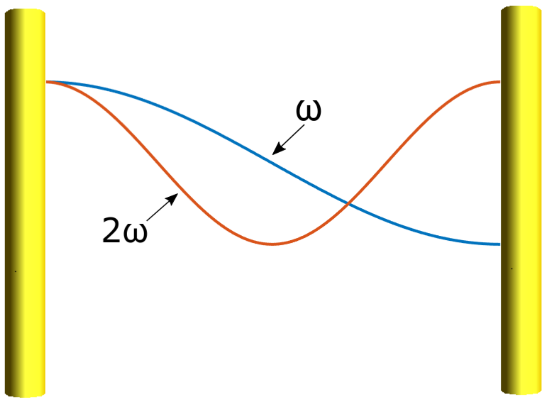

Figure 26: The two first force components for a system with phase lag $\beta_2 = \pi$. The blue line represents force acting with the wave frequency and the red line represents the force acting with double the wave frequency

4.2.2.2 Phase lag equal to $\beta_2 = \pi/2$

In Figure 27 the phase lag is $\beta_2 = \pi/2$. This phase lag lies in between the two eigenmodes, and there is therefore a peak present at both the two eigenfrequencies, ω_{n1} and ω_{n1}. The smaller peak at $\omega = 1.54$ corresponds to half of the second eigenfrequency. It is observed that there is no peak at half of the first eigenfrequency. This result can be explained by looking at Figure 28. The blue curve represents the force component acting with the the wave frequency ω while the red line is the force component with frequency equal to double the wave frequency, 2ω. It is seen that the forces from the red line act in counter-phase with each other, meaning that they excite the system with the second mode shape ϕ_2. Thus, the red line does only give a peak at $\omega_{n2}/2$, and not at $\omega_{n1}/2$.

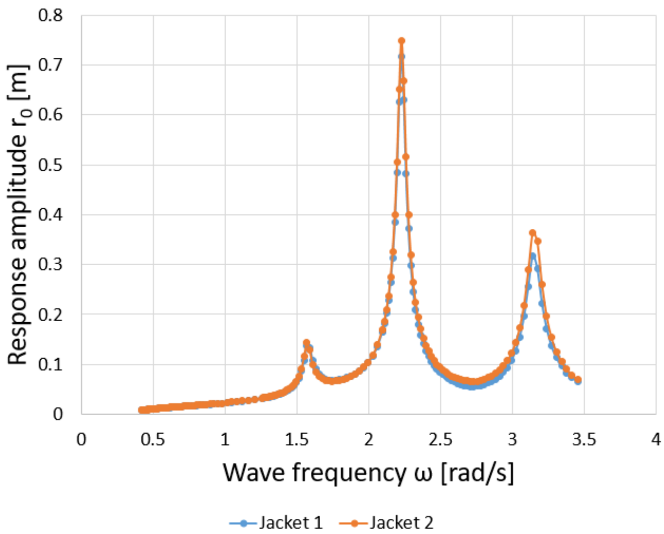

Figure 27: Response amplitude as function of wave frequency for a inertia dominated system with phase lag $\beta_2 = \pi/2$ and stiffness ratio $\mu = 0.5$

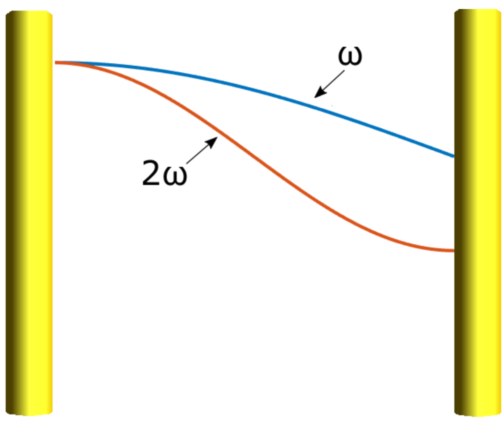

Figure 28: The two first force components for a system with phase lag $\beta_2 = \pi/2$. The blue line represents force acting with the wave frequency and the red line represents the force acting with double the wave frequency

4.2.3 Drag Dominated System, $C_M = 0$ and $C_D = 2$

4.2.3.1 Phase lag $\beta_2 = \pi/2$ and stiffness ratio $\mu = 0.5$

By comparing Figure 29 with Figure 27, the drag dominated system shows similar behaviour as the inertia dominated system for high frequencies, but the drag dominated system shows additional peaks at lower frequencies. This is in compliance with the results obtained in Section 4.2.1, where it was shown that a drag dominated system gives considerable force components with frequency 3ω and 4ω, in contrast to a inertia dominated system. The peaks at $\omega = 0.76$ and $\omega = 1.05$ correspond to $\omega_{n1}/3$ and $\omega_{n2}/3$, respectively, and there are also observed small peaks at $\omega_{n1}/4$ and $\omega_{n2}/4$.

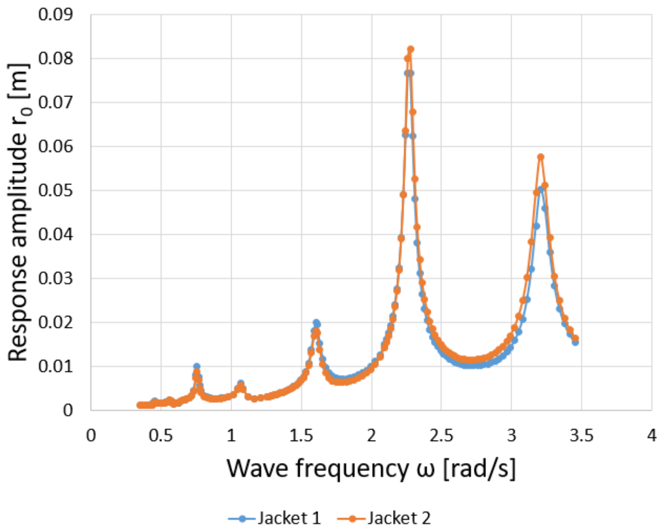

Figure 29: Response amplitude as function of wave frequency for a drag dominated system with phase lag $\beta_2 = \pi/2$ and stiffness ratio $\mu = 0.5$

4.2.3.2 Phase lag $\beta_2 = \pi/2$ and stiffness ratio $\mu = 0.05$

Figure 30 shows that for a lower stiffness ratio, the second eigenfrequency is moved to the left, which is in compliance with (2.25). Consequently, the peaks at $\omega = \omega_{n2}/2$ and $\omega = \omega_{n2}/3$ are also moved to the left, towards waves with more energy. On the other hand, it is seen that a lower stiffness ratio smaller range of critical frequencies.

4.2.3.3 Single Jacket

By comparing Figure 31 with Figure 30, it is seen that the main difference between a single jacket and jackets connected with a low stiffness ratio, is the difference in response of the two jackets around the eigenfrequency ω_{n1}. The reason for this, is that at the two eigenfrequencies, the system is forced oscillate with their corresponding mode shapes. The excitation on the second jacket will follow better the two mode shapes than the

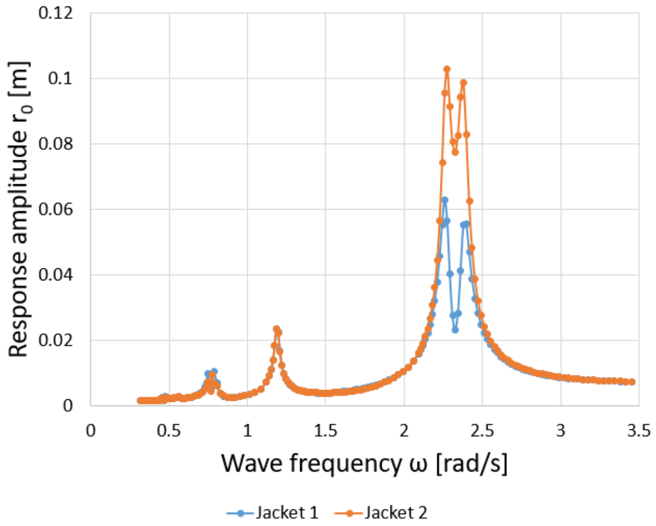

Figure 30: Response amplitude as function of wave frequency for a drag dominated system with phase lag $\beta_2 = \pi/2$ and stiffness ratio $\mu = 0.05$

excitation on the first jacket. Hence, the response will be largest on the second jacket. A more detailed explanation to this is found in Appendix A and B.

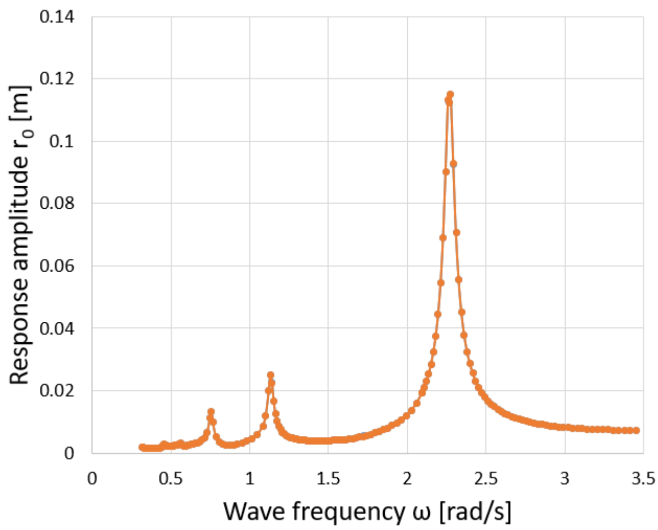

Figure 31: Response amplitude as function of wave frequency for a drag dominated single jacket

4.3 Stiffness from Piping

To get a feeling of the magnitude of the stiffness from the piping, an estimate was found by use of GeniE, see Section 3.3.2. The total piping stiffness together with the contribution from each pipe type is shown in Table 6.[11]

Diameter [m]	Thickness [m]	Reaction Force [N]	# Pipes	Total Stiffness [N/m]
1.0	0.012	1.0×10^6	2	2.0×10^6
0.5	0.006	64.0×10^3	4	256.0×10^3
0.2	0.003	7.8×10^3	10	78.0×10^3
				2.3×10^6

Table 6: Estimated total stiffness from piping, together with pipe dimensions and the number of each pipes used in the estimation.

In Section 3.2.1, the jacket stiffness was estimated to be $k_j = 182.65MN/m$. By assuming that all of the bridge stiffness comes from the piping, the stiffness ratio is equal to

$$\mu = \frac{k_b}{k_j} = \frac{2.3 \times 10^6}{182.65 \times 10^6} = 1.3\% \tag{4.1}$$

4.4 Friction

In Section 3.3 the mass of the bridge was set to be $m_{bridge} = 430$ t and the friction coefficient was assumed to be $\mu_f = 0.1$. By assuming that the weight is identically distributed on the two supports, the friction force in the sliding support is

$$F_f = \mu_f F_n = 0.1 \cdot 215 \times 10^3 kg \cdot 9.81 m/s^2 = 211 \times 10^3 N \tag{4.2}$$

A force of 211 kN is not large in this context. This suggests that the friction force can be neglected and the bridge can be modelled as a linear spring, as done in the simulations of this thesis.

4.5 Jacket Model Subjected to Point loads

In the same way as for the simplified model, the jacket model was initially subjected to point loads at the uppermost nodes of the jackets. This was done to verify that the jacket model behaves in the same way as the simplified model. Figure 32 shows the displacement response as function of excitation frequency for a system with two connected jackets, phase lag $\beta_2 = \pi/2$ and stiffness ratio $\mu = 0.5$. This is the same configurations that were used in Section 4.1 for the simplified model. By comparing Figure 32 with Figure 20 it is observed that the two models display similar behaviour in

[11] The reaction force in Table 6 is the reaction force due to a prescribed displacement of 1 m

the frequency domain, and that the jacket model has higher eigenfrequencies than the simplified model.

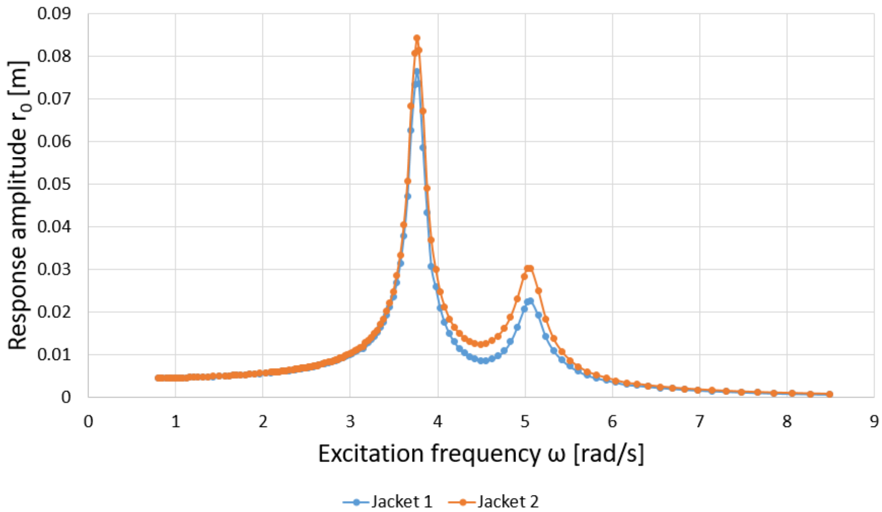

Figure 32: Response amplitude as function of wave frequency for jacket model subjected to point loads with phase lag $\beta_2 = \pi/2$ and stiffness ratio $\mu = 0.5$

4.6 Jacket Model Subjected to Extrapolated Airy Waves

The jacket model was subjected to wave excitation due to extrapolated airy waves. The wave height is $h = 5$ m, the water depth is $d = 80$ m and the hydrodynamic coefficients in Morison's equation are set to be $C_D = 0.7$ and $C_M = 2$. In reality the hydrodynamic coefficients are influenced by many parameters, such as Reynolds number R_e, the Keulegan-Carpenter number and the roughness, see Section 2.4.3. This means that the hydrodynamic coefficients will vary over the structure and with different loads. By a mistake, the mass of the topside was set to be 10000 tons instead of 11000 tons for this particular simulation. Figure 33 shows the displacement response as function of wave frequency for a system with two jackets, phase lag $\beta_2 = \pi/2$ and stiffness ratio $\mu = 0.5$. The two eigenfrequencies from this simulation are $\omega_{n1} = 4.10$ and $\omega_{n2} = 5.74$, which is a bit higher than the eigenfrequencies obtained when the correct mass is used. The eigenfrequencies are not included in Figure 33, since waves with frequencies this high have insignificant energy. In reality, frequencies higher than $\omega = 1.9$ are not physical for the given wave height. However, frequencies up to $\omega = 3$ are included to show the presence of all the higher order peaks. The peak at $\omega = 2.87$ is equal to half of $\omega_{n2} = 5.74$. The small peaks at $\omega = 1.37$ and $\omega = 1.91$ corresponds to one third of ω_{n1} and ω_{n2} respectively. Note that there is no peak at $\omega_{n1}/2$. These results are in compliance with the results obtained from the simplified model with phase lag $\pi/2$. In addition to the super-harmonic peaks, there are peaks at $\omega = 2.7$, $\omega = 2.4$ and $\omega = 1.7$. These peaks are explained in the following subsection.

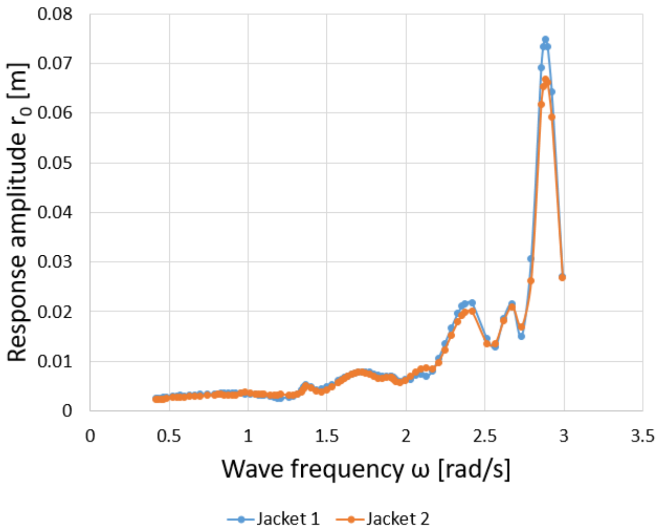

Figure 33: Response amplitude as function of wave frequency for two connected jackets with stiffness ratio $\mu = 0.5$ subjected to extrapolated Airy waves

4.6.1 Amplification and Cancellation Effects

Waves with frequency higher than $\omega = 1.7$, have wave lengths that are shorter than the width of the jacket[12]. Figure 34 shows that the wave length corresponding to $\omega = 2.4$ is half of the jacket width. This means that the forces, acting with the wave frequency, on the front legs and the back legs are in phase with each other, and the response becomes amplified. On the other hand, when the forces on the front legs and the back legs are in counter-phase with each other, they give cancellation effects. Due to these additional effects, the jacket model shows a more irregular plot in the frequency domain than the simplified model.

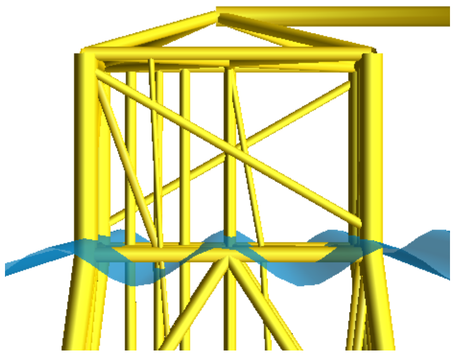

Figure 34: Wave length corresponding to wave frequency $\omega = 2.4$

[12]Jacket width: the distance between the center of the back legs and the center of the front legs at mean water level

The amplification/cancellation effects are presented in another way in Figure 35, which shows the power spectrum for the total wave force acting on one single jacket. The jacket is subjected to irregular waves given by a JONSWAP spectrum with $T_p = 6$ s. This means that there is a concentration of energy around $\omega_p = \frac{2\pi}{6s} = 1.05$, which explains the first peak in Figure 35. The three other peaks at higher frequencies correspond to the three peaks in Figure 33 which could not be explained by super-harmonic force components. The troughs in Figure 35 where there is almost no energy, correspond to frequencies giving forces on the front legs and back legs in counter-phase with each other. It is observed that the second trough is coinciding with the super-harmonic force component $2\omega_p$, which explains why there is no energy concentration around this frequency.

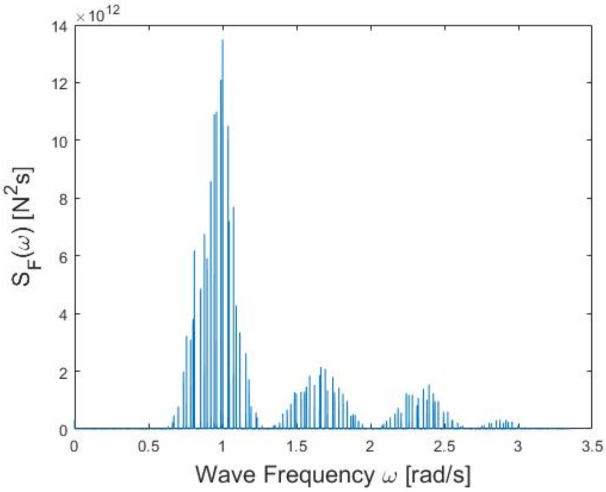

Figure 35: The power spectrum for the total wave force acting on one single jacket

4.7 Jacket Model Subjected to Irregular Waves

4.7.1 Comparing Quasi-Static and Dynamic Responses

The simulations presented in this subsection are done on a model consisting of two jackets connected by a spring with stiffness ratio $\mu = 0.5$. The stiffness was chosen to be this high to clearly demonstrate how the bridge affects the results. The eigenfrequencies for the model are $\omega_{n1} = 3.92$ and $\omega_{n2} = 5.54$.

4.7.1.1 Comparing Quasi-static and Dynamic Responses Visually by Time Series and Response Spectra

Figure 36 shows the displacement response as function of time from both quasi-static and dynamic analyses in USFOS. The jackets are subjected to irregular waves described by a JONSWAP spectrum with $T_p = 10$ m and $H_s = 5$ m. The dynamic and the quasi-static equation of motion are found in (2.1) and (2.74). It is seen from Figure 36b that the dynamic system oscillates with the fundamental eigenperiod $T_{n1} = 1.6$ s, on top of the oscillation from the quasi-static analysis, Figure 36a. This gave the motivation to investigate to what extent the fatigue damage is affected by dynamics, see Section 4.7.1.3.

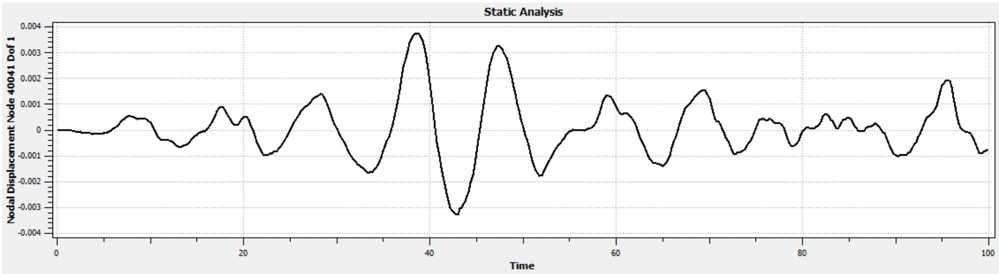

(a) Quasi-static analysis

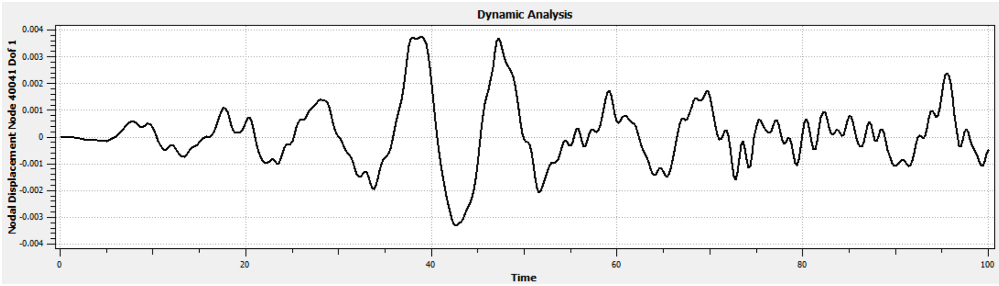

(b) Dynamic analysis

Figure 36: Displacement response as function of time from quasi-static and dynamic analysis in USFOS

Figure 37 shows the response spectrum of the displacement from dynamic and quasi-static analyses, for both a single and two connected jackets. The simulations were done for three hours, with sea state $T_p = 10$ m and $H_s = 5$ m. By comparing Figure 37a and Figure 37b, it is seen that the main difference between quasi-static and dynamic analysis for a single jacket is the dynamic amplification with peak close to 0.6 Hz. This frequency is close to the first eigenfrequency, f_{n1}=0.62. It is seen that the spectrum from two connected jackets have more irregular shape than the spectrum from a single jacket. This is explained by the interaction between the jackets. The additional peaks and bottoms correspond to frequencies where the waves hitting the jackets are in phase and counter-phase, respectively. The dynamic analysis for the connected jackets, Figure 37d, shows an additional low peak around $f = 0.8$ Hz. This peak is probably related to the second eigenfrequency $f_{02} = 0.88$ Hz. Again, the peak is given at a frequency lower than the eigenfrequency, in the same way as for the peak related to the first eigenfrequency. The reason to this is unknown.

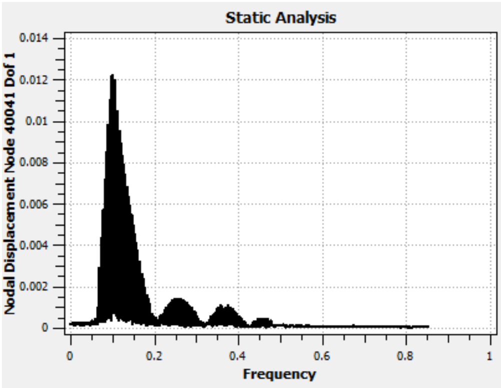

(a) Quasi-static analysis for single jacket

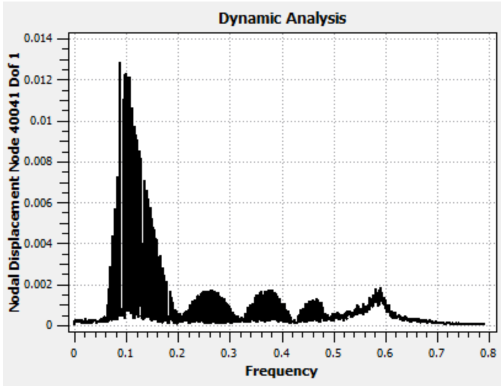

(b) Dynamic analysis for single jacket

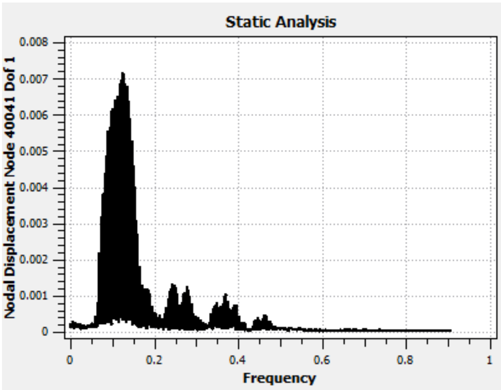

(c) Quasi-static analysis for two connected jackets

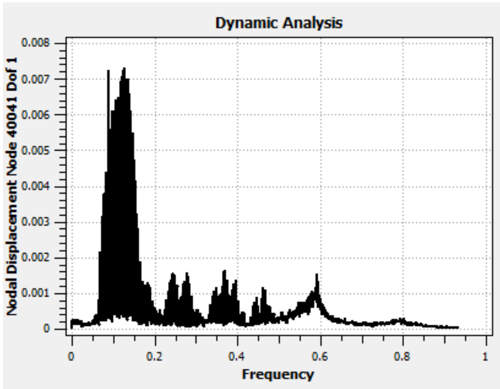

(d) Dynamic analysis for two connected jackets

Figure 37: Displacement response plotted in the frequency domain from dynamic and quasi-static analyses, for both a single and two connected jackets

4.7.1.2 Displacement Response

Table 7 shows the ratio between the mean square displacement response from dynamic and quasi-static analyses, $\frac{E[r^2_{0,dyn}]}{E[r^2_{0,stat}]}$, for three different sea states. As expected, the system behaves less dynamically for increasing wave periods. When the peak period is T_p=6 s, the mean square response from dynamic analysis is more than double the mean square response from quasi-static analysis. However, waves with periods in the range of T_p=6 s, do not have much energy, and it is therefore not likely that they will give a considerable effect to the dynamics of the structure. The larger waves with more energy are associated with less dynamic amplification. Thus, the system may after all behave almost quasi-statically.

Figure 38 shows the extreme displacement responses from 20 time series of 3 hours plotted in a Gumbel paper, together with their fitted regression lines. The data are located more or less along a straight line, which proposes that the Gumbel model is well

Sea State	$\frac{E[r^2_{0dyn}]}{E[r^2_{0,stat}]}$
T_p=6, H_s=2	2.16
T_p=10, H_s=5	1.19
T_p=15, H_s=10	1.06

Table 7: Ratio between the mean square displacement response from dynamic and quasi-static analysis, for three different sea states

suited for the analysis. The regression line for the dynamic analysis lies lower than the line for quasi-static analysis, which means that the dynamic analysis will give the largest q-probable response. Table 8 gives the values of the estimated parameters α and β used in the Gumbel distribution, together with the 10^{-2} annual probability response $r_{0,100}$.

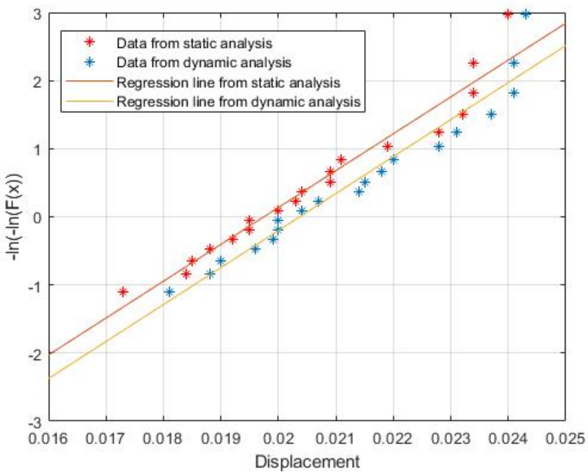

Figure 38: Gumbel plot of the extreme displacement response from 20 time series of 3 hours from both quasi-static and dynamic analyses

Analysis	α	β	$r_{0,100}$ [m]
Quasi-static	0.0197	0.0018	0.0239
Dynamic	0.0204	0.0018	0.0245

Table 8: Estimated parameters α and β used in the Gumbel distribution and 10^{-2} annual probability response $r_{0,100}$

The last column in Table 8 together with (3.28) give EDAF = 0.0245/0.0239 = 1.025. Thus, the dynamics amplification is almost insignificant for the extreme response of the displacement.

4.7.1.3 Force Response

In Table 9, the dynamic and quasi-static force response in the selected brace[13] are compared. The responses are compared with respect to fatigue damage C, in addition to the mean square response. By comparing Table 9 with Table 7, it is seen that there is less dynamic amplification, in terms of mean square response, for the force response than for the displacement response. Table 9 shows that the fatigue damage is highly affected by the dynamics for low values of T_p. Again, waves with low periods do not have much energy, so it is not sure that the fatigue lifetime of the system is highly affected by dynamics after all.

Sea State	$\frac{E[F_{0,dyn}^2]}{E[F_{0,stat}^2]}$	C_{dyn}/C_{stat}
T_p=6, H_s=2	1.19	1.83
T_p=10, H_s=5	1.03	1.12
T_p=15, H_s=10	1.01	1.04

Table 9: Ratio between dynamic and quasi-static analyses in terms of mean square force response and fatigue damage, for three different sea states

Figure 39 shows a Gumbel plot for extreme force responses from 20 times series of 3 hours. As for the displacement response, the data are located more or less along a straight line, which proposes that the Gumbel model is a suited model. Table 10 shows the Gumbel parameters α and β obtained from the regression analysis, together with the 10^{-2} annual probability response $F_{0,100}$.

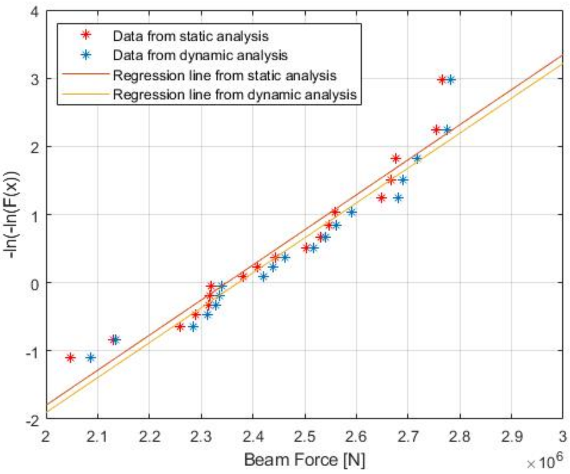

Figure 39: Gumbel plot of the extreme force response from 20 time series of 3 hours for both quasi-static and dynamic analysis

The last column in Table 10 together with (3.28) give EDAF $= 2.811/2.811 \times 10^6 =$

[13]See Section 3.6

Analysis	α	β	$F_{0,100}$ [N]
Quasi-static	2.349×10^6	1.945×10^5	2.787×10^6
Dynamic	2.372×10^6	1.953×10^5	2.811×10^6

Table 10: Estimated parameters α and β used in the Gumbel distribution and 10^{-2} annual probability response $F_{0,100}$

1.009. Thus, the dynamics amplification for the force is even lower than for the displacement, and can be neglected in the calculation of the long term extreme response. In this context, it can be said that the system behaves quasi-statically.

4.7.2 Sensitivity Study of the Bridge Stiffness

A sensitivity study of how the bridge stiffness affects the displacement response and the force response has been performed. The jackets are exposed to irregular waves described by JONSWAP spectra, and the responses are calculated by dynamic analyses. The mean square response and the fatigue damage have been found for several stiffness values of the bridge. The long term extreme response was found for the stiffness ratios μ=0.5, μ=0.05 and μ=0.0. The latter stiffness ratio is equivalent to the case of a single jacket.

4.7.2.1 Displacement Response

Figure 40 shows the mean square displacement response as function of the stiffness ratio μ. The jackets are subjected to a sea state with $T_p = 10$ s and $H_s = 5$ m. The estimated bridge stiffness ratio for a representative bridge done in Section 4.3, was found to be $\mu = 0.013$. Even though this was a very rough estimate including many assumptions, the author will not expect the stiffness ratio to be higher than $\mu = 0.1$. It is seen that for $\mu < 0.1$, the response decreases nearly linearly with the stiffness. This means that the presence of the bridge reduces the repose of the jackets. The logic behind this is that one single jacket must absorb all the energy by itself, while two connected jackets can work together since they have maximum displacement at different time. On the other hand, we have seen that with a bridge present, a second eigenfrequency is introduced with additional peaks due to super-harmonic forces. This gives a larger range of critical frequencies. However, the dynamic amplification around the eigenfrequencies becomes lower, and in addition, the additional eigenfrequency is higher than the first, and is therefore of less significance.

For $\mu = 0$, the mean square response is 1.73×10^{-6}, which is in compliance with the result obtained by doing the analysis on a single jacket. As the stiffness ratio becomes very high, the two jackets will behave like a SDOF system which explains why the graph goes towards an asymptotic value.

Table 11 shows the ratio between jackets connected with stiffness ratio μ=0 and μ=0.05, in terms of the mean square displacement response. The table gives this ratio for two

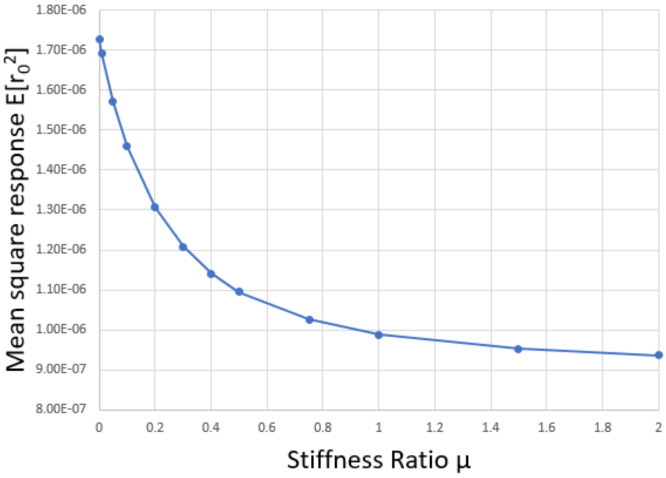

Figure 40: Mean square displacement response as function of the stiffness ratio μ

chosen sea states, as well as for both quasi-static and dynamic analysis. Again, it is seen that the dynamics do not play a big role, and that a single jacket has larger response than two connected jackets.

Sea State	$(E[r^2_{0,\mu=0}]/E[r^2_{0,\mu=0.05}])_{\text{static}}$	$(E[r^2_{0,\mu=0}]/E[r^2_{0,\mu=0.05}])_{\text{dynamic}}$
T_p=6, H_s=2	1.0955	1.1458
T_p=10, H_s=5	1.1393	1.1446

Table 11: Ratio of the mean square response between jackets connected with stiffness ratio μ=0 and μ=0.05

Figure 41 shows a Gumbel plot expressing the long term extreme displacement response, for jackets connected with bridges with stiffness ratios μ=0, μ=0.05 and μ=0.5. Table 12 shows the Gumbel parameters α and β obtained from the regression analysis, together with the 10^{-2} annual probability response $r_{0,100}$.

	α	β	$r_{0,100}$ [m]
$\mu = 0$	0.0252	0.0040	0.0342
$\mu = 0.05$	0.0242	0.0038	0.0328
$\mu = 0.5$	0.0197	0.0031	0.0266

Table 12: Estimated parameters α and β used in the Gumbel distribution and 10^{-2} annual probability response $r_{0,100}$

4.7.2.2 Force Response

Table 11 shows the response ratio between jackets connected with stiffness ratio μ=0 and μ=0.05. The responses are given with respect to mean square response and fatigue

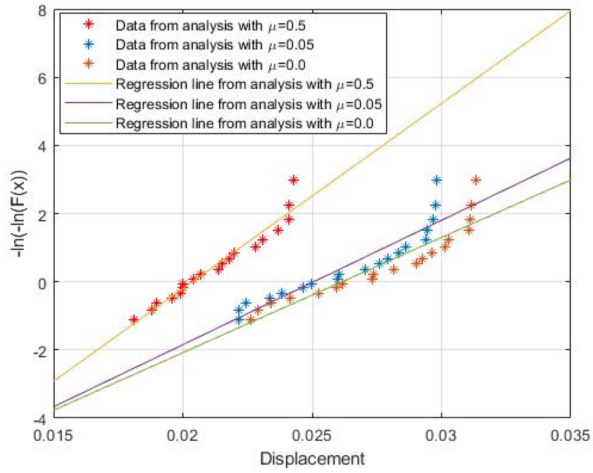

Figure 41: Gumbel plot of the extreme displacement response from 20 time series of 3 hours for the stiffness ratios $\mu = 0$, $\mu = 0.05$ and $\mu = 0.5$

damage. The ratio is given for two chosen sea states, from both quasi-static and dynamic analyses.

The ratio values from two sea states cannot be compared directly, since one of the sea states may include a larger range of wave lengths corresponding to phase lags close to one of the two eigenmodes. Additionally, one of the sea states may give more cancelling effects than the other. However, the ratio between the quasi-static and dynamic analyses can be investigated. It is seen that for the quasi-static analyses, the response ratios are largest for the second sea state, while for the dynamic analyses, the response ratios are largest for the first sea state. This is explained by that the first sea state contains small enough wave periods to excite the dynamics. Exactly how much of the dynamics that comes from the second eigenfrequency has not been quantified in this thesis. However, by comparing Figure 37b and Figure 37d, it seems like most of the dynamics have basis in the first eigenfrequency.

Sea State	$\left(\frac{E[r^2_{\mu=0}]}{E[r^2_{0,\mu=0.05}]}\right)_{static}$	$\left(\frac{E[r^2_{0,\mu=0}]}{E[r^2_{0,\mu=0.05}]}\right)_{dynamic}$	$\left(\frac{C_{\mu=0}}{C_{\mu=0.05}}\right)_{static}$	$\left(\frac{C_{\mu=0}}{C_{\mu=0.05}}\right)_{dynamic}$
T_p=6, H_s=2	1.031	1.055	1.079	1.137
T_p=10, H_s=5	1.040	1.043	1.105	1.119

Table 13: Ratio between jackets connected with stiffness ratio μ=0 and μ=0.05 in terms of mean square response and fatigue damage

Figure 41 shows a Gumbel expressing the long term extreme force response, for jackets connected with bridges with stiffness ratios μ=0, μ=0.05 and μ=0.5. Table 14 shows the Gumbel parameters α and β obtained from the regression analysis, together with the 10^{-2} annual probability response. From Table 12 it is seen that the 10^{-2} annual probability displacement response for a single jacket ($\mu = 0$) is 4% higher than for connected jackets with stiffness ratio $\mu = 0.05$. For the force response shown in Table 14, the difference is only 2%. Is it emphasized that a stiffness ratio of $\mu = 0.05$ corresponds to a bride which probably is stiffer than a typical bridge. This means that a typical bridge will not have a large influence on the long term maximum response.

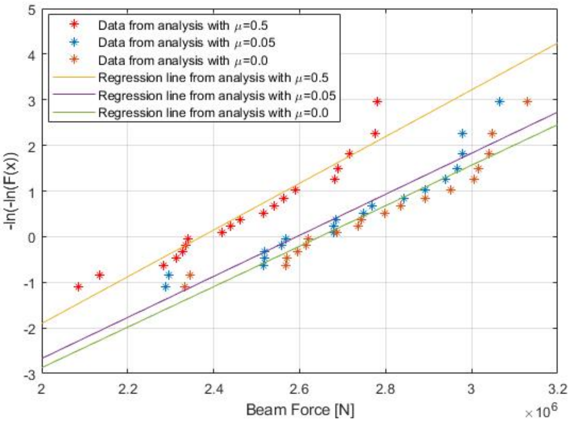

Figure 42: Gumbel plot of the extreme force response from 20 time series of 3 hours for the stiffness ratios $\mu = 0$, $\mu = 0.05$ and $\mu = 0.5$

	α $\times 10^{-6}$	β $\times 10^{-6}$	$F_{0,100}$ $\times 10^{-6}$ [N]
$\mu = 0$	2.647	2.254	3.15
$\mu = 0.05$	2.593	2.222	3.09
$\mu = 0.5$	2.372	1.952	2.81

Table 14: Estimated parameters α and β used in the Gumbel distribution and 10^{-2} annual probability response $r_{0,100}$

5 Conclusions and Recommendations for Further Work

5.1 Conclusions

The frequency plot of the displacement response for the simplified system gave the same results as obtained from the Matlab program made in the preparatory specialization project. A system of two identical jackets will have two eigenfrequencies with corresponding mode shapes. The first eigenfrequency is the same as the eigenfrequency for a single jacket, and is independent of the bridge stiffness. The other eigenfrequency introduced by the bridge is equal to $\omega_{n2} = \sqrt{1+2\mu}\omega_{n1}$. Thus, ω_{n2} is always higher than ω_{n1} and increases with higher bridge stiffness.

A jacket structure subjected to hydrodynamic loading of Morison type, will experience super-harmonic forces at multiples of the wave frequency, 2ω, 3ω,..., in addition to the force acting with the wave frequency ω. The super-harmonic force components are more important for a drag dominated system than for an inertia dominated system. Even though the super-harmonic forces are much smaller than the wave frequency force, they may coincide with one of the eigenfrequencies, and thus be of significant relevance. As follows, a structure that would be considered quasi-static without the super-harmonic forces, may have some dynamics due to these force components.

The bridge stiffness is assumed to be governed by the stiffness from the piping. A rough estimation for a representative bridge gave a relative stiffness ratio between the bridge and the jacket equal to $\mu = 1.3\%$. For stiffness values this low, the second eigenfrequency will only be 1.3% higher than the first, and the peaks in the frequency plot will appear as one single peak. However, already from very low stiffness values of the bridge, the peak of the second jacket will be higher than the first.

The equivalent dynamic amplification factor for the 10^{-2} annual probability displacement response of the first jacket was found to be EDAF = 1.025. This suggests that the dynamics are negligible for the long term extreme response. In terms of fatigue damage and mean square response, the system is more affected by dynamics. However, for waves with more energy, the dynamics become less significant. For a sea state with $T_p = 15$ s and $H_s = 10$ m, the ratio between the fatigue damage from a dynamic analysis and static analysis is $C_{dyn}/C_{stat} = 1.04$. In terms of the mean square force response, the ratio is only $E[F_{0,dyn}^2]/E[F_{0,stat}^2] = 1.01$. It can therefore be concluded that the dynamics do not play a big role in the system, and that the system displays a nearly quasi-statically behaviour.

The responses are higher for a single jacket than for connected jackets, and decrease with higher bridge stiffness. The logic behind this is that one single jacket must absorb all the energy by itself, while two connected jackets can work together since they have maximum response at different times. On the other hand, the bridge introduces a second eigenfrequency, with additional peaks due to super-harmonic forces, which gives a larger range of critical frequencies. However, since the system behaves nearly quasi-statically, the additional peaks are not of significant importance.

5.2 Recommendations for Further Work

This thesis has considered a simplified system. The complexity of the system should therefore gradually be further developed, to describe the reality in an improved way. The following steps are recommended for further work:

- Consider wave from different directions.
- Establish a more exact representation of the bridge, including shear stiffness.
- Study connected jackets that are not identical to each other.
- Expand the system from two to three (or more) different jackets.
- Use the understanding obtained in this study to do condition monitoring of connected jackets by assessing acceleration measurements.

References

[1] *USFOS Hydrodynamics - Theory Description of use Verification.*

[2] Standards Norway, *NORSOK Standard N-005, In-service integrity management of structures and maritime systems*, 2017.

[3] "Usfos non-linear static and dynamic analysis of space frame structures [online] available at: http://usfos.com/[accessed 30 may 2018]."

[4] "Conceptual modelling of offshore and maritime structures - genie [online] available at: https://www.dnvgl.com/services/conceptual-modelling-of-offshore-and-maritime-structures-genie-89128[accessed 30 may 2018]."

[5] A. E. Jørgen Amdahl *et al.*, *TMR 4100 - Marin teknikk intro, TMR 4105 - Marin teknikk 1 : kompendium.* Trondheim: Marin teknisk senter, NTNU, 4. utg. ed., 2011.

[6] D. Karunakaran and S. Haver, "Dynamic behaviour of kvitebjørn jacket structure - numerical predictions versus full-scale measurements," 2005.

[7] J. Amdahl, *TMR 4167 Marin teknikk 2 : Del 1 : Konstruksjonsanalyse*, vol. D. 1. Trondheim: Marinteknisk senter, Institutt for marin teknikk, 2010.

[8] S. Laik, *Offshore Petroleum Drilling and Production.* Taylor & Francis Inc, 2018.

[9] I. Langen, *Dynamisk analyse av konstruksjoner.* S.l.: [s.n.], 1979.

[10] O. M. Faltinsen, *Sea loads on ships and offshore structures.* Cambridge ocean technology series, Cambridge: Cambridge University Press, 1990.

[11] DNV GL, *DNVGL-RP-C205, Environmental conditions and environmental loads*, august 2017 ed.

[12] T. Moan, *Finite element modelling and analysis of marine structures*, vol. UK-03-98. Trondheim: Department of Marine Technology, NTNU, 2003.

[13] J. A. Tore H. Søreide *et al.*, *Theory Manual, USFOS - A Computer Program for Progressive Collapse Analysis of Steel Offshore Structures*, 1988.

[14] E. Pedersen and H. Valland, *Lecture Notes in Mechanical Vibrations, TMR 4222.* Department of Marine Technology, NTNU, 2014.

[15] O. Mo, *Stochastic time domain analysis of slender offshore structures.* PhD thesis, Trondheim, 1983.

[16] D. Myrhaug and W. Lian, *TMR4182 Marine Dynamics Irregular Waves.* Kompendieforlaget, 2009.

[17] D. E. Newland, *An introduction to random vibrations, spectral & wavelet analysis.* Mineola, N.Y: Dover, 3rd ed. ed., 2005.

[18] S. Haver, *Metocean Modelling and Prediction of Extreme Response.* 2017.

[19] K. v. Raaij, *Dynamic behaviour of jackets exposed to wave-in-deck forces.* PhD thesis, Stavanger, 2005.

[20] “Oiles global, metallic bearing [online] available at: https://www.oilesglobal.com/eu/en/products/[accessed 20 april 2018].”

[21] J. Schijve, *Fatigue of Structures and Materials.* Springer Netherlands, 2009.

[22] *DNVGL-RP-C203, Fatigue design of offshore steel structures*, 2016.

[23] J.-T. H. Horn, J. Amdahl, and S. K. Haver, “Dynamic amplification of drag dominated structures in irregular seas,” 2015.

Appendices

A Analytic Derivation of the Difference of Response for the two Jackets

The dynamic equation of motion for a system consisting of two connected jackets with stiffness k_j connected by a bridge with stiffness k_b, is given by:

$$\begin{bmatrix} k_j + k_b & -k_b \\ -k_b & k_j + k_b \end{bmatrix} \begin{bmatrix} x_1 \\ x_2 \end{bmatrix} + i\omega\alpha \begin{bmatrix} k_j + k_b + m & -k_b \\ -k_b & k_j + k_b + m \end{bmatrix} \begin{bmatrix} x_1 \\ x_2 \end{bmatrix} - \omega^2 \begin{bmatrix} m & 0 \\ 0 & m \end{bmatrix} \begin{bmatrix} x_1 \\ x_2 \end{bmatrix} = \begin{bmatrix} Q_0 \\ Q_0(cos\beta + isin\beta) \end{bmatrix} \tag{A.1}$$

In (A.1), Rayleigh damping is assumed with $\alpha_1 = \alpha_2 = \alpha$. Writing (A.1) on expanded form

$$\begin{bmatrix} (1 + i\omega\alpha)(k_j + k_b) + (i\omega\alpha - \omega^2)m & -(1 + i\omega\alpha)k_b \\ -(1 + i\omega\alpha)k_b & (1 + i\omega\alpha)(k_j + k_b) + (i\omega\alpha - \omega^2)m \end{bmatrix} \begin{bmatrix} x_1 \\ x_2 \end{bmatrix} = \begin{bmatrix} Q_0 \\ Q_0(cos\beta + isin\beta) \end{bmatrix} \tag{A.2}$$

Simplifying by introducing

$$a = (1 + i\omega\alpha)(k_j + k_b) + (i\omega\alpha - \omega^2)m \tag{A.3}$$

$$b = -(1 + i\omega\alpha)k_b \tag{A.4}$$

and equation (A.2) can then be written

$$ax_1 + bx_2 = Q_0 \tag{A.5}$$

$$bx_1 + ax_2 = Q_0(cos\beta + isin\beta) \tag{A.6}$$

Solving this set of equations for x_1 and x_2 and get

$$x_1 = \frac{-aQ_0 + bQ_0((cos\beta + isin\beta))}{b^2 - a^2} \tag{A.7}$$

$$x_2 = \frac{bQ_0 - aQ_0(cos\beta + isin\beta))}{b^2 - a^2} \tag{A.8}$$

The denominator is the same for x_1 and x_2, so it is sufficient to study the absolute value of the complex numerators. If the difference between the absolute value of the numerators is not equal to zero, then it is proved that the responses are not equal to each other. The absolute value for a complex number z is given by $|z| = \sqrt{z \cdot z^*}$, where

z^* is the complex conjugate. By use of Maple, the absolute value of the numerator of x_1 and x_2 are equal to

$$|num_{x1}| = \Big\{ \left[Q_0(\omega^2 m - k_j - k_b - k_j\cos(\beta) + \omega\alpha k_b \sin(\beta))\right]^2 + \left[Q_0(-\omega\alpha k_b \cos(\beta) - \omega\alpha k_j - \omega\alpha k_b - \omega\alpha m - k_b\sin(\beta))\right]^2 \Big\}^{1/2} \tag{A.9}$$

$$|num_{x2}| = \Big\{ \left[Q_0(-k_b + \omega\alpha k_j \sin(\beta) + \omega\alpha k_b \sin(\beta) + \omega\alpha m \sin(\beta) + \omega^2 m \cos(\beta) - k_j\cos(\beta) - k_b\cos(\beta))\right]^2 + \left[Q_0(-\omega\alpha k_b + \omega^2 m \sin(\beta) - \omega\alpha k_j \cos(\beta) - \omega\alpha k_b \cos(\beta) - \omega\alpha m \cos(\beta) - k_j \sin(\beta) - k_b \sin(\beta))\right]^2 \Big\}^{1/2} \tag{A.10}$$

The response amplitudes are not equal if

$$|num_{x1}| - |num_{x2}| \neq 0 \implies |num_{x1}|^2 - |num_{x2}|^2 \neq 0 \tag{A.11}$$

Use of Maple gives

$$|num_{x1}|^2 - |num_{x2}|^2 = 4Q_0\alpha m k_b \sin(\beta)\omega(\omega^2 + 1) \tag{A.12}$$

This shows that the response amplitudes are not necessarily equal. Since the expression includes α, it is shown that the difference is related to the Rayleigh damping. The response amplitudes are also equal for zero bride stiffness ($k_b = 0$) and for phase lag $\beta = 0$ or $\beta = \pi$. This is consistent with the results from the Matlab program made in the specialization project.

B Physical Explanation for the Difference in Response around the Eigenfrequencies

The difference in response amplitude can be explained physically by looking at Figure 43. The figure shows the phase angle as function of excitation frequency, with phase lag equal to $\pi/2$. The phase angle θ is here defined as the phase between the response of jacket j and the excitation acting of jacket 1. A negative phase angle results in a response acting behind the excitation. As explained in section 2.3.3, the jackets are forced at oscillate in phase with each other at ω_{n1}, which means that the phase angle θ will be the same. Figure 43 shows that they are $\theta_1 = \theta_2 = 3\pi/4$ at ω_{n2}. At this point, jacket 1 oscillates with a phase $3\pi/4$ behind the excitation acting on jacket 1, while

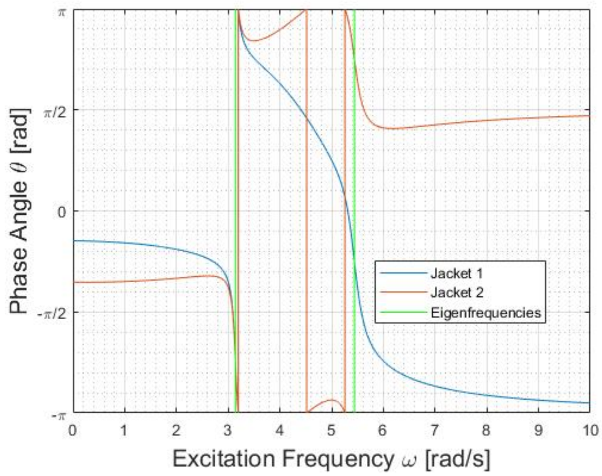

Figure 43: Phase angle as function of excitation frequency for a system with phase lag $\beta_2 = \pi/2$ and stiffness ratio $\mu = 1$. The figure is obtained from the Matlab program made in the specialization project.

jacket 2 oscillates with a phase $\pi/4$ behind the force excitation on jacket 2. This means that the system oscillates with a phase angle that follows better the excitation on jacket 2, than it follows the excitation on jacket 1. Hence, it is reasonable that jacket 2 has the largest response at ω_{n1}.

At the second eigenfrequency ω_{n2}, the jackets are forced to oscillate in counter-phase with each other. Figure 43 shows that the jackets oscillate in counter-phase with the their respective excitation forces at high values of ω. This means that the jacket that follows the counter-phase motion with excitation in the best way, will be the jacket with largest response at ω_{n2}. Figure 43 shows that jacket 1 oscillates with a phase $3\pi/4$ behind the counter-phase motion, while jacket 2 oscillates with a phase $\pi/4$ ahead the counter-phase motion. Hence, jacket 2 will also have the highest response amplitude at ω_{n2}.

C Matlab Codes

C.1 Code for Calculation of Key Response Data

```
clear all

%Loading data from file and write to time vector and displacement vector
load elem_force3.plo
t = elem_force3(:,1);
d = elem_force3(:,2);
n = length(t);
```

```
%Time step used in USFOS analysis
dt = (t(end) - t(1))/(n-1);

%Finding zero-up-crossing points
k = 0; %counting the number of zero-up-crossing points
Z = [];
for i = 1:n-1
    if d(i)<0 && d(i+1)>0
        k = k+1;
        Z(k) = i;  %Last point before zero-up-crossing
        TZ(k) = Z(k)*dt-d(i)*dt/(d(i+1)-d(i)); %Time for zero-up-crossing
                                               %assuming linear increasment
                                               %between the two points

    end
end

m = length(Z); %Number of zero-up-crossings

%Storing the wave periods in T
T = zeros(1,m-1);
for i = 1:m-1
    T(i) = dt*(Z(i+1)-Z(i));  %Wave periods
end

%Finding max and min diplacement in each interval
[mx,mn,H] = deal(zeros(1,m-1));
for i = 1:m-1
    displ = [];
    displ = d(Z(i):Z(i+1));
    mx(i) = max(displ);
    mn(i) = min(displ);
    H(i) = mx(i)-mn(i);  %Response height
end

%Find mean of 1/3 of higheset response heights
H_sort = sort(H);
nr = round((m-1)/3);
H_sort(1:2*nr) = [];
H_s = mean(H_sort);

%Find maximum response ampitude
mx_extreme = max([mx abs(mn)]);

%When mean value of d is zero, the zeroth moment can be calculated from
%the variance of h
m_0 = var(d);
H_s_var = 4*sqrt(m_0);

%Spectral analysis
df = 1/dt; %sample frequency
[pxx,f] = periodogram(d,[],[],df);
figure
```

```
plot(f(1:7000),pxx(1:7000))
%Solving integral m0=int{S(f)df}
%Using Trapezoidal numerical integration
m0 = trapz(f,pxx);
H_m0=4*sqrt(m_0);

%Pipe dimensions
D = 0.750; %m
r = D/2;
t = 0.035; %m
A = pi*(r^2-(r-t)^2); %m^2

% Rainflow counting
[c,hist,edges,rmm,idx] = rainflow(d/A,df);

% Stress ranges
range_dynamic = c(:,2);

% Load stress ranges from static analysis
load range_static.txt

% Make histogram
mx_val = max([max(range_dynamic) max(range_static)]);
figure
histogram(range_dynamic,0:mx_val/40:mx_val)
hold on
histogram(range_static,0:mx_val/40:mx_val)
xlabel('Stress Range')
ylabel('Cycle Counts')
legend('Dynamic','Static')
hold off

% Calculate number of cycles to failure for the stress range corresponding
% to the center of each bar, by use of SN-curve.
for i = 1:length(edges)-1
sigma(i) = edges(i)+(edges(i+1)-edges(i))/2;
end
sigma = sigma/1e6; %MPa
% Parameters used in SN-curve
lga1 = 12.48;
lga2 = 16.13;
m1 = 3;
m2 = 5;
%Solve for N
lgN = lga2 - m2*log10(sigma);
N = 10.^lgN;

% Number of cycles from in each stress range from rainflow counting
Num = sum(hist,2);
Num = Num';

% Calculating fatigue damage
rel = Num./N;
```

```
C = sum(rel);
```

C.2 Code for Plotting Extremes Values in Gumbel Paper

```
clear all

% Load file with extreme response for 20 3-hours simulation with different
% seeds, for both static and dynamic analysis
load extreme_values_double.txt

% Order the extreme values in two vectors
Extremes_stat = extreme_values_double(:,2);
Extremes_dyn = extreme_values_double(:,3);

% Calculating sample distribution F_stat
Extremes_stat = sort(Extremes_stat);
Extremes_stat = Extremes_stat';
for i = 1:length(Extremes_stat)
F_stat(i) = i/(1+length(Extremes_stat));
end
% Regression analysis for data plotted in Gubel paper
Y_stat = -log(-log(F_stat));
[r_stat,m_stat,b_stat] = regression(Extremes_stat,Y_stat);
x_stat = 0.016:0.0001:0.025;
reg_stat = b_stat+m_stat*x_stat;  %Regression line static analysis

% Find Gumber parameters
beta_stat = 1/m_stat;
alpha_stat = -b_stat*beta_stat;

%Calculate 100 anual probability response
r_stat_100 = alpha_stat - beta_stat*log(-log(0.9));

% Calculating sample distribution F_dyn
Extremes_dyn = sort(Extremes_dyn);
Extremes_dyn = Extremes_dyn';
for i = 1:length(Extremes_dyn)
F_dyn(i) = i/(1+length(Extremes_dyn));
end

% Regression analysis for data plotted in Gubel paper
Y_dyn = -log(-log(F_dyn));
[r_dyn,m_dyn,b_dyn] = regression(Extremes_dyn,Y_dyn);
x_dyn = 0.016:0.0001:0.025;
reg_dyn = b_dyn+m_dyn*x_dyn; %Regression line dynamic analysis

% Find Gumber parameters
beta_dyn = 1/m_dyn;
alpha_dyn = -b_dyn*beta_dyn;

%Calculate 100 anual probability response
r_dyn_100 = alpha_dyn -beta_dyn*log(-log(0.9));
```

```

% Plot the data together with the regression lines
plot(Extremes_stat,Y_stat,'r*')
hold on
plot(Extremes_dyn,Y_dyn,'*')
plot(x_stat,reg_stat)
plot(x_dyn,reg_dyn)
grid on
xlabel('Displacement')
ylabel('-ln(-ln(F(x))')
legend('Data from static analysis','Data from dynamic analysis',...
'Regression line from static analysis','Regression line from dynamic ...
    analysis')
```

C.3 Finding Random Frequencies and Phases for JONSWAP Spectrum

```
clear all
% Lower and upper limits for JONSWAP spectrum
Tmin = 2;
Tmax = 20;
Omin = 2*pi/Tmax;
Omax = 2*pi/Tmin;

% Number of wave components
N = 120;

% Length of intervals
Δ_O = (Omax-Omin)/120;

% Random number within Δ_O
r = Δ_O.*rand(1,N);

% Defining vector with equally spaced frequencies
omega = zeros(1,N);
omega(1) = Omin;
for i = 2:N
    omega(i) = omega(i-1) + Δ_O;
end

% Vector with random frequency value within each interval
omega_rand = omega + r;
% Corresponding time values used as input in USFOS
T_rand = 2*pi./omega_rand;

% Generating 120 radom phase angles
phase_rand = randi(360,120,1);

% Write random time values to txt.file
fileID = fopen('T_rand.txt','w');
fprintf(fileID,'%6.3f\n',T_rand);
```

```
fclose(fileID);

% Write random phase values to txt.file
fileID = fopen('Phase_rand.txt','w');
fprintf(fileID,'%6.3f\n',phase_rand);
fclose(fileID);
```

D Files Used to Run USFOS in Batch Mode

Here, the input files to USFOS, together with batch files used to automate the analysis, are presented. Since many different types of analysis have been done, only the following two cases are presented here

- Simplified model subjected to Airy waves with several periods (Appendix D.1)
- Full jacket model subjected to irregular sea ((Appendix D.2))

D.1 Simplified Model, Subjected to Wave Loads with phase lag $\beta = \pi/2$

D.1.1 Head file, *head.fem*

```
 HEAD                    Simplified model
                         Dynamic Analysis
                         Tarjei Sandal
'
# Eigenvalue analysis
'            KeyWord       Value
 Eigenval   Time           1         # Perform eigenval at time = 1
 Eigenval   NumberOf       5         # Compute 5 vectors
 Eigenval   Algorithm      Lanczos   # Use Lanczos solver
 Eigenval   ModeScale       5        # Scale modes by 5 for visualization
'
# Global results to be saved
'            Type      ID
DYNRES_N    Disp    1   1
DYNRES_N    Disp    3   1
Dynres_G    WaveElev
Dynres_G    WaveLoad
'
# Dynamic analysis
'          End_Time  D_t      dT_Res   dT_pri
 Dynamic  endT      0.01      0.1      0.1
'
'              ID    <type>  Dtime Factor   Start_time   ! Hydro Forces
 TimeHist       1    Switch  0.0    1.0        0.0
'
'              L_Case   TimeHist
 LOADHIST       1         1
'
# Wave load
'            l_case    Type  Height  Period Direct Phase   Surflev      Depth ...
      N_i
WAVEDATA     1       1       H1      T1      0     0       -20         80
'
# Number of integration points for wave calculation
Wave_Int          20
```

```
Wave_Int        30  1       2       102      103      202      203
'
# Hydrodynamic coefficients
Hyd_CdCm  Cd1 Cm1
'
# Sea dimension
SWITCHES WaveData SeaDim dimxy
'
# Control nodes
'          ncnods
 CNODES      1
'          nodex    idof     dfact
             1        1       1.
' -------------------------- E O F ------------------------
```

D.1.2 Structure file, *stru.fem*

```
 '        Node ID        X       Y           Z     Boundary code
 NODE        1        .000     .000        .000    0 1 0 0 0 0
 NODE        2        .000     .000    -100.000    1 1 1 1 1 1
 NODE        3         N2      .000        .000    0 1 0 0 0 0
 NODE        4         N2      .000    -100.000    1 1 1 1 1 1
'
'         Elem ID   np1    np2   material   geom
 BEAM      1         1      2        1         1
 BEAM      2         3      4        1         1
 BEAM      3         1      3        10        1
'
# Riser element used for slender structures
 BeamType   Riser    Mat      1
'
# Refine each beam element into 10 elements
'                nelem   elem1    elem2
 Refine   10        1        2
'
# Cross section data
'            Geom ID        Do       Thick     Shear_y   Shear_z
PIPE            1          10       0.50
'
# Node mass a top of each pipe
'           NodeID    M_x    M_y     M_z
 NODEMASS     1       20E6
 NODEMASS     3       20E6
'
# Rayleigh damping
'                          alpha1 alpha 2
 RAYLDAMP           0.01      0.01
'
# Define material
'         matno      E-mod    poiss   yield      density
 MISOIEP     1   210000E6  0.3     355.0E+30     0.000      0.0
'
```

```
# Material properties for spring element
'         Mat_ID     RefX  RefY  RefZ   RefMx  RefMy  RefMz
 MREF      10        101    0     0      0       0      0
'
# Define hyperelastic curve
'             Mat_ID       P         Delta
HypElastic     101    -106.056E6*0.5  -1
                       106.056E6*0.5   1
' ------------- E O F --------------------
```

D.1.3 Batch file to automate analysis , *run_case*

```
# ... ------------------------------------------------------------------------------------
# || Batch file to automate analysis                                     ... ||
# || Input parameters : Wave period, wave height, mass coefficient, drag ... coefficient ||
# || Usage: ./run_case Tp Hs Cm1 Cd1                                     ... ||
# ... ------------------------------------------------------------------------------------
'
 # - Make folder to store analysis
mkdir Tp=$1_endT=$2_Cm1=$3_Cd1=$4
'
# - Make file name defined by the input parameters
cp   head.fem      head_Tp=$1_endT=$2_Cm1=$3_Cd1=$4.fem
cp   stru.fem      stru_Tp=$1_endT=$2_Cm1=$3_Cd1=$4.fem
'
# - Insert input parameters to head file
 sed -i 's/Tp/'$1'/g'    head_Tp=$1_endT=$2_Cm1=$3_Cd1=$4.fem
 sed -i 's/endT/'$2'/g'  head_Tp=$1_endT=$2_Cm1=$3_Cd1=$4.fem
 sed -i 's/Cm1/'$3'/g'   head_Tp=$1_endT=$2_Cm1=$3_Cd1=$4.fem
 sed -i 's/Cd1/'$4'/g'   head_Tp=$1_endT=$2_Cm1=$3_Cd1=$4.fem
'
# - Calculate wave length from wave period
 lambda=$(echo "$1^2*9.81/6.2832" | bc -l)
'
# - Limit for when the formula above is valid
 T_lim=$(echo "sqrt ( 2*80*2*3.14159/9.81 )" | bc -l)
'
# - Calculate distance between jackets and sea dimension
if (( $(echo "$1 < 3" | bc -l) ));
 then
 var=$(echo "$lambda*6.25" | bc -l)
 seadim1=$(echo "$lambda*10" | bc -l)
 elif (( $(echo "$1 > $T_lim" | bc -l) ));
 then
 lambda2=$(echo "2*80*(2*$1/$T_lim-1)" | bc -l)
 var=$(echo "$lambda2*0.25" | bc -l)
 seadim1=$(echo "$lambda*2" | bc -l)
```

```
 elif (( $(echo "$1 > 5" | bc -l) )) && (( $(echo "$1 < $T_lim" | bc -l) ));
 then
 var=$(echo "$lambda*1.25" | bc -l)
 seadim1=$(echo "$lambda*4" | bc -l)
 else
 var=$(echo "$lambda*3.5" | bc -l)
 seadim1=$(echo "$lambda*8" | bc -l)
 fi
# - Inserte calculated values in input files
 sed -i 's/dimxy/'$seadim1'/g'   head_Tp=$1_endT=$2_Cm1=$3_Cd1=$4.fem
 sed -i 's/N2/'$var'/g'   stru_Tp=$1_endT=$2_Cm1=$3_Cd1=$4.fem
'
# - Run USFOS
./usfos.cmd   << ENDIN
head_Tp=$1_endT=$2_Cm1=$3_Cd1=$4
stru_Tp=$1_endT=$2_Cm1=$3_Cd1=$4
BT=USF
Tp=$1_endT=$2_Cm1=$3_Cd1=$4
ENDIN
'
# - Calculate starting time for Dynmax
if (( $(echo "$1 < 6" | bc -l) ));
then
TS1=$(echo "$2-5*$1" | bc )
else
TS1=$(echo "$2-3*$1" | bc )
fi
'
# - Run DynMax
./dynmax.cmd   << ENDIN
1
0
Tp=$1_endT=$2_Cm1=$3_Cd1=$4.dyn
dynmax
$TS1   $2
1
2
0
ENDIN
'
# - Write stationary response amplitude and wave period to file
grep "PeakValue for DynRes   1" dynmax >> res1
grep "PeakValue for DynRes   2" dynmax >> res2
echo -n "$1 " >> result
awk 'FNR==NR{a[$1]=$7 FS $6;next}{ print $6, a[$1]}' res2 res1 >> result
'
# - Move files to folder
mv stru_Tp=$1_endT=$2_Cm1=$3_Cd1=$4.fem Tp=$1_endT=$2_Cm1=$3_Cd1=$4
mv Tp=$1_endT=$2_Cm1=$3_Cd1=$4.raf Tp=$1_endT=$2_Cm1=$3_Cd1=$4
mv Tp=$1_endT=$2_Cm1=$3_Cd1=$4.dyn Tp=$1_endT=$2_Cm1=$3_Cd1=$4
mv Tp=$1_endT=$2_Cm1=$3_Cd1=$4_status.text Tp=$1_endT=$2_Cm1=$3_Cd1=$4
mv head_Tp=$1_endT=$2_Cm1=$3_Cd1=$4.fem Tp=$1_endT=$2_Cm1=$3_Cd1=$4
mv Tp=$1_endT=$2_Cm1=$3_Cd1=$4.out Tp=$1_endT=$2_Cm1=$3_Cd1=$4
```

```
mv dynmax Tp=$1_endT=$2_Cm1=$3_Cd1=$4
# - Delete files
rm res1
rm res2
' ------------- E O F --------------------
```

D.1.4 Run Loop with Different Wave Periods, *run_loop*

The batch file *run_case* is automatically run for many wave periods as defined in the for-loops in the file *run_loop*.

```
# - Assign values to variables
H=5       # Wave height
Cm=2      # Hydrodynamic mass coefficient
Cd=0      # Hydrodynamic drag coefficient
'
# - Run loops
for i in $(seq 1.82 0.02 2)
 do
 var=$(echo "$i*100" | bc )
    ./run_case  $i  $H  $var  $Cm  $Cd
  done
'
for i in $(seq 2.02 0.02 3)
 do
 var=$(echo "$i*150" | bc )
    ./run_case   $i  $H  $var  $Cm  $Cd
  done
'
for i in $(seq 3.00 0.05 5.5)
 do
 var=$(echo "$i*100" | bc )
    ./run_case   $i  $H  $var  $Cm  $Cd
  done
'
for i in $(seq 5.60 0.2 10)
 do
 var=$(echo "$i*50" | bc )
    ./run_case   $i  $H  $var  $Cm  $Cd
  done
'
for i in $(seq 10.20 0.2 15)
 do
 var=$(echo "$i*30" | bc )
    ./run_case   $i  $H  $var  $Cm  $Cd
  done
'
for i in $(seq 15.50 0.5 20)
 do
 var=$(echo "$i*20" | bc )
    ./run_case   $i  $H  $var  $Cm  $Cd
```

```
  done
'
mv result results
' ------------- E O F ---------------
```

D.2 Full Jacket Model, Subjected to Irregular Waves

D.2.1 Head file, *head.fem*

```
HEAD                 Full Jacket Model
                     Dynamic Analysis, Irregular Waves
                     Tarjei Sandal
'
# - Eigenvalue analysis
'           KeyWord       Value
 Eigenval    Time           1        # Perform eigenval at time = 1
 Eigenval    NumberOf       5        # Compute 20 vectors
 Eigenval    ModeScale      5        # Scale modes by 2  for visualization
 Eigenval    Algorithm    SubSpace   # Use Lanczos solver
'
# - Global results to be saved
'             Type      ID
DYNRES_N      Disp    40041    1
DYNRES_N      Disp    140041   1
Dynres_G      WaveElev
Dynres_G      WaveLoad
DynRes_Elem  Force  14105   2   1
'
# - Dynamic analysis
'         End_Time  D_t      dT_Res    dT_pri
 Dynamic  endT     0.2      10      1
'
'              ID    <type>   Dtime Factor    Start_time    ! Hydro Forces
 TimeHist       2     Switch  0.0     1.0        0.0
'
'            L_case    Tim Hist
 LOADHIST      2          2
'
# - Wave load from, with initialization of wave
'            Ildcs   <type>   Sign_H     Period    Dir Phase_Seed Surf_Lev ...
    Depth nIni
 WAVEDATA       2     Spect      Hs         Tp     0      1.0        80.0     80 ...
       4
'
             -1000  1
              -200  1
                 0  0
               100  0
'            nFreq     Type   T_Min    T_Max   iGrid Gamma
              120       Read !
```

```
'
# - User defined wave spectrum
'              Key       Name
 FileName      Spec     spect_120.txt
'
# - Number of integration points for wave calculation
Wave_Int         20
'
# Hydrodynamic coefficients
Hyd_CdCm   0.7   2
'
# - Sea dimension
SWITCHES WaveData SeaDim dimxy
'
# Control nodes
'          ncnods
CNODES       1
'          nodex     idof      dfact
           40041      1.         1.0
'
# - Max number of steps in analysis
CMAXSTEP 100000
' ------------- E O F --------------------
```

D.2.2 Structure File, *stru.fem*

```
'    Node ID X       Y          Z  Boundary code
NODE    10101   42          21          0     1 1 1 1 1 1
NODE    10107   42          1           0     1 1 1 1 1 1
NODE    10113   0           21          0     1 1 1 1 1 1
NODE    10119   0           -21         0     1 1 1 1 1 1
NODE    10201   41.75       -20.75      2
NODE    10202   41.75       -7.62       2
NODE    10203   44.13       -7.62       2
NODE    10204   41.75       0           2
NODE    10205   44.13       7.62        2
NODE    10206   41.75       7.62        2
NODE    10207   41.75       20.75       2
NODE    10209   21          0.75        2
NODE    10213   0.25        20.75       2
NODE    10216   0.25        0           2
NODE    10219   0.25        -20.75      2
NODE    10222   21          -20.75      2
NODE    10223   41.39       -20.39      4.884
NODE    10224   41.39       20.39       4.884
NODE    10225   0.61        20.39       4.884
NODE    10226   0.61        -20.39      4.884
NODE    10229   34.13       -7.62       2
NODE    10232   43.067      -7.62       10.5
NODE    10233   33.067      -7.621      10.5
NODE    10239   34.13       7.62        2
NODE    10241   40.873      -19.873     9.02
NODE    10242   43.067      7.62        10.5
NODE    10243   33.067      7.621       10.5
NODE    10247   40.873      19.873      9.02
NODE    10253   1.127       19.873      9.02
NODE    10259   1.127       -19.873     9.02
NODE    10301   39.5        -18.5       20
NODE    10302   39.5        -7.622      20
NODE    10303   41.88       -7.62       20.001
NODE    10304   39.5        0           20
NODE    10305   41.88       7.62        20.001
NODE    10306   39.5        7.622       20
NODE    10307   39.5        18.5        20
NODE    10309   21          18.5        20
NODE    10310   17.2        18.5        20
```

41	NODE	10311	14.9	18.5	20
42	NODE	10312	12.6	18.5	20
43	NODE	10313	2.5	18.5	20
44	NODE	10316	2.5	0	20
45	NODE	10317	15.5	-13	20
46	NODE	10319	2.5	-18.5	20
47	NODE	10322	21	-18.5	20
48	NODE	10329	31.878	-7.622	20
49	NODE	10332	40.63	-7.62	30
50	NODE	10333	30.631	-7.619	30
51	NODE	10339	31.878	7.622	20
52	NODE	10342	40.63	7.62	30
53	NODE	10343	30.631	7.619	30
54	NODE	10401	37	-16	40
55	NODE	10402	37	-7.616	40
56	NODE	10403	39.38	-7.62	39.999
57	NODE	10404	37	0	40
58	NODE	10405	39.38	7.62	39.999
59	NODE	10406	37	7.616	40
60	NODE	10407	37	16	40
61	NODE	10409	21	16	40
62	NODE	10412	12.6	16	40
63	NODE	10413	5	16	40
64	NODE	10416	5	0	40
65	NODE	10417	15.5	-10.5	40
66	NODE	10419	5	-16	40
67	NODE	10422	21	-16	40
68	NODE	10429	29.384	-7.616	40
69	NODE	10432	38.442	-7.62	47.505
70	NODE	10433	28.446	-7.616	47.505
71	NODE	10439	29.384	7.616	40
72	NODE	10442	38.442	7.62	47.505
73	NODE	10443	28.446	7.616	47.505
74	NODE	10501	34.625	-13.625	59
75	NODE	10502	34.625	-7.616	59
76	NODE	10503	37.005	-7.62	59
77	NODE	10504	34.625	0	59
78	NODE	10505	37.005	7.62	59
79	NODE	10506	34.625	7.616	59
80	NODE	10507	34.625	13.625	59
81	NODE	10509	21	13.625	59
82	NODE	10510	15.52	13.625	59
83	NODE	10511	13.22	13.625	59
84	NODE	10512	10.92	13.625	59
85	NODE	10513	7.375	13.625	59
86	NODE	10514	7.375	10.325	59
87	NODE	10516	7.375	0	59
88	NODE	10517	15.5	-8.125	59
89	NODE	10519	7.375	-13.625	59
90	NODE	10520	13.847	-13.625	59
91	NODE	10521	17.464	-10.089	59
92	NODE	10522	21	-13.625	59
93	NODE	10525	17.7	10.325	59
94	NODE	10527	21	5	59
95	NODE	10528	29.629	-4.996	59
96	NODE	10529	27.009	-7.616	59
97	NODE	10530	17.2	11.94	59
98	NODE	10531	14.9	11.94	59
99	NODE	10532	12.6	11.94	59
100	NODE	10533	15.5	10.325	59
101	NODE	10534	13.206	10.325	59
102	NODE	10535	10.911	10.325	59
103	NODE	10538	29.629	4.996	59
104	NODE	10539	27.009	7.616	59
105	NODE	10540	25.064	9.561	59
106	NODE	10600	29.454	-11	80
107	NODE	10601	32	-11	80
108	NODE	10602	32	-8.456	80
109	NODE	10603	32	-6.204	80
110	NODE	10604	32	0	80
111	NODE	10605	32	6.204	80
112	NODE	10606	32	8.456	80
113	NODE	10607	32	11	80
114	NODE	10608	29.454	11	80
115	NODE	10609	21	11	80
116	NODE	10610	15.52	11	80
117	NODE	10611	13.22	11	80
118	NODE	10612	10.92	11	80
119	NODE	10613	10	11	80
120	NODE	10614	10	7.7	80
121	NODE	10616	10	0	80
122	NODE	10617	15.5	-5.5	80
123	NODE	10618	10	-8.454	80

```
NODE     10619   10        -11       80
NODE     10620   12.546    -11       80
NODE     10621   15.78     -11       80
NODE     10622   21        -11       80
NODE     10623   21        0         80
NODE     10624   17.7      7.7       80
NODE     10625   15.502    7.7       80
NODE     10626   13.21     7.7       80
NODE     10627   10.917    7.7       80
NODE     10628   17.2      9.313     80
NODE     10629   14.9      9.313     80
NODE     10630   12.6      9.313     80
NODE     10631   23.75     8.25      80
NODE     10638   21        5         80
NODE     20621   32        -11       81.855
NODE     20624   32        -11       94.45
NODE     20631   32        11        81.855
NODE     20634   32        11        94.45
NODE     20641   10        11        81.855
NODE     20644   10        11        94.45
NODE     20651   10        -11       81.855
NODE     20654   10        -11       94.45
NODE     20712   32        11        95.5
NODE     20715   21        11        95.5
NODE     20716   17.2      11        95.5
NODE     20717   15        11        95.5
NODE     20718   12.6      11        95.5
NODE     20719   10        11        95.5
NODE     20732   10        -11       95.5
NODE     20734   15        -11       95.5
NODE     20739   32        -11       95.5
NODE     20750   32        -5.5      95.5
NODE     20752   32        5.5       95.5
NODE     20760   21        5.5       95.5
NODE     20765   10        -8.25     95.5
NODE     30210   17.2      20        2          1   1   0   0   0   0
NODE     30211   14.9      20        2          1   1   0   0   0   0
NODE     30212   12.6      20        2          1   1   0   0   0   0
NODE     30217   15.5      -15.25    2          1   1   0   0   0   0
NODE     30421   17.464    -10.089   55
NODE     30427   21        5         58
NODE     30428   29.626    -5        58
NODE     30438   29.626    5         58
NODE     30440   25.063    9.563     58

'
'    Elem ID np1 np2 material geom  lcoor ecc1 ecc2
BEAM 11201 10101 10201 10001 10001 10193
BEAM 11202 10107 10207 10001 10001 10194
BEAM 11302 10113 10213 10001 10001 10195
BEAM 11402 10119 10219 10001 10001 10196
BEAM 12103 10219 10222 10001 10010 10197
BEAM 12104 10222 10201 10001 10010 10197
BEAM 12105 10319 10222 10001 10006 10199 10013 0
BEAM 12106 10222 10322 10001 10009 10200
BEAM 12107 10301 10222 10001 10006 10199 10015 0
BEAM 12200 10204 10206 10001 10010 10202
BEAM 12201 10201 10223 10001 10001 10193
BEAM 12202 10207 10224 10001 10001 10194
BEAM 12203 10201 10202 10001 10010 10202
BEAM 12204 10202 10204 10001 10010 10202
BEAM 12205 10301 10204 10001 10006 10207 10015 0
BEAM 12206 10206 10207 10001 10010 10202
BEAM 12207 10307 10204 10001 10006 10209 10029 0
BEAM 12208 10223 10241 10001 10002 10193
BEAM 12209 10224 10247 10001 10002 10194
BEAM 12210 10241 10301 10001 10002 10193
BEAM 12211 10247 10307 10001 10002 10194
BEAM 12302 10213 10225 10001 10001 10195
BEAM 12303 10207 10209 10001 10010 10217
BEAM 12304 10209 10213 10001 10010 10217
BEAM 12305 10307 10209 10001 10006 10219 10029 0
BEAM 12306 10209 10309 10001 10009 10220
BEAM 12307 10313 10209 10001 10006 10219 10031 0
BEAM 12309 10225 10253 10001 10002 10195
BEAM 12311 10253 10313 10001 10002 10195
BEAM 12402 10219 10226 10001 10001 10196
BEAM 12403 10213 10216 10001 10010 10226
BEAM 12404 10216 10219 10001 10010 10226
BEAM 12405 10313 10216 10001 10006 10209 10031 0
BEAM 12406 10216 10316 10001 10009 10229
BEAM 12407 10319 10216 10001 10006 10207 10013 0
BEAM 12409 10226 10259 10001 10002 10196
```

207	BEAM	12411	10259	10319	10001	10002	10196			
208	BEAM	12501	10222	10229	10001	10010	10234	10082	0	
209	BEAM	12502	10229	10204	10001	10010	10234	0	10087	
210	BEAM	12503	10204	10239	10001	10010	10234	10079	0	
211	BEAM	12504	10239	10209	10001	10010	10234	0	10082	
212	BEAM	12505	10209	10216	10001	10010	10001	10083	10079	
213	BEAM	12506	10216	10222	10001	10010	10001	10087	10083	
214	BEAM	12507	10202	10229	10001	10011	10234			
215	BEAM	12508	10201	10229	10001	10012	10241			
216	BEAM	12509	10206	10239	10001	10011	10234			
217	BEAM	12510	10207	10239	10001	10012	10243			
218	BEAM	12511	10209	10222	10001	10011	10220			
219	BEAM	12600	10203	10202	10001	10011	10234			
220	BEAM	12601	10203	10233	10001	10020	10246			
221	BEAM	12602	10229	10233	10001	10016	10247			
222	BEAM	12603	10203	10232	10001	10018	10247			
223	BEAM	12604	10232	10233	10001	10020	10234			
224	BEAM	12605	10233	10329	10001	10015	10247			
225	BEAM	12606	10303	10233	10001	10021	10251			
226	BEAM	12607	10232	10303	10001	10019	10247			
227	BEAM	12610	10205	10206	10001	10011	10234			
228	BEAM	12611	10205	10243	10001	10020	10246			
229	BEAM	12612	10239	10243	10001	10016	10247			
230	BEAM	12613	10205	10242	10001	10018	10247			
231	BEAM	12614	10242	10243	10001	10020	10234			
232	BEAM	12615	10243	10339	10001	10015	10247			
233	BEAM	12616	10305	10243	10001	10021	10251			
234	BEAM	12617	10242	10305	10001	10019	10247			
235	BEAM	13103	10319	10322	10001	10013	10197			
236	BEAM	13104	10322	10301	10001	10034	10197			
237	BEAM	13105	10319	10422	10001	10007	10263	0	10010	
238	BEAM	13107	10301	10422	10001	10007	10263	0	10012	
239	BEAM	13200	10304	10306	10001	10013	10202			
240	BEAM	13201	10301	10401	10001	10003	10113			
241	BEAM	13202	10307	10407	10001	10003	10133			
242	BEAM	13203	10301	10302	10001	10013	10202			
243	BEAM	13204	10302	10304	10001	10013	10202			
244	BEAM	13205	10301	10404	10001	10007	10268	0	10042	
245	BEAM	13206	10306	10307	10001	10013	10202			
246	BEAM	13207	10307	10404	10001	10007	10270	0	10044	
247	BEAM	13302	10313	10413	10001	10003	10153			
248	BEAM	13303	10307	10309	10001	10034	10217			
249	BEAM	13305	10307	10409	10001	10007	10272	0	10012	
250	BEAM	13307	10313	10409	10001	10007	10272	0	10010	
251	BEAM	13321	10309	10310	10001	10038	10217			
252	BEAM	13322	10310	10311	10001	10038	10217			
253	BEAM	13323	10311	10312	10001	10038	10217			
254	BEAM	13324	10312	10313	10001	10013	10217			
255	BEAM	13402	10319	10419	10001	10003	10173			
256	BEAM	13403	10313	10316	10001	10013	10226			
257	BEAM	13404	10316	10319	10001	10013	10226			
258	BEAM	13405	10313	10416	10001	10007	10270	0	10044	
259	BEAM	13407	10319	10416	10001	10007	10268	0	10042	
260	BEAM	13500	10317	10322	10001	10010	10001	0	10083	
261	BEAM	13501	10322	10329	10001	10013	10234	10082	0	
262	BEAM	13502	10329	10304	10001	10010	10234	0	10087	
263	BEAM	13503	10304	10339	10001	10010	10234	10079	0	
264	BEAM	13504	10339	10309	10001	10013	10234	0	10082	
265	BEAM	13505	10309	10316	10001	10010	10001	10083	10079	
266	BEAM	13506	10316	10317	10001	10010	10001	10087	0	
267	BEAM	13507	10302	10329	10001	10010	10234			
268	BEAM	13508	10301	10329	10001	10012	10290			
269	BEAM	13509	10306	10339	10001	10010	10234			
270	BEAM	13510	10307	10339	10001	10012	10292			
271	BEAM	13511	10309	10322	10001	10012	10220			
272	BEAM	13600	10303	10302	10001	10010	10234			
273	BEAM	13601	10329	10332	10001	10013	10295			
274	BEAM	13602	10329	10333	10001	10014	10247			
275	BEAM	13603	10303	10332	10001	10018	10247			
276	BEAM	13604	10332	10333	10001	10012	10234			
277	BEAM	13605	10333	10429	10001	10014	10247			
278	BEAM	13606	10333	10403	10001	10020	10300			
279	BEAM	13607	10332	10403	10001	10017	10247			
280	BEAM	13610	10305	10306	10001	10010	10234			
281	BEAM	13611	10339	10342	10001	10013	10295			
282	BEAM	13612	10339	10343	10001	10014	10247			
283	BEAM	13613	10305	10342	10001	10018	10247			
284	BEAM	13614	10342	10343	10001	10012	10234			
285	BEAM	13615	10343	10439	10001	10014	10247			
286	BEAM	13616	10343	10405	10001	10020	10300			
287	BEAM	13617	10342	10405	10001	10017	10247			
288	BEAM	14103	10419	10422	10001	10014	10197			
289	BEAM	14104	10422	10401	10001	10031	10197			

290	BEAM	14105	10419	10522	10001	10007	10263	10005	10006
291	BEAM	14107	10401	10522	10001	10007	10263	10007	10008
292	BEAM	14200	10404	10406	10001	10014	10202		
293	BEAM	14201	10401	10501	10001	10004	10193		
294	BEAM	14202	10407	10507	10001	10004	10194		
295	BEAM	14203	10401	10402	10001	10014	10202		
296	BEAM	14204	10402	10404	10001	10014	10202		
297	BEAM	14205	10401	10504	10001	10007	10319	10007	10038
298	BEAM	14206	10406	10407	10001	10014	10202		
299	BEAM	14207	10407	10504	10001	10007	10321	10021	10040
300	BEAM	14302	10413	10513	10001	10004	10195		
301	BEAM	14303	10407	10409	10001	10031	10217		
302	BEAM	14305	10407	10509	10001	10007	10272	10021	10008
303	BEAM	14307	10413	10509	10001	10007	10272	10023	10006
304	BEAM	14322	10409	10412	10001	10036	10217		
305	BEAM	14324	10412	10413	10001	10014	10217		
306	BEAM	14402	10419	10519	10001	10004	10196		
307	BEAM	14403	10413	10416	10001	10014	10226		
308	BEAM	14404	10416	10419	10001	10014	10226		
309	BEAM	14405	10413	10516	10001	10007	10321	10023	10040
310	BEAM	14407	10419	10516	10001	10007	10319	10005	10038
311	BEAM	14500	10417	10422	10001	10010	10001	0	10083
312	BEAM	14501	10422	10429	10001	10034	10234	10082	0
313	BEAM	14502	10429	10404	10001	10010	10234	0	10087
314	BEAM	14503	10404	10439	10001	10010	10234	10079	0
315	BEAM	14504	10439	10409	10001	10034	10234	0	10082
316	BEAM	14505	10409	10416	10001	10010	10001	10083	10079
317	BEAM	14506	10416	10417	10001	10010	10001	10087	0
318	BEAM	14507	10402	10429	10001	10022	10234		
319	BEAM	14508	10401	10429	10001	10012	10343		
320	BEAM	14509	10406	10439	10001	10022	10234		
321	BEAM	14510	10407	10439	10001	10012	10345		
322	BEAM	14511	10409	10422	10001	10012	10220		
323	BEAM	14600	10403	10402	10001	10022	10234		
324	BEAM	14601	10403	10433	10001	10023	10348		
325	BEAM	14602	10429	10433	10001	10015	10247		
326	BEAM	14603	10403	10432	10001	10018	10350		
327	BEAM	14604	10432	10433	10001	10012	10234		
328	BEAM	14605	10433	10529	10001	10015	10350		
329	BEAM	14606	10433	10503	10001	10012	10353		
330	BEAM	14607	10432	10503	10001	10018	10247		
331	BEAM	14610	10405	10406	10001	10022	10234		
332	BEAM	14611	10405	10443	10001	10023	10348		
333	BEAM	14612	10439	10443	10001	10015	10247		
334	BEAM	14613	10405	10442	10001	10018	10350		
335	BEAM	14614	10442	10443	10001	10012	10234		
336	BEAM	14615	10443	10539	10001	10015	10350		
337	BEAM	14616	10443	10505	10001	10012	10353		
338	BEAM	14617	10442	10505	10001	10018	10247		
339	BEAM	15102	10519	10520	10001	10031	10197		
340	BEAM	15103	10520	10522	10001	10031	10197		
341	BEAM	15104	10522	10501	10001	10031	10197		
342	BEAM	15105	10519	10622	10001	10008	10263	0	10002
343	BEAM	15107	10501	10622	10001	10008	10263	0	10004
344	BEAM	15200	10504	10506	10001	10014	10202		
345	BEAM	15201	10501	10601	10001	10005	10193		
346	BEAM	15202	10507	10607	10001	10005	10194		
347	BEAM	15203	10501	10502	10001	10031	10202		
348	BEAM	15204	10502	10504	10001	10014	10202		
349	BEAM	15205	10501	10604	10001	10008	10373	0	10034
350	BEAM	15206	10506	10507	10001	10031	10202		
351	BEAM	15207	10507	10604	10001	10008	10375	0	10036
352	BEAM	15302	10513	10613	10001	10005	10195		
353	BEAM	15303	10507	10509	10001	10031	10217		
354	BEAM	15305	10507	10609	10001	10008	10272	0	10004
355	BEAM	15307	10513	10609	10001	10008	10272	0	10002
356	BEAM	15321	10509	10510	10001	10036	10217		
357	BEAM	15322	10510	10511	10001	10036	10217		
358	BEAM	15323	10511	10512	10001	10036	10217		
359	BEAM	15324	10512	10513	10001	10036	10217		
360	BEAM	15401	10513	10514	10001	10039	10226		
361	BEAM	15402	10519	10619	10001	10005	10196		
362	BEAM	15403	10514	10516	10001	10039	10226		
363	BEAM	15404	10516	10519	10001	10031	10226		
364	BEAM	15405	10513	10616	10001	10008	10375	0	10036
365	BEAM	15407	10519	10616	10001	10008	10373	0	10034
366	BEAM	15500	10521	10522	10001	10032	10001	0	10083
367	BEAM	15501	10522	10529	10001	10040	10234	10082	0
368	BEAM	15502	10504	10528	10001	10012	10001	10087	0
369	BEAM	15503	10504	10538	10001	10012	10234	10079	0
370	BEAM	15504	10539	10540	10001	10040	10001		
371	BEAM	15507	10502	10529	10001	10037	10234		
372	BEAM	15508	10501	10529	10001	10012	10397		

373	BEAM	15509	10506	10539	10001	10037	10234		
374	BEAM	15510	10507	10539	10001	10012	10399		
375	BEAM	15511	10527	10522	10001	10045	10220		
376	BEAM	15512	10540	10509	10001	10040	10234	0	10082
377	BEAM	15514	10517	10521	10001	10032	10402		
378	BEAM	15515	10516	10517	10001	10032	10001	10087	0
379	BEAM	15517	10520	10521	10001	10009	10404		
380	BEAM	15520	10525	10516	10001	10032	10001	0	10079
381	BEAM	15521	10509	10527	10001	10045	10220		
382	BEAM	15522	10538	10539	10001	10012	10407		
383	BEAM	15523	10528	10529	10001	10012	10395		
384	BEAM	15524	10509	10525	10001	10032	10001	10083	0
385	BEAM	15525	10525	10533	10001	10025	10410		
386	BEAM	15526	10533	10534	10001	10025	10410		
387	BEAM	15527	10534	10535	10001	10025	10410		
388	BEAM	15528	10535	10514	10001	10025	10410		
389	BEAM	15529	10530	10533	10001	10043	10001		
390	BEAM	15530	10510	10530	10001	10043	10415		
391	BEAM	15531	10531	10534	10001	10044	10416		
392	BEAM	15532	10511	10531	10001	10044	10415		
393	BEAM	15533	10532	10535	10001	10043	10418		
394	BEAM	15534	10512	10532	10001	10043	10415		
395	BEAM	15600	10503	10502	10001	10037	10234		
396	BEAM	15610	10505	10506	10001	10037	10234		
397	BEAM	16100	10600	10602	10001	10012	10422		
398	BEAM	16101	10619	10620	10001	10031	10197		
399	BEAM	16102	10620	10621	10001	10031	10197		
400	BEAM	16103	10621	10622	10001	10031	10197		
401	BEAM	16104	10622	10600	10001	10031	10197		
402	BEAM	16105	10600	10601	10001	10031	10197		
403	BEAM	16200	10606	10608	10001	10012	10407		
404	BEAM	16201	10601	10602	10001	10031	10202		
405	BEAM	16202	10602	10603	10001	10031	10202		
406	BEAM	16203	10603	10604	10001	10031	10202		
407	BEAM	16204	10604	10605	10001	10031	10202		
408	BEAM	16205	10605	10606	10001	10031	10202		
409	BEAM	16206	10606	10607	10001	10031	10202		
410	BEAM	16302	10607	10608	10001	10031	10217		
411	BEAM	16303	10608	10609	10001	10031	10217		
412	BEAM	16321	10609	10610	10001	10031	10217		
413	BEAM	16322	10610	10611	10001	10031	10217		
414	BEAM	16323	10611	10612	10001	10031	10217		
415	BEAM	16324	10612	10613	10001	10031	10217		
416	BEAM	16400	10618	10620	10001	10012	10402		
417	BEAM	16403	10614	10616	10001	10031	10226		
418	BEAM	16404	10616	10618	10001	10031	10226		
419	BEAM	16405	10618	10619	10001	10031	10226		
420	BEAM	16420	10613	10614	10001	10031	10226		
421	BEAM	16500	10617	10622	10001	10032	10001	0	10069
422	BEAM	16501	10622	10604	10001	10032	10234	10068	10073
423	BEAM	16502	10604	10631	10001	10032	10234	10065	0
424	BEAM	16503	10624	10616	10001	10032	10001	0	10065
425	BEAM	16504	10616	10617	10001	10032	10001	10073	0
426	BEAM	16511	10609	10638	10001	10009	10220		
427	BEAM	16512	10623	10622	10001	10009	10220		
428	BEAM	16513	10604	10623	10001	10009	10410		
429	BEAM	16514	10623	10616	10001	10009	10410		
430	BEAM	16515	10638	10623	10001	10009	10220		
431	BEAM	16520	10631	10609	10001	10032	10234	0	10068
432	BEAM	16521	10609	10624	10001	10032	10001	10069	0
433	BEAM	16522	10624	10625	10001	10025	10234		
434	BEAM	16523	10625	10626	10001	10025	10234		
435	BEAM	16524	10626	10627	10001	10025	10234		
436	BEAM	16525	10627	10614	10001	10025	10234		
437	BEAM	16526	10628	10625	10001	10043	10463		
438	BEAM	16527	10610	10628	10001	10043	10464		
439	BEAM	16528	10629	10626	10001	10044	10465		
440	BEAM	16529	10611	10629	10001	10044	10001		
441	BEAM	16530	10630	10627	10001	10043	10467		
442	BEAM	16531	10612	10630	10001	10043	10464		
443	BEAM	26106	20654	20621	10001	20003	20001		
444	BEAM	26107	10601	20621	10001	10005	10200		
445	BEAM	26109	20621	20624	10001	10005	10200		
446	BEAM	26110	20624	20739	10001	10005	10200		
447	BEAM	26206	20624	20631	10001	20003	20005		
448	BEAM	26301	10607	20631	10001	10005	10220		
449	BEAM	26306	20634	20641	10001	20003	20007		
450	BEAM	26307	10613	20641	10001	10005	10220		
451	BEAM	26309	20641	20644	10001	10005	10220		
452	BEAM	26310	20644	20719	10001	10005	10220		
453	BEAM	26406	20644	20651	10001	20003	20011		
454	BEAM	26601	10619	20651	10001	10005	10200		
455	BEAM	26602	20651	20654	10001	10005	10200		

```
BEAM 26603 20654 20732 10001 10005 10200
BEAM 26604 20631 20634 10001 10005 10220
BEAM 26605 20634 20712 10001 10005 10220
BEAM 30020 30217 10317 10001 30003 10199
BEAM 30021 30210 10310 10001 30001 30002
BEAM 30022 30211 10311 10001 30002 30002
BEAM 30023 30212 10312 10001 30001 30002
BEAM 30030 10317 10417 10001 30003 10199
BEAM 30040 10417 10517 10001 30003 10199
BEAM 30041 10310 10530 10001 30001 30010
BEAM 30042 10311 10531 10001 30002 30010
BEAM 30043 10312 10532 10001 30001 30010
BEAM 30044 30428 10528 10001 30812 30013
BEAM 30045 30438 10538 10001 30812 30014
BEAM 30046 30440 10540 10001 30005 10410
BEAM 30047 30427 10527 10001 30005 10410
BEAM 30049 30421 10521 10001 30006 10410
BEAM 30050 10517 10617 10001 30003 10199
BEAM 30051 10530 10628 10001 30001 10272
BEAM 30052 10531 10629 10001 30002 10272
BEAM 30053 10532 10630 10001 30001 10272
BEAM 30054 10528 10603 10001 30812 30022
BEAM 30055 10538 10605 10001 30812 30023
BEAM 30056 10540 10631 10001 30005 30024
BEAM 30057 10527 10638 10001 30005 10410
BEAM 30059 10521 10621 10001 30006 30026
BEAM 30060 10617 20765 10001 30003 30027
BEAM 30061 10628 20716 10001 30001 30028
BEAM 30062 10629 20717 10001 30002 30029
BEAM 30063 10630 20718 10001 30001 30028
BEAM 30064 10603 20750 10001 30812 30031
BEAM 30065 10605 20752 10001 30812 30032
BEAM 30066 10631 20760 10001 30005 30033
BEAM 30067 10638 20760 10001 30005 30034
BEAM 30069 10621 20734 10001 30006 30035
BEAM 30209 10209 10309 10001 31066 10272
BEAM 30309 10309 10409 10001 31066 10272
BEAM 30409 10409 10509 10001 31066 10272
BEAM 30509 10509 10609 10001 31066 10272
BEAM 30609 10609 20715 10001 31066 10410
'
' Geom ID Do Thick Shear_y Shear_z
PIPE 10001 3.000 0.050
PIPE 10002 3.000 0.075
PIPE 10003 2.400 0.050
PIPE 10004 2.400 0.040
PIPE 10005 1.800 0.040
PIPE 10006 1.300 0.030
PIPE 10007 1.300 0.035
PIPE 10008 1.100 0.035
PIPE 10009 0.650 0.020
PIPE 10010 1.000 0.025
PIPE 10011 0.900 0.025
PIPE 10012 0.800 0.025
PIPE 10013 1.000 0.030
PIPE 10014 1.200 0.030
PIPE 10015 1.200 0.025
PIPE 10016 1.200 0.020
PIPE 10017 1.600 0.045
PIPE 10018 1.600 0.035
PIPE 10019 1.600 0.030
PIPE 10020 0.800 0.020
PIPE 10021 0.900 0.020
PIPE 10022 1.100 0.030
PIPE 10023 1.000 0.020
PIPE 10024 1.940 0.095
PIPE 10025 0.800 0.035
PIPE 10031 1.200 0.035
PIPE 10032 0.800 0.030
PIPE 10034 1.000 0.035
PIPE 10036 1.200 0.040
PIPE 10037 1.100 0.025
PIPE 10038 1.000 0.040
PIPE 10039 1.200 0.055
PIPE 10040 0.800 0.040
PIPE 10043 0.560 0.025
PIPE 10044 0.510 0.025
PIPE 10045 1.000 0.045
PIPE 20003 0.750 0.035
PIPE 30001 0.935 0.038
PIPE 30002 0.722 0.033
PIPE 30003 0.780 0.033
PIPE 30005 0.559 0.025
```

```
PIPE 30006 0.457 0.025
PIPE 30812 0.813 0.025
PIPE 31066 1.067 0.025
'
' Loc-Coo dx dy dz
UNITVEC 10001 0.000 0.000 1.000
UNITVEC 10113 0.696 -0.696 0.174
UNITVEC 10125 0.948 0.092 0.304
UNITVEC 10133 0.696 0.696 0.174
UNITVEC 10153 -0.696 0.696 0.174
UNITVEC 10173 -0.696 -0.696 0.174
UNITVEC 10193 0.992 0.015 0.122
UNITVEC 10194 -0.992 0.015 -0.122
UNITVEC 10195 -0.992 -0.015 0.122
UNITVEC 10196 0.992 -0.015 -0.122
UNITVEC 10197 0.000 -0.124 -0.992
UNITVEC 10199 0.000 -0.992 0.124
UNITVEC 10200 1.000 0.000 0.000
UNITVEC 10202 0.124 0.000 -0.992
UNITVEC 10207 0.000 -0.696 -0.718
UNITVEC 10209 0.000 -0.696 0.718
UNITVEC 10217 0.000 0.124 -0.992
UNITVEC 10219 0.000 -0.992 -0.124
UNITVEC 10220 -1.000 0.000 0.000
UNITVEC 10226 -0.124 0.000 -0.992
UNITVEC 10229 0.000 -1.000 0.000
UNITVEC 10234 0.000 0.000 -1.000
UNITVEC 10241 0.865 0.502 0.000
UNITVEC 10243 -0.865 0.502 0.000
UNITVEC 10246 -0.609 0.000 -0.793
UNITVEC 10247 -0.992 0.000 -0.124
UNITVEC 10251 0.733 0.000 -0.680
UNITVEC 10263 0.000 0.992 -0.124
UNITVEC 10268 0.000 0.737 -0.676
UNITVEC 10270 0.000 0.737 0.676
UNITVEC 10272 0.000 0.992 0.124
UNITVEC 10290 0.819 0.574 0.000
UNITVEC 10292 -0.819 0.574 0.000
UNITVEC 10295 -0.753 0.000 0.659
UNITVEC 10300 -0.753 0.000 0.658
UNITVEC 10319 0.000 0.767 -0.642
UNITVEC 10321 0.000 0.767 0.642
UNITVEC 10343 0.740 0.672 0.000
UNITVEC 10345 -0.740 0.672 0.000
UNITVEC 10348 -0.566 0.000 -0.824
UNITVEC 10350 0.992 0.000 0.124
UNITVEC 10353 -0.802 0.000 0.597
UNITVEC 10373 0.000 0.839 -0.545
UNITVEC 10375 0.000 0.839 0.545
UNITVEC 10395 -0.707 0.707 0.000
UNITVEC 10397 0.619 0.785 0.000
UNITVEC 10399 -0.619 0.785 0.000
UNITVEC 10402 -0.707 -0.707 0.000
UNITVEC 10404 0.699 -0.715 0.000
UNITVEC 10407 0.707 0.707 0.000
UNITVEC 10410 0.000 1.000 0.000
UNITVEC 10415 -0.708 -0.706 0.000
UNITVEC 10416 -0.690 0.724 0.000
UNITVEC 10418 -0.691 0.723 0.000
UNITVEC 10422 0.707 -0.707 0.000
UNITVEC 10463 -0.689 0.725 0.000
UNITVEC 10464 -0.709 -0.706 0.000
UNITVEC 10465 -0.690 0.723 0.000
UNITVEC 10467 -0.692 0.722 0.000
UNITVEC 20001 -0.496 0.000 -0.868
UNITVEC 20005 0.000 -0.496 -0.868
UNITVEC 20007 0.496 0.000 -0.868
UNITVEC 20011 0.000 0.496 -0.868
UNITVEC 30002 0.000 0.997 0.083
UNITVEC 30010 0.000 0.978 0.209
UNITVEC 30013 -0.588 -0.809 0.005
UNITVEC 30014 -0.588 0.809 0.005
UNITVEC 30022 -0.885 0.449 0.126
UNITVEC 30023 -0.885 -0.449 0.126
UNITVEC 30024 0.704 0.704 0.088
UNITVEC 30026 0.876 0.474 0.091
UNITVEC 30027 0.831 0.416 0.369
UNITVEC 30028 0.000 -0.994 0.108
UNITVEC 30029 -0.059 -0.992 0.108
UNITVEC 30031 0.000 -0.999 0.045
UNITVEC 30032 0.000 0.999 0.045
UNITVEC 30033 0.686 0.686 0.243
UNITVEC 30034 0.000 -0.999 0.032
```

```
UNITVEC 30035 0.999 0.000 0.050
'
' Ecc-ID Ex Ey Ez
ECCENT 10002 0.015 0.000 0.000
ECCENT 10004 -0.015 0.000 0.000
ECCENT 10005 0.026 0.026 0.207
ECCENT 10006 -0.235 0.000 0.000
ECCENT 10007 -0.026 0.026 0.207
ECCENT 10008 0.235 0.000 0.000
ECCENT 10010 -0.145 0.000 0.000
ECCENT 10012 0.145 0.000 0.000
ECCENT 10013 -0.009 -0.009 -0.069
ECCENT 10015 0.009 -0.009 -0.069
ECCENT 10021 -0.026 -0.026 0.207
ECCENT 10023 0.026 -0.026 0.207
ECCENT 10029 0.009 0.009 -0.069
ECCENT 10031 -0.009 0.009 -0.069
ECCENT 10034 0.000 0.015 0.000
ECCENT 10036 0.000 -0.015 0.000
ECCENT 10038 0.000 -0.235 0.000
ECCENT 10040 0.000 0.235 0.000
ECCENT 10042 0.000 -0.145 0.000
ECCENT 10044 0.000 0.145 0.000
ECCENT 10065 0.000 -0.080 0.000
ECCENT 10068 -0.080 0.000 0.000
ECCENT 10069 0.080 0.000 0.000
ECCENT 10073 0.000 0.080 0.000
ECCENT 10079 0.000 -0.105 0.000
ECCENT 10082 -0.105 0.000 0.000
ECCENT 10083 0.105 0.000 0.000
ECCENT 10087 0.000 0.105 0.000
 '
 '
 # - Material specifications
 ' -----------------------
 '
 '       Mat ID E-mod     Poiss Yield    Density    Thermal
 MISOIEP 10001 2.100E+11 0.3 355.0E+6 7.850E+03 .000E+00
 MISOIEP 40001 2.100E+14 0.3 355.0E+6*100 1.000E-05 .000E+00
 '
 '
 # - Dummy cross section for deck dummy structure
 ' --------------------------------------------
 '
 PIPE 40001 1.000 0.100
 '
 ' Extra nodes for dummy structure attracting wave-in-deck loads
 ' -------------------------------------------------------------
 '
 NODE 40021 21.000 0.000 95.500
 NODE 40041 19.916 -1.107 99.000
 '
 '
 # - Extra elements for dummy structure representing topside
 ' ----------------------------------------------------------------
 '
 '     Elem ID np1 np2 material geom
BEAM 40021 20719 20718 40001 40001 10001
BEAM 40022 20718 20717 40001 40001 10001
BEAM 40023 20717 20716 40001 40001 10001
BEAM 40024 20716 20715 40001 40001 10001
BEAM 40025 20715 20712 40001 40001 10001
BEAM 40026 20732 20765 40001 40001 10001
BEAM 40027 20765 20719 40001 40001 10001
BEAM 40028 20732 20734 40001 40001 10001
BEAM 40029 20734 20739 40001 40001 10001
BEAM 40030 20739 20750 40001 40001 10001
BEAM 40031 20750 20752 40001 40001 10001
BEAM 40032 20752 20712 40001 40001 10001
BEAM 40033 20719 40021 40001 40001 10001
BEAM 40034 40021 20712 40001 40001 10001
BEAM 40035 20732 40021 40001 40001 10001
BEAM 40036 40021 20739 40001 40001 10001
BEAM 40037 40021 20760 40001 40001 10001
BEAM 40038 20760 20715 40001 40001 10001
BEAM 40041 20719 40041 40001 40001 10001
BEAM 40042 40041 20712 40001 40001 10001
BEAM 40043 20732 40041 40001 40001 10001
BEAM 40044 40041 20739 40001 40001 10001
 '
 '
 # - Node mass representing weight of topside                                   ' ...
     ---------------------------------------                               ...
```

```
        NODEMASS 40041 11000E+03
 '
 #  Jacket 2, where J defines the distance between the jackets                 '
'       Node ID    X            Y           Z      Boundary code
NODE    110101   42.00+J2     -21.00      0.00    1 1 1 1 1 1
NODE    110107   42.00+J2     21.00       0.00    1 1 1 1 1 1
NODE    110113   0.000+J2     21.00       0.00    1 1 1 1 1 1
NODE    110119   0.000+J2     -21.00      0.00    1 1 1 1 1 1
NODE    110201   41.75+J2     -20.75      2.00
NODE    110202   41.75+J2     -7.62       2.00
NODE    110203   44.13+J2     -7.62       2.00
NODE    110204   41.75+J2     0.00        2.00
NODE    110205   44.13+J2     7.62        2.00
NODE    110206   41.75+J2     7.62        2.00
NODE    110207   41.75+J2     20.75       2.00
NODE    110209   21.00+J2     20.75       2.00
NODE    110213   0.250+J2     20.75       2.00
NODE    110216   0.250+J2     0.00        2.00
NODE    110219   0.250+J2     -20.75      2.00
NODE    110222   21.00+J2     -20.75      2.00
NODE    110223   41.39+J2     -20.39      4.88
NODE    110224   41.39+J2     20.39       4.88
NODE    110225   0.610+J2     20.39       4.88
NODE    110226   0.610+J2     -20.39      4.88
NODE    110229   34.13+J2     -7.62       2.00
NODE    110232   43.07+J2     -7.62       10.50
NODE    110233   33.07+J2     -7.62       10.50
NODE    110239   34.13+J2     7.62        2.00
NODE    110241   40.87+J2     -19.87      9.02
NODE    110242   43.07+J2     7.62        10.50
NODE    110243   33.07+J2     7.62        10.50
NODE    110247   40.87+J2     19.87       9.02
NODE    110253   1.130+J2     19.87       9.02
NODE    110259   1.130+J2     -19.87      9.02
NODE    110301   39.50+J2     -18.50      20.00
NODE    110302   39.50+J2     -7.62       20.00
NODE    110303   41.88+J2     -7.62       20.00
NODE    110304   39.50+J2     0.00        20.00
NODE    110305   41.88+J2     7.62        20.00
NODE    110306   39.50+J2     7.62        20.00
NODE    110307   39.50+J2     18.50       20.00
NODE    110309   21.00+J2     18.50       20.00
NODE    110310   17.20+J2     18.50       20.00
NODE    110311   14.90+J2     18.50       20.00
NODE    110312   12.60+J2     18.50       20.00
NODE    110313   2.500+J2     18.50       20.00
NODE    110316   2.500+J2     0.00        20.00
NODE    110317   15.50+J2     -13.00      20.00
NODE    110319   2.500+J2     -18.50      20.00
NODE    110322   21.00+J2     -18.50      20.00
NODE    110329   31.88+J2     -7.62       20.00
NODE    110332   40.63+J2     -7.62       30.00
NODE    110333   30.63+J2     -7.62       30.00
NODE    110339   31.88+J2     7.62        20.00
NODE    110342   40.63+J2     7.62        30.00
NODE    110343   30.63+J2     7.62        30.00
NODE    110401   37.00+J2     -16.00      40.00
NODE    110402   37.00+J2     -7.62       40.00
NODE    110403   39.38+J2     -7.62       40.00
NODE    110404   37.00+J2     0.00        40.00
NODE    110405   39.38+J2     7.62        40.00
NODE    110406   37.00+J2     7.62        40.00
NODE    110407   37.00+J2     16.00       40.00
NODE    110409   21.00+J2     16.00       40.00
NODE    110412   12.60+J2     16.00       40.00
NODE    110413   5.000+J2     16.00       40.00
NODE    110416   5.000+J2     0.00        40.00
NODE    110417   15.50+J2     -10.50      40.00
NODE    110419   5.000+J2     -16.00      40.00
NODE    110422   21.00+J2     -16.00      40.00
NODE    110429   29.38+J2     -7.62       40.00
NODE    110432   38.44+J2     -7.62       47.51
NODE    110433   28.45+J2     -7.62       47.51
NODE    110439   29.38+J2     7.62        40.00
NODE    110442   38.44+J2     7.62        47.51
NODE    110443   28.45+J2     7.62        47.51
NODE    110501   34.63+J2     -13.63      59.00
NODE    110502   34.63+J2     -7.62       59.00
NODE    110503   37.01+J2     -7.62       59.00
NODE    110504   34.63+J2     0.00        59.00
NODE    110505   37.01+J2     7.62        59.00
NODE    110506   34.63+J2     7.62        59.00
NODE    110507   34.63+J2     13.63       59.00
```

786	NODE	110509	21.00+J2	13.63	59.00						
787	NODE	110510	15.52+J2	13.63	59.00						
788	NODE	110511	13.22+J2	13.63	59.00						
789	NODE	110512	10.92+J2	13.63	59.00						
790	NODE	110513	7.380+J2	13.63	59.00						
791	NODE	110514	7.380+J2	10.33	59.00						
792	NODE	110516	7.380+J2	0.00	59.00						
793	NODE	110517	15.50+J2	-8.13	59.00						
794	NODE	110519	7.380+J2	-13.63	59.00						
795	NODE	110520	13.85+J2	-13.63	59.00						
796	NODE	110521	17.46+J2	-10.09	59.00						
797	NODE	110522	21.00+J2	-13.63	59.00						
798	NODE	110525	17.70+J2	10.33	59.00						
799	NODE	110527	21.00+J2	5.00	59.00						
800	NODE	110528	29.63+J2	-5.00	59.00						
801	NODE	110529	27.01+J2	-7.62	59.00						
802	NODE	110530	17.20+J2	11.94	59.00						
803	NODE	110531	14.90+J2	11.94	59.00						
804	NODE	110532	12.60+J2	11.94	59.00						
805	NODE	110533	15.50+J2	10.33	59.00						
806	NODE	110534	13.21+J2	10.33	59.00						
807	NODE	110535	10.91+J2	10.33	59.00						
808	NODE	110538	29.63+J2	5.00	59.00						
809	NODE	110539	27.01+J2	7.62	59.00						
810	NODE	110540	25.06+J2	9.56	59.00						
811	NODE	110600	29.45+J2	-11.00	80.00						
812	NODE	110601	32.00+J2	-11.00	80.00						
813	NODE	110602	32.00+J2	-8.46	80.00						
814	NODE	110603	32.00+J2	-6.20	80.00						
815	NODE	110604	32.00+J2	0.00	80.00						
816	NODE	110605	32.00+J2	6.20	80.00						
817	NODE	110606	32.00+J2	8.46	80.00						
818	NODE	110607	32.00+J2	11.00	80.00						
819	NODE	110608	29.45+J2	11.00	80.00						
820	NODE	110609	21.00+J2	11.00	80.00						
821	NODE	110610	15.52+J2	11.00	80.00						
822	NODE	110611	13.22+J2	11.00	80.00						
823	NODE	110612	10.92+J2	11.00	80.00						
824	NODE	110613	10.00+J2	11.00	80.00						
825	NODE	110614	10.00+J2	7.70	80.00						
826	NODE	110616	10.00+J2	0.00	80.00						
827	NODE	110617	15.50+J2	-5.50	80.00						
828	NODE	110618	10.00+J2	-8.45	80.00						
829	NODE	110619	10.00+J2	-11.00	80.00						
830	NODE	110620	12.55+J2	-11.00	80.00						
831	NODE	110621	15.78+J2	-11.00	80.00						
832	NODE	110622	21.00+J2	-11.00	80.00						
833	NODE	110623	21.00+J2	0.00	80.00						
834	NODE	110624	17.70+J2	7.70	80.00						
835	NODE	110625	15.50+J2	7.70	80.00						
836	NODE	110626	13.21+J2	7.70	80.00						
837	NODE	110627	10.92+J2	7.70	80.00						
838	NODE	110628	17.20+J2	9.31	80.00						
839	NODE	110629	14.90+J2	9.31	80.00						
840	NODE	110630	12.60+J2	9.31	80.00						
841	NODE	110631	23.75+J2	8.25	80.00						
842	NODE	110638	21.00+J2	5.00	80.00						
843	NODE	120621	32.00+J2	-11.00	81.86						
844	NODE	120624	32.00+J2	-11.00	94.45						
845	NODE	120631	32.00+J2	11.00	81.86						
846	NODE	120634	32.00+J2	11.00	94.45						
847	NODE	120641	10.00+J2	11.00	81.86						
848	NODE	120644	10.00+J2	11.00	94.45						
849	NODE	120651	10.00+J2	-11.00	81.86						
850	NODE	120654	10.00+J2	-11.00	94.45						
851	NODE	120712	32.00+J2	11.00	95.50						
852	NODE	120715	21.00+J2	11.00	95.50						
853	NODE	120716	17.20+J2	11.00	95.50						
854	NODE	120717	15.00+J2	11.00	95.50						
855	NODE	120718	12.60+J2	11.00	95.50						
856	NODE	120719	10.00+J2	11.00	95.50						
857	NODE	120732	10.00+J2	-11.00	95.50						
858	NODE	120734	15.00+J2	-11.00	95.50						
859	NODE	120739	32.00+J2	-11.00	95.50						
860	NODE	120750	32.00+J2	-5.50	95.50						
861	NODE	120752	32.00+J2	5.50	95.50						
862	NODE	120760	21.00+J2	5.50	95.50						
863	NODE	120765	10.00+J2	-8.25	95.50						
864	NODE	130210	17.20+J2	20.00	2.00	1	1	0	0	0	0
865	NODE	130211	14.90+J2	20.00	2.00	1	1	0	0	0	0
866	NODE	130212	12.60+J2	20.00	2.00	1	1	0	0	0	0
867	NODE	130217	15.50+J2	-15.25	2.00	1	1	0	0	0	0
868	NODE	130421	17.46+J2	-10.09	55.00						

```
NODE      130427   21.00+J2       5.00          58.00
NODE      130428   29.63+J2      -5.00          58.00
NODE      130438   29.63+J2       5.00          58.00
NODE      130440   25.06+J2       9.56          58.00
'
'
'    Elem ID   np1     np2  material  geom   lcoor  ecc1  ecc2
BEAM 111201 110101 110201 10001 10001 10193
BEAM 111202 110107 110207 10001 10001 10194
BEAM 111302 110113 110213 10001 10001 10195
BEAM 111402 110119 110219 10001 10001 10196
BEAM 112103 110219 110222 10001 10010 10197
BEAM 112104 110222 110201 10001 10010 10197
BEAM 112105 110319 110222 10001 10006 10199 10013 0
BEAM 112106 110222 110322 10001 10009 10200
BEAM 112107 110301 110222 10001 10006 10199 10015 0
BEAM 112200 110204 110206 10001 10010 10202
BEAM 112201 110201 110223 10001 10001 10193
BEAM 112202 110207 110224 10001 10001 10194
BEAM 112203 110201 110202 10001 10010 10202
BEAM 112204 110202 110204 10001 10010 10202
BEAM 112205 110301 110204 10001 10006 10207 10015 0
BEAM 112206 110206 110207 10001 10010 10202
BEAM 112207 110307 110204 10001 10006 10209 10029 0
BEAM 112208 110223 110241 10001 10002 10193
BEAM 112209 110224 110247 10001 10002 10194
BEAM 112210 110241 110301 10001 10002 10193
BEAM 112211 110247 110307 10001 10002 10194
BEAM 112302 110213 110225 10001 10001 10195
BEAM 112303 110207 110209 10001 10010 10217
BEAM 112304 110209 110213 10001 10010 10217
BEAM 112305 110307 110209 10001 10006 10219 10029 0
BEAM 112306 110209 110309 10001 10009 10220
BEAM 112307 110313 110209 10001 10006 10219 10031 0
BEAM 112309 110225 110253 10001 10002 10195
BEAM 112311 110253 110313 10001 10002 10195
BEAM 112402 110219 110226 10001 10001 10196
BEAM 112403 110213 110216 10001 10010 10226
BEAM 112404 110216 110219 10001 10010 10226
BEAM 112405 110313 110216 10001 10006 10209 10031 0
BEAM 112406 110216 110316 10001 10009 10229
BEAM 112407 110319 110216 10001 10006 10207 10013 0
BEAM 112409 110226 110259 10001 10002 10196
BEAM 112411 110259 110319 10001 10002 10196
BEAM 112501 110222 110229 10001 10010 10234 10082 0
BEAM 112502 110229 110204 10001 10010 10234 0 10087
BEAM 112503 110204 110239 10001 10010 10234 10079 0
BEAM 112504 110239 110209 10001 10010 10234 0 10082
BEAM 112505 110209 110216 10001 10010 10001 10083 10079
BEAM 112506 110216 110222 10001 10010 10001 10087 10083
BEAM 112507 110202 110229 10001 10011 10234
BEAM 112508 110201 110229 10001 10012 10241
BEAM 112509 110206 110239 10001 10011 10234
BEAM 112510 110207 110239 10001 10012 10243
BEAM 112511 110209 110222 10001 10011 10220
BEAM 112600 110203 110202 10001 10011 10234
BEAM 112601 110203 110233 10001 10020 10246
BEAM 112602 110229 110233 10001 10016 10247
BEAM 112603 110203 110232 10001 10018 10247
BEAM 112604 110232 110233 10001 10020 10234
BEAM 112605 110233 110329 10001 10015 10247
BEAM 112606 110303 110233 10001 10021 10251
BEAM 112607 110232 110303 10001 10019 10247
BEAM 112610 110205 110206 10001 10011 10234
BEAM 112611 110205 110243 10001 10020 10246
BEAM 112612 110239 110243 10001 10016 10247
BEAM 112613 110205 110242 10001 10018 10247
BEAM 112614 110242 110243 10001 10020 10234
BEAM 112615 110243 110339 10001 10015 10247
BEAM 112616 110305 110243 10001 10021 10251
BEAM 112617 110242 110305 10001 10019 10247
BEAM 113103 110319 110322 10001 10013 10197
BEAM 113104 110322 110301 10001 10034 10197
BEAM 113105 110319 110422 10001 10007 10263 0 10010
BEAM 113107 110301 110422 10001 10007 10263 0 10012
BEAM 113200 110304 110306 10001 10013 10202
BEAM 113201 110301 110401 10001 10003 10113
BEAM 113202 110307 110407 10001 10003 10133
BEAM 113203 110301 110302 10001 10013 10202
BEAM 113204 110302 110304 10001 10013 10202
BEAM 113205 110301 110404 10001 10007 10268 0 10042
BEAM 113206 110306 110307 10001 10013 10202
BEAM 113207 110307 110404 10001 10007 10270 0 10044
```

952	BEAM	113302	110313	110413	10001	10003	10153		
953	BEAM	113303	110307	110309	10001	10034	10217		
954	BEAM	113305	110307	110409	10001	10007	10272	0	10012
955	BEAM	113307	110313	110409	10001	10007	10272	0	10010
956	BEAM	113321	110309	110310	10001	10038	10217		
957	BEAM	113322	110310	110311	10001	10038	10217		
958	BEAM	113323	110311	110312	10001	10038	10217		
959	BEAM	113324	110312	110313	10001	10013	10217		
960	BEAM	113402	110319	110419	10001	10003	10173		
961	BEAM	113403	110313	110316	10001	10013	10226		
962	BEAM	113404	110316	110319	10001	10013	10226		
963	BEAM	113405	110313	110416	10001	10007	10270	0	10044
964	BEAM	113407	110319	110416	10001	10007	10268	0	10042
965	BEAM	113500	110317	110322	10001	10010	10001	0	10083
966	BEAM	113501	110322	110329	10001	10013	10234	10082	0
967	BEAM	113502	110329	110304	10001	10010	10234	0	10087
968	BEAM	113503	110304	110339	10001	10010	10234	10079	0
969	BEAM	113504	110339	110309	10001	10013	10234	0	10082
970	BEAM	113505	110309	110316	10001	10010	10001	10083	10079
971	BEAM	113506	110316	110317	10001	10010	10001	10087	0
972	BEAM	113507	110302	110329	10001	10010	10234		
973	BEAM	113508	110301	110329	10001	10012	10290		
974	BEAM	113509	110306	110339	10001	10010	10234		
975	BEAM	113510	110307	110339	10001	10012	10292		
976	BEAM	113511	110309	110322	10001	10012	10220		
977	BEAM	113600	110303	110302	10001	10010	10234		
978	BEAM	113601	110329	110332	10001	10013	10295		
979	BEAM	113602	110329	110333	10001	10014	10247		
980	BEAM	113603	110303	110332	10001	10018	10247		
981	BEAM	113604	110332	110333	10001	10012	10234		
982	BEAM	113605	110333	110429	10001	10014	10247		
983	BEAM	113606	110333	110403	10001	10020	10300		
984	BEAM	113607	110332	110403	10001	10017	10247		
985	BEAM	113610	110305	110306	10001	10010	10234		
986	BEAM	113611	110339	110342	10001	10013	10295		
987	BEAM	113612	110339	110343	10001	10014	10247		
988	BEAM	113613	110305	110342	10001	10018	10247		
989	BEAM	113614	110342	110343	10001	10012	10234		
990	BEAM	113615	110343	110439	10001	10014	10247		
991	BEAM	113616	110343	110405	10001	10020	10300		
992	BEAM	113617	110342	110405	10001	10017	10247		
993	BEAM	114103	110419	110422	10001	10014	10197		
994	BEAM	114104	110422	110401	10001	10031	10197		
995	BEAM	114105	110419	110522	10001	10007	10263	10005	10006
996	BEAM	114107	110401	110522	10001	10007	10263	10007	10008
997	BEAM	114200	110404	110406	10001	10014	10202		
998	BEAM	114201	110401	110501	10001	10004	10193		
999	BEAM	114202	110407	110507	10001	10004	10194		
1000	BEAM	114203	110401	110402	10001	10014	10202		
1001	BEAM	114204	110402	110404	10001	10014	10202		
1002	BEAM	114205	110401	110504	10001	10007	10319	10007	10038
1003	BEAM	114206	110406	110407	10001	10014	10202		
1004	BEAM	114207	110407	110504	10001	10007	10321	10021	10040
1005	BEAM	114302	110413	110513	10001	10004	10195		
1006	BEAM	114303	110407	110409	10001	10031	10217		
1007	BEAM	114305	110407	110509	10001	10007	10272	10021	10008
1008	BEAM	114307	110413	110509	10001	10007	10272	10023	10006
1009	BEAM	114322	110409	110412	10001	10036	10217		
1010	BEAM	114324	110412	110413	10001	10014	10217		
1011	BEAM	114402	110419	110519	10001	10004	10196		
1012	BEAM	114403	110413	110416	10001	10014	10226		
1013	BEAM	114404	110416	110419	10001	10014	10226		
1014	BEAM	114405	110413	110516	10001	10007	10321	10023	10040
1015	BEAM	114407	110419	110516	10001	10007	10319	10005	10038
1016	BEAM	114500	110417	110422	10001	10010	10001	0	10083
1017	BEAM	114501	110422	110429	10001	10034	10234	10082	0
1018	BEAM	114502	110429	110404	10001	10010	10234	0	10087
1019	BEAM	114503	110404	110439	10001	10010	10234	10079	0
1020	BEAM	114504	110439	110409	10001	10034	10234	0	10082
1021	BEAM	114505	110409	110416	10001	10010	10001	10083	10079
1022	BEAM	114506	110416	110417	10001	10010	10001	10087	0
1023	BEAM	114507	110402	110429	10001	10022	10234		
1024	BEAM	114508	110401	110429	10001	10012	10343		
1025	BEAM	114509	110406	110439	10001	10022	10234		
1026	BEAM	114510	110407	110439	10001	10012	10345		
1027	BEAM	114511	110409	110422	10001	10012	10220		
1028	BEAM	114600	110403	110402	10001	10022	10234		
1029	BEAM	114601	110403	110433	10001	10023	10348		
1030	BEAM	114602	110429	110433	10001	10015	10247		
1031	BEAM	114603	110403	110432	10001	10018	10350		
1032	BEAM	114604	110432	110433	10001	10012	10234		
1033	BEAM	114605	110433	110529	10001	10015	10350		
1034	BEAM	114606	110433	110503	10001	10012	10353		

1035	BEAM	114607	110432	110503	10001	10018	10247		
1036	BEAM	114610	110405	110406	10001	10022	10234		
1037	BEAM	114611	110405	110443	10001	10023	10348		
1038	BEAM	114612	110439	110443	10001	10015	10247		
1039	BEAM	114613	110405	110442	10001	10018	10350		
1040	BEAM	114614	110442	110443	10001	10012	10234		
1041	BEAM	114615	110443	110539	10001	10015	10350		
1042	BEAM	114616	110443	110505	10001	10012	10353		
1043	BEAM	114617	110442	110505	10001	10018	10247		
1044	BEAM	115102	110519	110520	10001	10031	10197		
1045	BEAM	115103	110520	110522	10001	10031	10197		
1046	BEAM	115104	110522	110501	10001	10031	10197		
1047	BEAM	115105	110519	110622	10001	10008	10263	0	10002
1048	BEAM	115107	110501	110622	10001	10008	10263	0	10004
1049	BEAM	115200	110504	110506	10001	10014	10202		
1050	BEAM	115201	110501	110601	10001	10005	10193		
1051	BEAM	115202	110507	110607	10001	10005	10194		
1052	BEAM	115203	110501	110502	10001	10031	10202		
1053	BEAM	115204	110502	110504	10001	10014	10202		
1054	BEAM	115205	110501	110604	10001	10008	10373	0	10034
1055	BEAM	115206	110506	110507	10001	10031	10202		
1056	BEAM	115207	110507	110604	10001	10008	10375	0	10036
1057	BEAM	115302	110513	110613	10001	10005	10195		
1058	BEAM	115303	110507	110509	10001	10031	10217		
1059	BEAM	115305	110507	110609	10001	10008	10272	0	10004
1060	BEAM	115307	110513	110609	10001	10008	10272	0	10002
1061	BEAM	115321	110509	110510	10001	10036	10217		
1062	BEAM	115322	110510	110511	10001	10036	10217		
1063	BEAM	115323	110511	110512	10001	10036	10217		
1064	BEAM	115324	110512	110513	10001	10036	10217		
1065	BEAM	115401	110513	110514	10001	10039	10226		
1066	BEAM	115402	110519	110619	10001	10005	10196		
1067	BEAM	115403	110514	110516	10001	10039	10226		
1068	BEAM	115404	110516	110519	10001	10031	10226		
1069	BEAM	115405	110513	110616	10001	10008	10375	0	10036
1070	BEAM	115407	110519	110616	10001	10008	10373	0	10034
1071	BEAM	115500	110521	110522	10001	10032	10001	0	10083
1072	BEAM	115501	110522	110529	10001	10040	10234	10082	0
1073	BEAM	115502	110504	110528	10001	10012	10001	10087	0
1074	BEAM	115503	110504	110538	10001	10012	10234	10079	0
1075	BEAM	115504	110539	110540	10001	10040	10001		
1076	BEAM	115507	110502	110529	10001	10037	10234		
1077	BEAM	115508	110501	110529	10001	10012	10397		
1078	BEAM	115509	110506	110539	10001	10037	10234		
1079	BEAM	115510	110507	110539	10001	10012	10399		
1080	BEAM	115511	110527	110522	10001	10045	10220		
1081	BEAM	115512	110540	110509	10001	10040	10234	0	10082
1082	BEAM	115514	110517	110521	10001	10032	10402		
1083	BEAM	115515	110516	110517	10001	10032	10001	10087	0
1084	BEAM	115517	110520	110521	10001	10009	10404		
1085	BEAM	115520	110525	110516	10001	10032	10001	0	10079
1086	BEAM	115521	110509	110527	10001	10045	10220		
1087	BEAM	115522	110538	110539	10001	10012	10407		
1088	BEAM	115523	110528	110529	10001	10012	10395		
1089	BEAM	115524	110509	110525	10001	10032	10001	10083	0
1090	BEAM	115525	110525	110533	10001	10025	10410		
1091	BEAM	115526	110533	110534	10001	10025	10410		
1092	BEAM	115527	110534	110535	10001	10025	10410		
1093	BEAM	115528	110535	110514	10001	10025	10410		
1094	BEAM	115529	110530	110533	10001	10043	10001		
1095	BEAM	115530	110510	110530	10001	10043	10415		
1096	BEAM	115531	110531	110534	10001	10044	10416		
1097	BEAM	115532	110511	110531	10001	10044	10415		
1098	BEAM	115533	110532	110535	10001	10043	10418		
1099	BEAM	115534	110512	110532	10001	10043	10415		
1100	BEAM	115600	110503	110502	10001	10037	10234		
1101	BEAM	115610	110505	110506	10001	10037	10234		
1102	BEAM	116100	110600	110602	10001	10012	10422		
1103	BEAM	116101	110619	110620	10001	10031	10197		
1104	BEAM	116102	110620	110621	10001	10031	10197		
1105	BEAM	116103	110621	110622	10001	10031	10197		
1106	BEAM	116104	110622	110600	10001	10031	10197		
1107	BEAM	116105	110600	110601	10001	10031	10197		
1108	BEAM	116200	110606	110608	10001	10012	10407		
1109	BEAM	116201	110601	110602	10001	10031	10202		
1110	BEAM	116202	110602	110603	10001	10031	10202		
1111	BEAM	116203	110603	110604	10001	10031	10202		
1112	BEAM	116204	110604	110605	10001	10031	10202		
1113	BEAM	116205	110605	110606	10001	10031	10202		
1114	BEAM	116206	110606	110607	10001	10031	10202		
1115	BEAM	116302	110607	110608	10001	10031	10217		
1116	BEAM	116303	110608	110609	10001	10031	10217		
1117	BEAM	116321	110609	110610	10001	10031	10217		

1118	BEAM	116322	110610	110611	10001	10031	10217		
1119	BEAM	116323	110611	110612	10001	10031	10217		
1120	BEAM	116324	110612	110613	10001	10031	10217		
1121	BEAM	116400	110618	110620	10001	10012	10402		
1122	BEAM	116403	110614	110616	10001	10031	10226		
1123	BEAM	116404	110616	110618	10001	10031	10226		
1124	BEAM	116405	110618	110619	10001	10031	10226		
1125	BEAM	116420	110613	110614	10001	10031	10226		
1126	BEAM	116500	110617	110622	10001	10032	10001	0	10069
1127	BEAM	116501	110622	110604	10001	10032	10234	10068	10073
1128	BEAM	116502	110604	110631	10001	10032	10234	10065	0
1129	BEAM	116503	110624	110616	10001	10032	10001	0	10065
1130	BEAM	116504	110616	110617	10001	10032	10001	10073	0
1131	BEAM	116511	110609	110638	10001	10009	10220		
1132	BEAM	116512	110623	110622	10001	10009	10220		
1133	BEAM	116513	110604	110623	10001	10009	10410		
1134	BEAM	116514	110623	110616	10001	10009	10410		
1135	BEAM	116515	110638	110623	10001	10009	10220		
1136	BEAM	116520	110631	110609	10001	10032	10234	0	10068
1137	BEAM	116521	110609	110624	10001	10032	10001	10069	0
1138	BEAM	116522	110624	110625	10001	10025	10234		
1139	BEAM	116523	110625	110626	10001	10025	10234		
1140	BEAM	116524	110626	110627	10001	10025	10234		
1141	BEAM	116525	110627	110614	10001	10025	10234		
1142	BEAM	116526	110628	110625	10001	10043	10463		
1143	BEAM	116527	110610	110628	10001	10043	10464		
1144	BEAM	116528	110629	110626	10001	10044	10465		
1145	BEAM	116529	110611	110629	10001	10044	10001		
1146	BEAM	116530	110630	110627	10001	10043	10467		
1147	BEAM	116531	110612	110630	10001	10043	10464		
1148	BEAM	126106	120654	120621	10001	20003	20001		
1149	BEAM	126107	110601	120621	10001	10005	10200		
1150	BEAM	126109	120621	120624	10001	10005	10200		
1151	BEAM	126110	120624	120739	10001	10005	10200		
1152	BEAM	126206	120624	120631	10001	20003	20005		
1153	BEAM	126301	110607	120631	10001	10005	10220		
1154	BEAM	126306	120634	120641	10001	20003	20007		
1155	BEAM	126307	110613	120641	10001	10005	10220		
1156	BEAM	126309	120641	120644	10001	10005	10220		
1157	BEAM	126310	120644	120719	10001	10005	10220		
1158	BEAM	126406	120644	120651	10001	20003	20011		
1159	BEAM	126601	110619	120651	10001	10005	10200		
1160	BEAM	126602	120651	120654	10001	10005	10200		
1161	BEAM	126603	120654	120732	10001	10005	10200		
1162	BEAM	126604	120631	120634	10001	10005	10220		
1163	BEAM	126605	120634	120712	10001	10005	10220		
1164	BEAM	130020	130217	110317	10001	30003	10199		
1165	BEAM	130021	130210	110310	10001	30001	30002		
1166	BEAM	130022	130211	110311	10001	30002	30002		
1167	BEAM	130023	130212	110312	10001	30001	30002		
1168	BEAM	130030	110317	110417	10001	30003	10199		
1169	BEAM	130040	110417	110517	10001	30003	10199		
1170	BEAM	130041	110310	110530	10001	30001	30010		
1171	BEAM	130042	110311	110531	10001	30002	30010		
1172	BEAM	130043	110312	110532	10001	30001	30010		
1173	BEAM	130044	130428	110528	10001	30812	30013		
1174	BEAM	130045	130438	110538	10001	30812	30014		
1175	BEAM	130046	130440	110540	10001	30005	10410		
1176	BEAM	130047	130427	110527	10001	30005	10410		
1177	BEAM	130049	130421	110521	10001	30006	10410		
1178	BEAM	130050	110517	110617	10001	30003	10199		
1179	BEAM	130051	110530	110628	10001	30001	10272		
1180	BEAM	130052	110531	110629	10001	30002	10272		
1181	BEAM	130053	110532	110630	10001	30001	10272		
1182	BEAM	130054	110528	110603	10001	30812	30022		
1183	BEAM	130055	110538	110605	10001	30812	30023		
1184	BEAM	130056	110540	110631	10001	30005	30024		
1185	BEAM	130057	110527	110638	10001	30005	10410		
1186	BEAM	130059	110521	110621	10001	30006	30026		
1187	BEAM	130060	110617	120765	10001	30003	30027		
1188	BEAM	130061	110628	120716	10001	30001	30028		
1189	BEAM	130062	110629	120717	10001	30002	30029		
1190	BEAM	130063	110630	120718	10001	30001	30028		
1191	BEAM	130064	110603	120750	10001	30812	30031		
1192	BEAM	130065	110605	120752	10001	30812	30032		
1193	BEAM	130066	110631	120760	10001	30005	30033		
1194	BEAM	130067	110638	120760	10001	30005	30034		
1195	BEAM	130069	110621	120734	10001	30006	30035		
1196	BEAM	130209	110209	110309	10001	31066	10272		
1197	BEAM	130309	110309	110409	10001	31066	10272		
1198	BEAM	130409	110409	110509	10001	31066	10272		
1199	BEAM	130509	110509	110609	10001	31066	10272		
1200	BEAM	130609	110609	120715	10001	31066	10410		

```
'
# - Extra nodes for dummy structure attracting wave-in-deck loads
' ------------------------------------------------------------
'
 NODE 140021   21.000+J2   0.000  95.500
 NODE 140041  19.916+J2  -1.107  99.000
'
'
# - Extra elements for dummy structure representing topside
' ---------------------------------------------------------------
'
'     Elem ID np1   np2   material geom lcoor ecc1  ecc2
BEAM 140021 120719 120718 40001 40001 10001
BEAM 140022 120718 120717 40001 40001 10001
BEAM 140023 120717 120716 40001 40001 10001
BEAM 140024 120716 120715 40001 40001 10001
BEAM 140025 120715 120712 40001 40001 10001
BEAM 140026 120732 120765 40001 40001 10001
BEAM 140027 120765 120719 40001 40001 10001
BEAM 140028 120732 120734 40001 40001 10001
BEAM 140029 120734 120739 40001 40001 10001
BEAM 140030 120739 120750 40001 40001 10001
BEAM 140031 120750 120752 40001 40001 10001
BEAM 140032 120752 120712 40001 40001 10001
BEAM 140033 120719 140021 40001 40001 10001
BEAM 140034 140021 120712 40001 40001 10001
BEAM 140035 120732 140021 40001 40001 10001
BEAM 140036 140021 120739 40001 40001 10001
BEAM 140037 140021 120760 40001 40001 10001
BEAM 140038 120760 120715 40001 40001 10001
BEAM 140041 120719 140041 40001 40001 10001
BEAM 140042 140041 120712 40001 40001 10001
BEAM 140043 120732 140041 40001 40001 10001
BEAM 140044 140041 120739 40001 40001 10001
'
 # - Node mass representing weight of topside
 ' --------------------------------------
 NODEMASS 140041  11000E+03

 # - Element representing the bridge
 '            Elem ID      np1       np2      material     geom
 BEAM         150001        40041     140041     50001        10001
 '
 # - Material properties for spring element
 '          Mat_ID      RefX   RefY   RefZ     RefMx   RefMy   RefMz
 MREF       50001        101      0       0        0         0        0
 '
 # - Define hyperelastic curve
 '              Mat_ID      P                Delta
HYPELAST        101      -182.65E6*mu    -1
                          182.65E6*mu     1
'
 # - Define damping by damping ratio at two frequencies
'             d1          d2          fq1      fq2
DampRatio     0.02      0.02          0.067       0.667
' ------------- E O F --------------------
```

D.2.3 Batch file to automate analysis, *run_case*

```
# ...
    --------------------------------------------------------------------------------------------
# || Batch file to automate analysis                                        ...
                              ||
# || Input parameters : Peak period, significant wave height, time of ...
    analysis, stiffness ratio ||
# || Usage: ./run_case Tp Hs endT mu                                        ...
                              ||
# ...
    --------------------------------------------------------------------------------------------
'
'
# - Make folder to store analysis
```

```
mkdir Tp=$1_Hs=$2_endT=$3_mu=$4
'
# - Make file name defined by the input parameters
cp   head.mal              head_Tp=$1_Hs=$2_endT=$3_mu=$4.fem
cp   stru.mal              stru_Tp=$1_Hs=$2_endT=$3_mu=$4.fem
'
# - Insert input parameters to head file
 sed -i 's/Tp/'$1'/g'      head_Tp=$1_Hs=$2_endT=$3_mu=$4.fem
 sed -i 's/Hs/'$2'/g'      head_Tp=$1_Hs=$2_endT=$3_mu=$4.fem
 sed -i 's/endT/'$3'/g'    head_Tp=$1_Hs=$2_endT=$3_mu=$4.fem
 sed -i 's/mu/'$4'/g'      head_Tp=$1_Hs=$2_endT=$3_mu=$4.fem
'
# - Calculate wave length from wave period
 lambda=$(echo "$1^2*9.81/6.2832" | bc -l)
'
# - Calculate sea dimension
if (( $(echo "$1 < 4" | bc -l) ));
 then
 seadim1=$(echo "$lambda*8" | bc -l)
 elif (( $(echo "$1 > 10" | bc -l) ));
 then
 seadim1=$(echo "$lambda*2" | bc -l)
 else
 seadim1=$(echo "$lambda*4" | bc -l)
 fi
# - Insert sea dimension to head file
 sed -i 's/dimxy/'$seadim1'/g'   head_Tp=$1_Hs=$2_endT=$3_mu=$4.fem
# - Insert distance between jackets = 80 m to struture file
 sed -i 's/J2/'80'/g'   stru_Tp=$1_Hs=$2_endT=$3_mu=$4.fem
 #
# - Run USFOS
./usfos.cmd   << ENDIN
head_Tp=$1_Hs=$2_endT=$3_mu=$4
stru_Tp=$1_Hs=$2_endT=$3_mu=$4
BT=USF
Tp=$1_Hs=$2_endT=$3_mu=$4
ENDIN
'
# - Run Dynres
./dynres.cmd   << ENDIN
Tp=$1_Hs=$2_endT=$3_mu=$4
3
2
res_$2
ENDIN
# - Move files to folder
mv stru_Tp=$1_Hs=$2_endT=$3_mu=$4.fem Tp=$1_Hs=$2_endT=$3_mu=$4
mv Tp=$1_Hs=$2_endT=$3_mu=$4.raf Tp=$1_Hs=$2_endT=$3_mu=$4
mv Tp=$1_Hs=$2_endT=$3_mu=$4.dyn Tp=$1_Hs=$2_endT=$3_mu=$4
mv Tp=$1_Hs=$2_endT=$3_mu=$4_status.text Tp=$1_Hs=$2_endT=$3_mu=$4
mv head_Tp=$1_Hs=$2_endT=$3_mu=$4.fem Tp=$1_Hs=$2_endT=$3_mu=$4
mv Tp=$1_Hs=$2_endT=$3_mu=$4.out Tp=$1_Hs=$2_endT=$3_mu=$4
mv res_$2_Nodal_Displacement_Node_40041_Dof_1.plo displacement.plo
```

```
mv res_$2_Nodal_Displacement_Node_140041_Dof_1.plo displacement2.plo
mv res_$2_Surface_Elevation.plo elevation.plo
mv res_$2_Total_Wave_Load.plo wave_load.plo
mv res_$2_Element_Force_Elem_14105_End_2_Dof_1.plo elem_force3.plo
mv displacement.plo Tp=$1_Hs=$2_endT=$3_mu=$4
mv displacement2.plo Tp=$1_Hs=$2_endT=$3_mu=$4
mv elevation.plo Tp=$1_Hs=$2_endT=$3_mu=$4
mv wave_load.plo Tp=$1_Hs=$2_endT=$3_mu=$4
mv elem_force3.plo Tp=$1_Hs=$2_endT=$3_mu=$4
' ------------- E O F --------------------
```